DOCTORAL THESIS

Online Fibre Property Measurements

Foundations for a method based on ultrasound attenuation

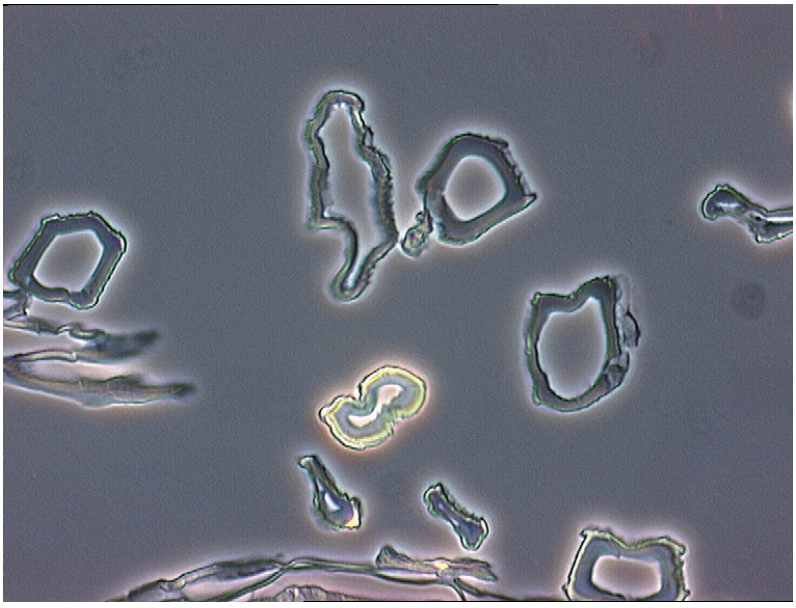

Yvonne Aitomäki

Luleå University of Technology

Online Fibre Property Measurements

Foundations for a method based on ultrasound attenuation

Yvonne Aitomäki

EISLAB
Dept. of Computer Science and Electrical Engineering
Luleå University of Technology
Luleå, Sweden

Supervisors:

Torbjörn Löfqvist, Jerker Delsing

Tryck: Universitetstryckeriet, Luleå

ISSN: 1402-1544
ISBN 978-91-86233-54-9

Luleå 2009

www.ltu.se

To Erik

Abstract

This thesis presents the foundations of a method for estimating fibre properties of pulp suitable for online application in the pulp and paper industry.

In the pulp and paper industry, increased efficiency and greater paper quality control are two of the industry's main objectives. It is proposed that online fibre property measurements are a means of achieving progress in both of these objectives.

Optical based systems that provide valuable geometric data on the fibres and other pulp characteristics are commercially available. However, measurements of the elastic properties of the fibres are not feasible using these systems.

To fill this gap an ultrasound based system for measuring the elastic properties of the wood fibres in pulp is proposed. Ultrasound propagation through a medium depends on its elastic properties. Thus the attenuation of an ultrasonic wave propagating through pulp will be affected by the elastic properties of the wood fibres. The method is based on solving the inverse problem where the output is known and the objective is to establish the inputs. In this case, attenuation is measured and a model of attenuation based on ultrasound scattering is developed. A search algorithm is used for finding elastic properties that minimize the error between the model and measured attenuation. The results of the search are estimates of the elastic properties of the fibres in suspension.

The results show resonance peaks in the attenuation in the frequency region tested. These peaks are found in both the measured and modelled attenuation spectra. Further investigation of these resonances suggests that they are due to modes of vibration in the fibre. These resonances are shown to aid in the identification of the elastic properties.

The attenuation is found to depend heavily on the geometry of the fibres. Hence fibre geometry, which can be obtained from online optical fibre measurement system, provides the key to extracting the elastic properties from the attenuation signal.

Studies are also carried out on the effect of viscosity on attenuation as well as the differences in attenuation between hollow and solid synthetic fibres in suspensions. The measurement method is also applied to hardwood and softwood kraft pulps. The results of these studies show that using the model derived in the thesis and attenuation measurements, estimates of the elastic properties can be obtained. The elastic property estimates for synthetic fibres agree well with values from other methods. These elastic property estimates for pulps agree well with previous studies of individual fibre tests though further validation is required.

The conclusions, based on the work so far and under three realizable conditions, are that the shear modulus and the transverse Young's modulus of pulp fibres can be measured. Once these conditions are met, a system based on this method can be implemented. By doing this the industry would benefit from the increase in paper quality control and energy saving such system could provide.

Contents

Acknowledgements

I would like to thank my supervisor Torbjörn Löfqvist for his enthusiasm and ideas as well as his advice and support. I would also like to thank Jerker Delsing for keeping me in mind of the main objectives and, more recently, for the constructive remarks that have helped pull the thesis together. I would also like to thank Jan Niemi for being such an excellent work colleague and coauthor. It has been great having someone to bounce ideas off and I feel we've learnt a huge amount about acoustics, measurements and we've also found time to compare notes on parenting.

Thomas Brännström has been my mentor for the last year and has been a great source of wisdom and clever thinking for which I am most grateful. I would also like to thank Jan van Deventer for listening to my rantings on cylinder modes and life in general - I forgot to thank him in my licentiate so I am making sure I do it now. Thanks also go to Johan Carlson, who has found the time to read and re-read my recent articles and has made some valuable suggestions. Thanks also to Mikael Sjödahl and Niklas Brännström for commenting on my thesis.

I would also like to thank my friends and colleagues at the CSEE department for making the department an enjoyable place to work. Not only that but there are so many of you who have helped me that were I to list some, I would be leaving out others, so I have to thank you collectively and hope that will suffice. My thanks also go to the fantastic group of researchers, who made up the research school for women, for sharing your experiences with me. Your support has increased my self-confidence.

Following convention, I would finally like to thank my family, but in all truth you are up there highest on my list of people to thank. Especially you, Erik. I couldn't have managed without you. So, thank-you Emelie(7) for my lyckosten. Thank-you James(5) for telling me to break-a-leg when I go off to write this thesis. Thank-you Daisy(2) for making sure I get up in the morning and reminding me that work is only part of life. Thank-you Astrid(12) for being so thoughtful and for helping Erik with the little ones. Thank-you Martin(15) for reminding me that it's not easy being a teenager either. Thank-you mum for reading and correcting my English and for being 'on my side'.

Part I

Chapter 1

Introduction

Paper products are an essential part of our daily lives and the paper and pulp industry, which provide these products, is a cornerstone of World industry. In 2007, the European pulp and paper industry employed 260 000 people, produced 100 million tonnes of paper, 40 million tonnes of pulp and had a turnover of €80 billion. This accounted for 26% and 23% of the World's paper and pulp production, respectively [1]. It is a mature industry striving to adapt to the new demands of customers and to take advantage of its access to forest-based energy resources.

The energy consumption of the paper industry is high. In countries belonging to the Confederation of European Paper Industries (CEPI) this was 1.3 million TJ[1] in 2006 [1]. Increased efficiency is therefore an obvious means of reducing costs as not only does this reduce the amount of energy, which has to be bought, but any energy by-products from the process can be sold. This is exemplified by the Södra business strategy that states that energy is becoming an increasingly important element of operations [2].

One of the most energy intensive parts of the pulp manufacturing process is the refining of the pulp. In a typical plant this uses 1 GJ per tonne dry material [3]. Hence increased efficiency in this part of the process can have a large economic impact.

Online fibre property measurement could improve energy efficiency and optimise paper quality, for example:

1. In the refiner by allowing the refining energy level to be set according to the particular fibre properties or by reducing the percentage of fibres refined, if the fibres already have suitable properties.

2. By reducing waste - early detection of faults associated with the fibre properties can allow the pulp to be reprocessed at an earlier stage in the paper manufacturing.

3. Paper quality could be optimised by improving fractionation of the pulp. The aim of fractionation is to separate the pulp according to its properties. With online

[1] $1 \cdot 10^{18}$ Joules

fibre property measurement the fractionation process can be improved. These improvements would lead to the fibres, and hence the pulp, being better suited to the end product.

Optical fibre property measurements are currently available and their use in improving paper quality is shown by Hagedorn [4]. The flexibility of the fibres is an important property since greater flexibility increases the strength of the paper. This flexibility depends on both geometry and Young's modulus [5]. In optical systems such as the STFI Fibermaster, (Lorentsen-Wettre, Sweden) [6], bendibility is used as a relative measure of flexibility. However, using this measure the influence of bendibility cannot be separated from the geometry since they are interdependent variables [4]. The consequence of this is that there is ambiguity as to whether it is the elastic properties of the fibre (such as Young's modulus) or the geometry that needs to be modified by the process.

Ultrasound measurements have the potential to measure the elastic properties of the fibres in suspension. This is because ultrasound propagation is a function of these elastic properties. If an ultrasound method can measure elastic properties then a future paper manufacturing plant could have sensors based on this technology at crucial stages in the process. This would work alongside an online optical pulp analyser providing geometric fibre data. The result would be increased process efficiency, which results in reduced energy usage, and greater paper quality control. Thus profit margins are increased.

In addition, if the optical and ultrasound sensors were combined with an online paper measurement system, such as a laser ultrasonic web stiffness sensor [7], it would allow the relationship between pulp properties and paper quality to be more precisely established.

The objective of this thesis is to provide the first step towards an online method of measuring the elastic properties of fibres. Hence, the following hypothesis is tested:

> *The measurement of the ultrasound attenuation can be used to estimate the elastic properties of wood fibres in pulp online.*

This hypothesis can be broken down into three research questions,

1. Can elastic properties be estimated from ultrasound attenuation?
2. Can the method be applied to wood fibres in pulp?
3. Can the measurement method be used online?

Can elastic properties be estimated from ultrasound attenuation?

The method of estimating the elastic properties from ultrasound attenuation consists of three parts: a model, measurements and an algorithm for finding the parameters of the model that minimizes the difference between the model output and the measurements. Since the method is to be applied to wood fibres in pulp, the model is based on the acoustic scattering of particles in suspension (Chapters 3 & 5). The measurements are of ultrasound attenuation. The algorithm searches through the range of elastic properties to find the values that minimize the difference between the modelled attenuation and the

measured attenuation. The outcome of the algorithm, being the estimates of the elastic properties, gives the best-fit to measured attenuation (Chapter 6).

This question is central to the thesis and is addressed in all the papers as well as the chapters specified in the text.

Can the method be applied to wood fibres in pulp?

To apply this method to pulp a model is required, which captures only the wood fibre properties that are important to attenuation. From this, the elastic properties of the fibres can be extracted.

Again this question is central to the thesis but is particularly addressed in the final paper, Paper G and Chapter 2.

Can the method be used online?

The ultimate aim is to have an online method. This will influence decisions about the complexity of the model chosen. Hence, the need to establish the simplest model that will allow estimates of the elastic fibre properties to be made. Consideration should also be made of the computational efficiency of such a method and the equipment required.

The thesis is made up of two parts: a summary of the work and a collection of papers. The first part presents more detailed information on wood fibres in pulp and the background physics, followed by more detailed issues not covered in the scientific papers. The papers are then summarised before conclusions are drawn and further work is discussed. The second part is a collection of seven papers.

Chapter 2

Fibres in Pulp

2.1 Fibres and the effects of processing

Paper in the broadest sense of the word dates back to the ancient Egyptians who used the papyrus plant to make sheets on which to write. Our modern day paper making however, has its roots in China, possibly as early as 8 BC [8]. The basic steps are gathering the raw material, breaking it down to a pulp with the addition of water then forming it into a sheet before drying it. Although these steps may not have changed, the process is now high speed (up to 1,900 m/min [9]), high volume, and fully automated. The huge variations in the processes and the type of wood or even the organic and non-organic material used as input in the process reflect the differences required in the final products. The focus of this research is on the measurement of the properties of fibres used in the manufacture of paper products; more specifically wood fibre properties because wood is by far the most common source of fibres used in paper making.

Before discussing fibre property measurements and the effect the pulp process has on their properties it is worthwhile introducing some of the elements of the fibre that are important to its mechanical properties.

A wood fibre has a layered structure as shown in figure 2.1. The hollow in the centre of the fibre is called the lumen and the outer edge of the fibre is the primary cell wall. In wood, the fibres are held together by the middle lamella which is also shown in the diagram. The lines on the primary cell wall and secondary walls (s1, s2 and s3 in the diagram) illustrate fibrils that are part of the cell walls. Fibrils or microfibrils are made of cellulose molecules and their orientation, as indicated in the diagram, can vary considerably. The s2 layer has fibrils that are parallel and form a steep spiral about the axis of the fibre. The microfibrillar angle (MFA) of this layer has been measured and has been found to relate to the strength of individual fibres [10]. These results show that the more axially aligned the microfibrils (smaller MFA), the greater the strength of the fibres. On a larger scale, the MFA has been related to the Young's modulus of wood where a decrease in MFA correlates to increased stiffness (higher modulus) [11]. Interpreting the data on individual fibre measurements [12] shows that when MFA decreases, the

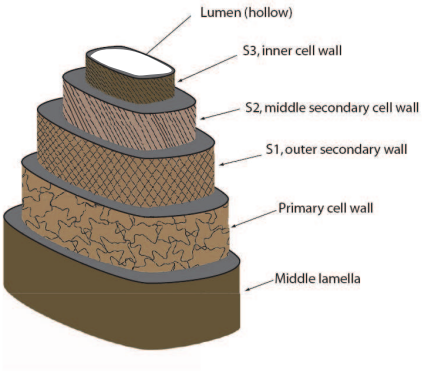

Figure 2.1: Illustration of the layered structure of a fibre [13]

Table 2.1: Table of fibre geometry

	Swedish Pine		Birch
	Earlywood	Latewood	
Fibre width (μm)	35	25	22
Lumen diameter (μm)	30	10	16
Fibre length (μm)	2500-4900		1000-1500

Young's modulus increases but this relationship is not clear because the fibre perimeter also decreases and thus would cause the modulus to increase.

The geometry of the fibres affects the properties of the paper produced. For example, long thin-walled fibres, as found in earlywood, provide good strength since their compliance and length means that they form a better bond between the fibres. However, the resulting paper will also have a low bending stiffness. In contrast, thick-walled fibres, from latewood, give high bending stiffness but their rigidity results in weaker bonds between the fibres and hence ultimately weaker paper [13].

In trees, fibre geometry varies not only from species to species but also within a species since the thickness of the wall depends on the age of the wood. A young tree will have mainly earlywood and hence long slender fibres, whereas a mature tree will have earlywood near the top and towards the outer edge of the trunk. Table 2.1 with data taken from [13], gives an example of the variation of the geometry of earlywood and latewood fibres.

The table also illustrates the geometrical differences between hardwoods and softwoods. Birch, acacia and eucalyptus are all examples of hardwood trees often used in making fine paper. Softwoods include species such as pine and spruce. There are also differences in their chemical composition of which will not be discussed here.

Pulp manufacturing is the method by which the fibres are extracted from wood. There are two basic types of pulp manufacturing: chemical and mechanical. In a typical chemi-

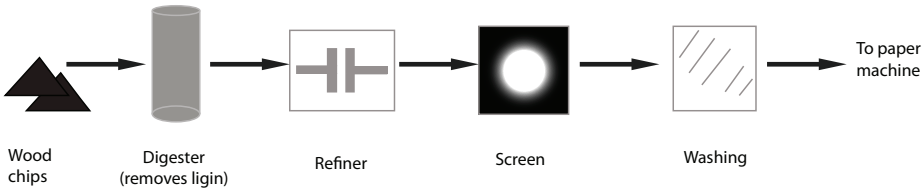

Figure 2.2: Simplified process diagram of a chemical pulp process (no bleach)

cal pulp manufacturing process, illustrated in figure 2.2, the wood is cooked in a solution of chemicals. The lignin of the wood is made soluble (digested) and the fibres separate as whole fibres. These softened fibres are then fed at high pressure into a refiner (refining process) where they are mechanically beaten. In a typical mechanical pulp manufacturing process, the wood fibres are exposed to heat and pressure (thermomechanical pulps [14]) before being separated by grinding or milling. These pulps can then be refined to improve the fibre properties for paper making. An overview of these different processes and the variations that exist between them is provided by Wikström [15] and Karlsson [13].

From the brief description of pulp manufacturing, it is obvious that one of the fundamental steps in making paper is the mechanical treatment of the fibres, typically in the refiner. One of the objectives of this stage is to fibrillate the fibre. This is where the fibres are beaten to increase their flexibility and their ability to swell, before paper formation [16]. There is some evidence to show that this increased flexibility is independent of geometry and hence due to elasticity of the fibre wall [17]. Collapsing of the fibre structure, so that the fibres have a ribbon geometry results in greater paper strength [13]. The relationship between flexibility and collapsed fibres is expected since in theory,

$$F = 1/EI \tag{2.1}$$

where F is the flexibility, E is the Young's modulus and I is the second moment of area [12]. If the fibre collapses, then I decreases and consequently F increases. From the equation it can been seen that the elastic modulus of the fibre is important in fibre flexibility directly. It could also have an indirect affect since from general studies of hollow cylinders [18], low E values lead to an increased tendency to collapse. Since collapsed fibres are more flexible it follows then low E will both directly and indirectly lead to greater fibre flexibility and hence stronger paper.

Refining also causes some of the microfibrils to be either released from the cell wall or bowed out. This increases the bonding of the fibres to each other, increases the strength of the paper and its homogeneity [10]. The relationship between the frequency of refining and the viscoelastic properties of water saturated lignin, which is related to the viscoelasticity of the fibres since they are composed on lignin, has also been investigated [19]. Although it was found that refining frequencies would not soften the lignin, the study does provide some data on the viscoelasticity of saturated wood and hence to some degree fibres.

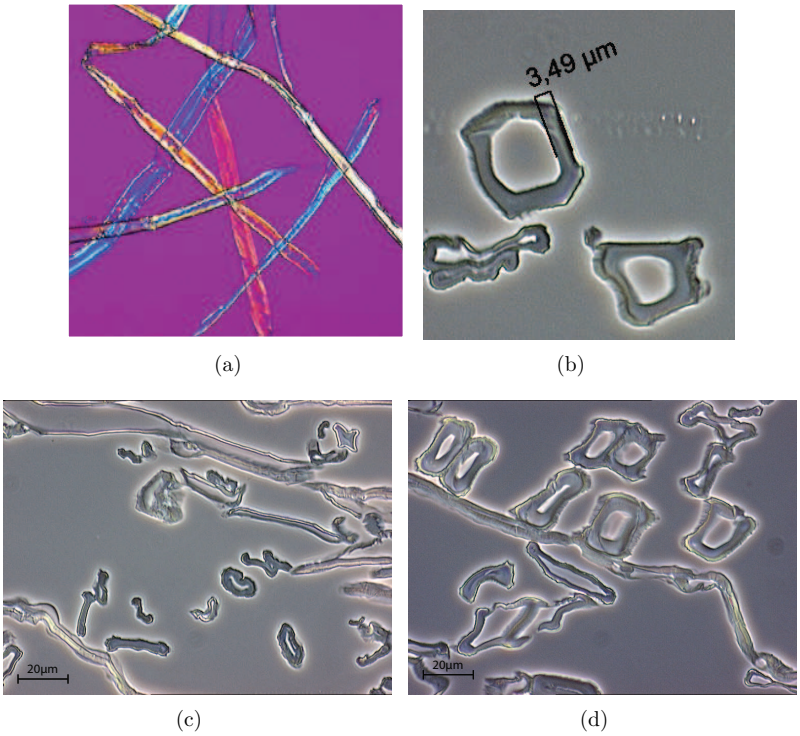

(a) (b)

(c) (d)

Figure 2.3: Examples of refined fibres in pulp: 2.3(b) Softwood fibres from chemical pulp (magnification x75), 2.3(a) Cross section of fibre in softwood chemical pulp showing two collapsed fibres. 2.3(c) Hardwood chemical pulp (bleached), 2.3(d) Softwood chemical pulp

Figure 2.3 are photographs of refined pulp fibres. Figure 2.3(a) illustrates their variability along the their length. Note also from the photograph and the dimensions given in Table 2.1 that the length is much greater than the fibre diameter, which is the reason for the assumption of infinite length used in the model. Figure 2.3(c) and 2.3(d) are at higher magnification and show the cross sectional variation between a hardwood pulp and a softwood pulp, respectively.

The cross sectional view of a group of refined pulp fibres is shown in the figure 2.3(b). Two of the fibres can clearly be seen to have maintained their structure whereas the other two fibres have collapsed and lie together.

In the processing of fibres their material properties and their geometric properties are altered in order to make a better quality paper product. It follows then that measuring and monitoring these properties can improve paper quality and this is exemplified in a study done by Hagedorn [4].

2.2 Measurement methods of mechanical properties of fibres

As customers, our demands on paper vary from the softness of tissue to the strength and durability of cardboard, and from the porous nature of vacuum bags to non-porous milk cartons. In addition are the demands made on the printing surfaces of most paper products. To match these demands on the final paper products, there is a wide range of pulp characteristics that require monitoring and measuring. The flexibility and the elastic properties of the fibres are two of these characteristics but, as discussed in section 2.1, their influence on paper strength means they have an important role in paper quality.

The flexibility of fibres depends on the elasticity of the fibres and their geometry. Fractioning fibres using a mesh separates long or stiff fibres from shorter or flexible fibres since the long and/or stiff fibres do not pass as easily through the mesh as shorter and/or more flexible fibres. Some assessment of fibre flexibility can therefore be made using different sizes of mesh. However, the problem of separating the length property from the flexibility property of the fibre remains.

The stiffness of individual fibres can be measured and through this Young's modulus established. The first of the two main methods used is carried out by setting the fibre in a v-shaped notch on the tip of a thin capillary tube submersed in water. Water is then allowed to flow through the capillary. This water flow is increased until the middle part of the fibre reaches a preset mark [20]. The second method is to measure the extent to which a fibre has followed the contour of a wire set between the fibre and a glass plate, when a hydraulic pressure is applied. This process has been automated and is available [20].

The L&W STFI Fibermaster [6] gives an indication of the stiffness through a measurement quantity referred to as bendability. This is defined as the difference in form factor when measured with high and normal flows in the measuring cell. The form factor is the ratio of the greatest extension of the fibre to the real length of the fibre in the same projected plane [21]. The use of flow and optical measurement results in the ability of the system to provide a measurement related to the elasticity of the fibre. One of the problems with this method is that the fibre is projected onto a plane so that deflections out of plane cause distortions and hence are a source of inaccuracy. Another issue is that the current measurement is a relative measurement of the flexibility of the fibres and not an absolute one. An industrial study measuring the bendability and paper quality showed a correlation between these two properties, however this correlation was explained as being due to the fact that the bendibility uses the shape factor, which is also correlated with paper quality, and hence the two could not be separated [4].

In research investigation of fibre flexibility, individual fibres are tested [12, 22]. One method was to test individual fibres by applying epoxy glue to each end of carefully selected long, straight fibres [12]. The fibre was then mounted in a loading machine and the load was measured under cyclic displacement. From this and the geometric measurements, the Young's modulus, and the flexiblity was calculated. This was done for approximately 400 fibres and provides figures for comparison with other methods.

Measurements of other elastic properties such as shear modulus and intrinsic loss have not been found for pulp fibres.

It can be seen from this overview of the current measurement methods that a rapid online method for measuring the elastic properties of the fibres directly does not yet exist.

Chapter 3

Ultrasound in Suspensions

3.1 Overview of acoustic waves

Ultrasound is simply sound with higher frequencies than that the human ear can detect (>20kHz), hence theories on audible sound also apply to ultrasound. The mechanism by which a sound wave propagates through a medium depends on its material properties. Hence by measuring the velocity of the wave and its attenuation information can be obtained about these material properties. The term wave velocity will in this thesis and refers to the phase velocity of the wave. As the wave propagates through a medium it tends to diminish in amplitude. This is due the dissipation of energy as the wave advances. This is quantified by the attenuation, α, and its relationship to the amplitude, S_o, at a point in space is

$$S' = S_o e^{-\alpha d}, \tag{3.1}$$

where S' is the wave amplitude after it has travelled a distance d in the medium. Hence

$$\alpha = \frac{1}{d} \ln \left(\frac{S_o}{S'} \right). \tag{3.2}$$

Sound waves with different frequencies are absorbed, or attenuated, by different amounts depending on the medium. Hence α is frequency dependent and the equation above is valid for a particular frequency.

If the sound is a pulse then it will contain different frequencies and the shorter the pulse, the more frequencies it will contain. The advantage of measuring using a pulse is that the frequency response of the medium can be obtained in a single measurement. However, the transient effects are more complex to model and hence it is common to model the system as a steady state one.

3.1.1 Waves in fluids

In fluids, the classical explanation for attenuation is that it is due to viscosity, η, and thermal conduction. For non-metallic fluids, the attenuation due to thermal conduction

is negligible compared to that due to viscosity [23]. Unfortunately for most common liquids this does not account for all the attenuation mechanisms. In water, this excess attenuation is attributed to structural relaxation [24] and an additional viscous term, η_B is used. For water, η_B is approximately three times that of the η. The relationship for the attenuation, α, can be written in terms of the relaxation time τ [23] such that

$$\alpha \approx \frac{1}{2}\frac{\omega^2}{c}\tau, \tag{3.3}$$

where ω is the angular frequency and τ is

$$\tau = (\frac{4}{3}\eta + \eta_B)/\rho_1 c^2. \tag{3.4}$$

From this it can be seen that as the frequency increases, the attenuation becomes increasingly significant, even in low viscous fluids such as water, as it is a function of ω^2.

In a non-viscous fluid the wave velocity, c_c, equals the thermodynamic speed of sound, c. This is defined as [23]

$$c = \sqrt{\frac{B}{\rho}}, \tag{3.5}$$

where B is the adiabatic bulk modulus and ρ_1 is the density of the fluid [23]. c is a constant in the wave equation which is derived from the linearised mass conservation and linearised conservation of momentum [25] such that

$$\nabla^2 p - \frac{1}{c^2}\frac{\partial^2 p}{\partial t^2} = 0 \tag{3.6}$$

If the fluid is unbound and viscous, then the effect of the viscosity can be approximated by the introduction of τ into the wave equation such that

$$c_c \approx c(1 + \frac{3}{8}\omega^2\tau^2). \tag{3.7}$$

Although c_c has a term depending on ω^2, τ^2 is very small for low viscosity fluids like water and hence the dispersion, which is where waves of different frequencies travel at different velocities, is small.

3.1.2 Waves in Solids

The wave motion in solids is more complex and it is described by Navier's displacement equation, which is expressed for a isotropic, elastic medium as

$$(\lambda + 2G)\nabla\nabla\cdot\boldsymbol{\zeta} + G\nabla^2\boldsymbol{\zeta} = \rho_2\frac{\partial^2\boldsymbol{\zeta}}{\partial t^2} \tag{3.8}$$

where $\boldsymbol{\zeta}$ is the displacement vector and ρ is the density. λ and G are elastic moduli where λ is Lamé constant and G is the shear modulus. ∇^2 is the three dimensional Laplace

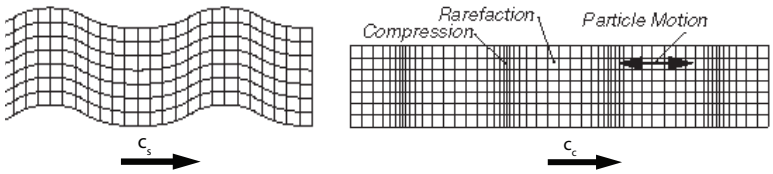

(a) (b)

Figure 3.1: Illustrations of a shear wave (3.1.2) and a pure compression wave 3.1.2 propagating in a solid

operator [26]. This can be re-written to divide the motion into a dilation (compression) and rotation.

$$(\lambda + 2G)\nabla(\nabla \cdot \boldsymbol{\zeta}) + G\nabla \times (\nabla \times \boldsymbol{\zeta}) = \rho_2 \frac{\partial^2 \boldsymbol{\zeta}}{\partial t^2} \tag{3.9}$$

Thus in an unbound solid two types of waves can exist: a compressional wave and a shear wave (rotational) wave. The shear wave is a transverse wave, where the particle motion is perpendicular to the direction of propagation (Figure 3.1.2) and hence is termed a rotational wave.

The velocity of a shear wave depends only on the shear modulus of the solid such that

$$c_s = \sqrt{\frac{G}{\rho_2}}. \tag{3.10}$$

In a compression wave, the particle motion and the wave direction are concurrent. The simplest case of a compression wave propagation in a solid is when it is along the axis of a narrow bar or rod of isotropic material, where surface of the rod is allowed to move freely and the frequency is low (theoretically when the frequency is zero). The velocity of this wave will solely depend on the Young's modulus such that [27]

$$c_o = \sqrt{\frac{E}{\rho_2}}. \tag{3.11}$$

However, if the isotropic media is now extended, it can be thought of as if the surface were fixed. It therefore requires a greater stress to cause the same strain. It can be shown that wave velocity of a compression wave is then dependent on the shear modulus, G as well as the bulk elasticity of the material, K [28]. Its velocity becomes

$$c_c = \sqrt{\frac{K + \frac{4}{3}G}{\rho_2}}. \tag{3.12}$$

For a volume of the material where the force, p, is applied uniformly on each side of an cubic element of the medium, K is defined as $p = K/\rho_2$ [28]. A full derivation of these

wave velocities and how they relate to the stress and strain in a solid medium is given in [28].

In solids, the intrinsic attenuation per wavelength can be approximated by the phase difference between the stress and the strain, also referred to as the loss tangent, $\tan\delta$ [29]. Stress and strain are related by a general elastic modulus, M. The specific modulus or combination of moduli will depend on the geometry, the type of loading, the specific material etc. To model this phase difference, M is made complex such that

$$M = M' + iM''$$

and

$$\tan\delta = \frac{M''}{M'} \tag{3.13}$$

In terms of the attenuation, α, this becomes, if $\tan\delta \ll 1$

$$\alpha \;=\; \pi\tan\delta \tag{3.14}$$

This phase difference will cause dispersion and the effect can be calculated by using the complex elastic modulus in the calculation of the wave velocity. Hence c_c can be expressed as a complex wave speed, $\mathbf{c_c} = c_c\sqrt{1 - i\tan\delta}$

In a suspension, the wave travels from a fluid to either a solid or another fluid. As the wave hits the boundary of the two media, part of the wave is reflected and part of the wave is transmitted. In the simple case of a plane wave arriving at a boundary that is perpendicular to the direction of the wave, calculating the ratio of the intensity of the transmitted wave to the reflected wave is straightforward. This is done by considering the boundary condition at the interface and assuming the velocity and pressure to be continuous at this point. The result is that the amplitude of the wave being reflected depends on the difference in the characteristic impedances of the two media. The characteristic impedance is the product of the density and the velocity of the wave. Since a plane wave and a flat boundary are considered, the only waves propagating are compression waves. The calculation is more elaborate if the wave progression is not perpendicular to the boundary and particularly if the interface is on a solid [30].

3.1.3 Thermoelastic Scattering

Associated with an ultrasonic pressure wave is a temperature field which is in phase with the pressure wave and depends on the thermal properties of the medium. In a suspension, there are two media that normally have different thermal properties. The result is that the temperature field inside the suspended particle is different in amplitude to that of the surrounding liquid away from the boundary. In order to maintain the equilibrium at the boundary, the temperature field in the boundary layer varies and causes the boundary layer to expand and contract and hence become the source of a secondary wave (Figure 3.2). This is known as thermoelastic scattering. Considering the $\theta - r$ plane, of a cylindrical scatterer in a fluid media, this thermal elastic scatter appears as a symmetric monopole wave emanating from the scatterer. This wave decays quickly

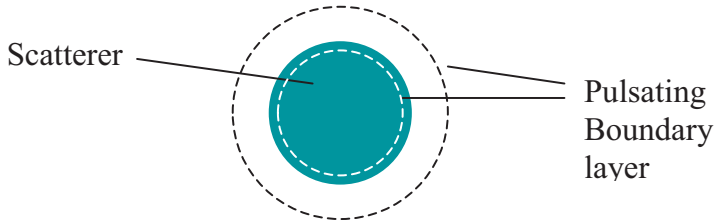

Figure 3.2: Diagram of an pulsating boundary layer, the source of a secondary sound wave.

and is not noticeable at a large distance from the scatterer. It does however dissipate energy and in some cases, such as for an emulsion of sunflower oil and water, it can be the dominant effect in attenuation [31]. For fibres where the scatterer has a larger diameter and for higher frequency this effect is small [32].

3.1.4 Viscous boundary effects

In the previous section the attenuation and motion of an unbound fluid was discussed. The added effect of a boundary is apparent when a viscous fluid flows close to and parallel to the surface of a wall. In this case there exists a primary wave with motion at a distance from the wall, with only a component in the x direction parallel to the wall, u_x. There also exists a secondary wave, u', with motion in x that is a function of z (direction perpendicular to boundary) and time t. In studying the absorption arising from the shear at the boundary, the equation governing the flow is the rotation part of the Navier Stokes equation,

$$\rho\frac{\partial \mathbf{u}}{\partial t} = \eta\nabla\times(\nabla\times\mathbf{u}). \tag{3.15}$$

The boundary conditions are that the velocity approaches the free stream velocity far from the boundary and the wall is fixed which means that the velocity is zero at this point such that $\mathbf{u} = (u_x + u')$. Hence equation 3.15 for the x direction is

$$\frac{\partial u'}{\partial t} = \frac{\eta}{\rho}\frac{\partial^2 u'}{\partial z^2}. \tag{3.16}$$

This is a diffusion equation, rather than a wave equation and hence no wave propagation is possible [33]. The solution for equation 3.15 that satisfies the boundary condition are that the complex secondary wave u' is [23]

$$u' = -u_x e^{-(1+i)z/\delta} \tag{3.17}$$

$$\delta = \sqrt{2\eta/\rho_1\omega} \tag{3.18}$$

The quantity δ is the viscous penetration depth or viscous skin depth. The final expression for the secondary wave if $u_x = U_o e^{i(\omega t - k_c x)}$ is

$$u = U_o e^{-z/\delta} e^{i(\omega t - k_c x - z/\delta)} \tag{3.19}$$

where k_c is the wave number of the primary wave in the fluid.

As can be clearly seen from this equation, this wave attenuates exponentially and its effect is confined to the distance given by the viscous skin. This description is for a moving fluid but it is also valid for a when the fluid is motionless and the solid surface is moving.

At a large distance from the scatterer this wave is not noticeable, but as with the thermoelastic wave, it does dissipate energy at the boundary. The above expression is valid if the wavelength is much greater than the skin depth, which for water is above the GHz region.

3.1.5 Summary

The attenuation of the sound or ultrasound wave reflects the nature of the medium the wave has passed through. Considering a sound wave travelling through a suspension of solid particles in a fluid, the attenuation of the sound wave will depend on the viscosity and the bulk viscosity of the fluid, the difference in the characteristic impedance between the fluid and the solid i.e. differences in density and wave velocity in these two media, and the attenuation in the solid itself. This illustrates the possibility of being able to estimate a number of fluid and solid properties by measuring the attenuation of sound in a suspension of solid particles in a fluid. The additional attenuation of thermoelastic scattering could potentially provide the thermal properties of the media. The viscous boundary effects reinforce the effects of the viscosity and hence could potentially lead to a means of establishing the viscosity of the fluid [34].

3.2 Attenuation Models of two phase suspensions

3.2.1 Historical background

The propagation of sound in suspensions has been discussed for over hundred years. Rayleigh [35] calculated the attenuation of sound due to small spherical obstacles in a non-viscous atmosphere, when considering the effect of fog on sound. He showed that the attenuation depends on the number of scattering particles and the ratio of their diameter to the wavelength of the sound. Knudsen [36] used expressions by Sewell [37] in the calculation of attenuation for spherical and cylindrical particles in a viscous fluid to model audible sound in fog and smoke. Incidentally, Sewell's work confirmed the futility of using suspended or stretched wires for absorbing sound in rooms. In 1953, Epstein and Carhart [38] developed a model for the attenuation of sound by spherical particles where energy loss is due to the thermal and viscous losses in the boundary layer as well as scattering from the particle itself.

This model was modified slightly by Allegra and Hawley [39] and the resulting Epstein-Carhart [38]/Allegra-Hawley [39] (ECAH) model has been the basis for investigations on attenuation and velocity measurements in emulsions [31]. A summary of different experiments on suspensions based on acoustic scattering theories is given in [40], though

which specific model has been used in each case is not mentioned. In 1982, Habeger [32] derived a version of the ECAH model for cylindrical scatterers and tested this with experiments on suspensions of viscoelastic polymer fibres in water. The fibre properties that were known or could be measured, using alternative methods, were used in the model with no adjustments. The values of the loss tangent and Poisson's ratio were set to fit the experimental data.

As the concentration of the scatterers increases, models based on a linear relationship between the attenuation of a single particle and the number particles start to become less appropriate [41]. Multiple scattering models [42] have been developed for spherical particles but these cannot be directly applied to other shapes.

Another type of model that has been applied to paper pulp is Biot's model by Adams [43]. The Biots model treats the suspension as a solid permeated by tubes through which the fluid phase passses. This type of model is suitable for high concentrations where the fibres can be allow to interact with each other to form a structure. The results showed some promising results but required four parameter to be estimated, two of which are the compression and the shear wave velocities of the fibre material and the other two are structural parameters of the suspension. Habeger [32] claims that more difficulties lie in trying to assess the structural and material properties required in this model than in establishing the material properties in a scattering model.

Habeger [32] used the results of work on synthetic fibres to explain qualitatively the effect of the refining process on paper pulp using the results of ultrasound attenuation measurement and suggested more work was warranted [44].

The three research questions in the introduction were:

1. Can the measurement of ultrasound be used to estimate the elastic properties from ultrasound attenuation?

2. Can the method be applied to wood fibres in pulp? and

3. Can the method be used online?

Basing the model of attenuation on Habeger's work provided a good basis for answering the first question because his work showed that the model captures the behaviour of fibres in suspension. In addition, his results showed that it was possible, to obtain estimates for one of the material properties when the others are defined [32]. However, his model is complex as it involves thermoelastic scattering, viscous boundary effect as well as the general wave propagation behaviour in the suspension. Hence to make the model more amenable to use in solving the inverse problem, where material properties are estimated from measurement of attenuation, an analytical solution for the attenuation was sought.

At first glance, it would seem that Habeger's work in part answers the second question in that he used the results of polymer fibres to interpret attenuation measurements of pulp [44]. However, the dependance of the attenuation on the geometric properties of the fibres, makes interpretation of these measurements without accurate size information, highly speculative. With the onset of optical measurements systems, accurate size information

on the wood fibres in pulp is available and hence basing a system on this model is more feasible.

One of the implications of the third question is that a simple model is sought. Although Habeger's model may be a good basis for the system, it is complex and hence simpler version of it that captures the necessary behaviour of the fibres was sought.

3.2.2 Assumptions and Modification of the attenuation model

A number of assumption are used in the attenuation models in work covered by this thesis (JED[1] models) and in the model derived by Habeger [32]. There is also a difference in the derivation between that of Habeger and that used in the JED models. In this section a summary of the different assumptions used in each model is presented. The difference in the derivations is also summarised. The summary includes reference to the appropriate equations in the full derivation of the JED model is given in the next section (section 3.2.3)

All the JED models assume:

- The scatterer is an infinitely long cylinder
- Thermal properties can be neglected.
- The suspension is dilute hence multiple scattering do not occur and there is interaction between fibres.
- The effect of viscosity on the stress at a large distance from the scatterer can be approximated by the addition of the attenuation of the fluid to the attenuation due to fibre interaction. This is shown in equations 3.41-3.45 and equations 3.52 and 3.53

In all the JED models there is a scaling factor that differs from that of Habeger's model but is similar to that used in the ECAH model. This is explained in more detail in and after equation 3.45.

JED v1

The initial version of the JED model is derived in detail in Paper A. The evanescent waves in the fluid are neglected (equation 3.27). This modifies the stress in the fluid (equation 3.28). The boundary conditions are modified.

JED non-viscous

This is derived in Paper E. Viscosity, η_1 is assumed to be negligible. Hence, as above the evanescent waves in the fluid are neglected (equation 3.27) and the stress in the fluid modified (equation 3.28) by setting $\eta_1 = 0$. The boundary conditions are modified.

[1] a Just Estimate of Damping

JED non-viscous distributed radii

As above but the attenuation allows for non-uniform radii.

JED viscous

This is also derived in Paper E. The evanescent waves in the fluid are included (equation 3.27) and all the terms in the stress (equation 3.28) are included. The boundary conditions are modified.

JED hollow distributed radii

This is derived in Paper F. The cylinder is hollow and the centre is assumed to be fluid filled. Viscosity, η_1 is assumed to be negligible. Hence, as above the evanescent waves in the fluid are neglected (equation 3.27) and the stress in the fluid modified (equation 3.28) by setting $\eta_1 = 0$. The boundary conditions are modified. The attenuation allows for non-uniform radii as in the JED non-viscous distributed radii.

3.2.3 General description of the JED model

A similar model is used in all the works covered by this thesis, hence a description is given here. It is presented in detail so as to allow the differences to be clearly seen between these JED models and the model developed by Habeger [32].

In the JED model, the energy loss of an ultrasound wave after it has interacted with an infinitely long, cylindrical scatterer is calculated. The basic geometry is show in Figure 3.3. The material of the scatterer is assumed to be viscoelastic and isotropic. For a solid, it can be seen from equation 3.9, that the displacement can be separated into a compressional part and a rotational part. These are expressed for the solid scatterer, where the time dependence is taken as $e^{-i\omega t}$, so that $\partial/\partial t$ is replaced with $-i\omega$, such that

$$\mathbf{V_2} = i\omega\boldsymbol{\zeta} = i\omega(\nabla\phi_2 + \nabla \times \mathbf{A_2}). \tag{3.20}$$

where ϕ_2 and A_2 are scalar and vector displacement potentials. In this, $\mathbf{A_2}$ is purely rotational can be expressed as

$$\nabla \cdot \mathbf{A_2} = 0. \tag{3.21}$$

The wave numbers are related to these scalar or wave displacement potentials through the wave equations such that

$$\nabla^2\phi_2 = -k_{2c}^2\phi_2 \tag{3.22}$$

$$\nabla \times \nabla \times \mathbf{A_2} = k_{2s}^2\mathbf{A_2}. \tag{3.23}$$

The subscript 2 is used to indicate the terms related to the solid. Terms relating to the fluid have the subscript 1.

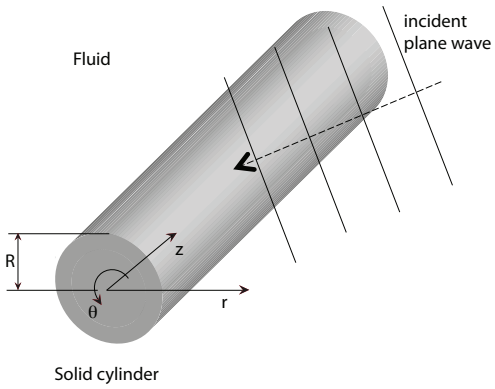

Figure 3.3: Diagram of an ultrasound plane wave being scattered off a cylindrical scatterer.

For the suspending fluid, similar expressions are used except the displacement potentials are replaced with velocity potentials. So,

$$\mathbf{V_1} = -\nabla\phi_1 - \nabla \times \mathbf{A_1}, \tag{3.24}$$

where

$$\nabla \cdot \mathbf{A_1} = 0. \tag{3.25}$$

The wave numbers are related to these scalar or vector velocity potentials through the wave equations such that

$$\nabla^2\phi_1 = -k_{1c}^2\phi_1 \tag{3.26}$$

$$\nabla \times \nabla \times \mathbf{A_1} = k_{1s}^2\mathbf{A_1}. \tag{3.27}$$

In the above equations $k_{2c} = \omega/(c_2(1 - i\tan\delta_2/2))$ and $k_{2s} = \sqrt{i\omega\rho_2/\mu_2}$.

The stress tensor can be expressed in terms of the wave potentials:

$$\tau_{1ij} = \eta_1\left[(k_{1s}^2 - 2k_{1c}^2)\phi_1\right]\delta_{ij} + 2\eta_1\dot{\epsilon}_{ij} \tag{3.28}$$

$$\tau_{2ij} = \left[(\omega^2\rho_2 - 2\mu_2 k_{2c}^2)\phi_2\right]\delta_{ij} + 2\mu_2\epsilon_{ij} \tag{3.29}$$

Where the strain is

$$\epsilon_{ij} = \frac{1}{2}(V_{i,j} + V_{j,i} - 2\Gamma_{ij}^l V_l) \tag{3.30}$$

The fluid wave potential is divided into an incident part and a reflected part, $\phi_1 = \phi_{1o} + \phi_{1r}$. The incident plane wave potential, ϕ_{1o}, is expressed in cylindrical coordinates and it behaves according to the wave equations and hence is set to equal $e^{i(k_{1cc}r + k_{1cs}z - \omega t)}$ [32]. Since the plane of the cylinder lies at an angle ψ to the incident wave, the wave numbers are expressed in terms of their components along the cylindrical coordinate axes.

$$k_{1cc} = k_{1c}\cos(\psi) \tag{3.31}$$

$$k_{1cs} = k_{1c}\sin(\psi). \tag{3.32}$$

ϕ_{1o} can then be expressed in terms of Bessels functions [45], such that

$$\phi_{1o} = \left(J_0(k_{1cc}r) + 2\sum_{n=1}^{\infty} i^n \cos(n\theta) J_n(k_{1cc}r) \right) e^{i(k_{1cs}z - \omega t)}. \tag{3.33}$$

where J_n is a Bessel function of the first kind of order n.

Since the reflected wave potentials in the fluid are not bounded at the origin in that they do not span $r = 0$, they are expanded in terms of Bessel functions of the third kind, subsequently referred to as Hankel functions, $H_n^{(1)}$, hence

$$\phi_{1r} = \left(B_{0_1} H_0^{(1)}(k_{1cc}r) + 2\sum_{n=1}^{\infty} i^n \cos(n\theta) B_{n_1} H_n^{(1)}(k_{1cc}r) \right) e^{i(k_{1cs}z - \omega t)}. \tag{3.34}$$

where B_{n_1} are the coefficients of expansion of the reflected wave potential, ϕ_{1r}. Note that any expansion coefficients which involves a wave number that is dependent ψ, will also be dependent ψ. Hence in the case B_{n_1} is dependent on ψ.

The combination of equations 3.33 and 3.34 gives an expression for ϕ_{1o} expanded in terms of Bessel and Hankel functions. To meet the boundary conditions for all values of z and t, the time and z dependence of the potentials must be the same as ϕ_{1o}. The equivalent expression for the compressional wave potential in the solid is then

$$\phi_2 = \left(B_{0_2} J_0(k_{2cc}r) + 2\sum_{n=1}^{\infty} i^n \cos(n\theta) B_{n_2} J_n(k_{2cc}r) \right) e^{i(k_{1cs}z - \omega t)} \tag{3.35}$$

where, $k_{2cc} = \sqrt{k_{2c}^2 - k_{1cs}^2}$ and B_{n_2} are the coefficients of expansion of ϕ_2. Note that all waves along the boundary surface in the z direction are equal (see Chapter 5). Hence, $k_{2c}\sin\psi = k_{1cs}$

To meet the boundary conditions in cylindrical coordinates, the transverse potential can be expanded in terms of two independent scalar potentials [46] such that, $\mathbf{M} = \nabla \times \chi\hat{\mathbf{k}}$, $\mathbf{N} = \nabla \times \nabla \times \xi\hat{\mathbf{k}}$ and $\mathbf{A} = \mathbf{M} + \mathbf{N}$. Where χ and ξ are solutions to the scalar Helmholtz equation so, $\nabla^2\chi = -k_{2s}^2\chi$ and $\nabla^2\xi = -k_{2s}^2\xi$ [32].

This means that the transverse waves in solid can be expanded in terms of Bessel

functions such that

$$k_{2s}^2\xi_2 = \left(D_{0_2}J_0(k_{2sc}r) + 2\sum_{n=1}^{\infty} i^n \frac{\partial \cos(n\theta)}{\partial\theta} D_{n_2} J_n(k_{2sc}r)\right) e^{i(k_{1cs}z-\omega t)} \quad (3.36)$$

$$ik_{1cs}\chi_2 = \left(E_{0_2}J_0(k_{2sc}r) + 2\sum_{n=1}^{\infty} i^n \cos(n\theta) E_{n_2} J_n(k_{2sc}r)\right) e^{i(k_{1cs}z-\omega t)} \quad (3.37)$$

where, $k_{2sc} = \sqrt{k_{2s}^2 - k_{1cs}^2}$ and D_{n_2} and E_{n_2} are the coefficients of expansion, ξ_2 and χ_2.

For a viscous fluid, evanescent waves in the boundary layer exists and these are expanded in terms of Hankel functions,

$$k_{1s}^2\xi_1 = \left(D_{0_1}H_0^{(1)}(k_{1sc}r) + 2\sum_{n=1}^{\infty} i^n \frac{\partial \cos(n\theta)}{\partial\theta} D_{n_1} H_n^{(1)}(k_{1sc}r)\right) e^{i(k_{1cs}z-\omega t)} \quad (3.38)$$

and

$$ik_{1cs}\chi_1 = \left(E_{0_1}H_0^{(1)}(k_{1sc}r) + 2\sum_{n=1}^{\infty} i^n \cos(n\theta) E_{n_1} H_n^{(1)}(k_{1sc}r)\right) e^{i(k_{1cs}z-\omega t)}. \quad (3.39)$$

where $k_{1sc} = k_{1s}cos(\psi)$ and D_{n_1} and En_1 are the coefficients of expansion of the evanescent wave potentials ξ_{n_1} and χ_{n_1}, repectively. Again, all waves on the surface in the z direction are equal hence $k_{2s}\sin\psi = k_{1cs}$.

The boundary conditions are that the velocities and the stresses in all directions are continuous at the solid-fluid interface. So at $r = R$, where R is the radius of the cylinder, $V_{1r} = V_{2r}$, $V_{1\theta} = V_{2\theta}$, $V_{1z} = V_{2z}$, $\tau_{1rr} = \tau_{1rr}$, $\tau_{1r\theta} = \tau_{2r\theta}$ and $\tau_{1rz} = \tau_{2rz}$.

The angular dependencies of the functions are orthogonal so the coefficients can be determined by applying the boundary condition to each order of expansion separately. The stresses and velocities (equation 3.28 and 3.29) are then expressed for a single n$^{\text{th}}$ order of the series and the appropriate boundary condition used. This results is a series of equations that can be solved for the unknown expansion coefficients. Since only B_{1n} is necessary for the calculation of the attenuation, the system of equations can be expressed as a matrix and Cramer's rule [47] used to solve for B_{1n}. This was done in Papers E and F.

The second part relates the coefficients of expansion to the energy loss of the incident wave as it interacts with a number of cylindrical scatterers. The average loss per unit time due to the viscous and thermal processes can be approximated by the product of the velocity and the stress integrated over the surface, S with its centre at the centre of the scatterer such that

$$U = \frac{1}{2}\Re\left(\int_S V_j^* \tau_{ij} dS_i\right), \quad (3.40)$$

where U is the energy loss per unit time, V_j^* is the conjugate of the velocity in the j axis, τ_{ij} is the stress tensor and $\Re$ indicates that only the real part is taken [38].

At a large distance from a cylindrical scatterer, the energy loss per unit time per unit length, L, can be expressed as

$$\lim_{r\to\infty} L = \frac{r}{2}\Re\bigg(\int V_r^*\tau_{rr}d\theta\bigg), \tag{3.41}$$

since the evanescent waves do not contribute. This can be simplified further by assuming that the effects of viscosity of the water on the compression wave are negligible and hence

$$\lim_{r\to\infty} \tau_{rr} = (i\omega\rho_1 - 2\eta k_{1c}^2)(\phi_{1o} + \phi_{1r}) - 2\eta(\phi_{1o,rr} + \phi_{1r,rr}) \tag{3.42}$$

becomes

$$\lim_{r\to\infty} \tau_{rr} \approx i\omega\rho_1(\phi_{1o} + \phi_{1r}), \tag{3.43}$$

where τ_{rr} is the stress in the radial direction is calculated using equation 3.42. Similarly

$$V_r \approx= -\phi_{1o,r} - \phi_{1r,r}. \tag{3.44}$$

Using 3.43 and 3.44 in 3.41 and using the expanded series for the potentials gives

$$L = -\omega\rho_1 \sum_{n=0}^{\infty} \epsilon_n \Re\left([J_n(k_{cc}r) + B_{1n}H_n^1(k_{cc}r)] \times [J_n'(k_{cc}r)^* + B_{1n}^* H_n^{1\prime}(k_{cc}r)^*]\right), \tag{3.45}$$

where $\epsilon_n = 1$ for $n = 0$, $\epsilon_n = 2$ for $n > 0$. In the above equation ϵ_n is not squared, which is similar to the approach used in Epstein and Carhart in their appendix [38]. This differs from Habeger's equation 37 where ϵ is squared. The reason for not squaring this term is unclear in Epstein and Carhart derivation. However, using ϵ^2 results in a poor match to experimental results. Note that in Paper A this difference was mistakingly attributed to a factor of two missing when asymptotic values are inserted in the Bessel functions.

Continuing with the derivation from equation 3.45, asymptotic values are inserted in the Bessel functions giving

$$L = -\omega\rho_1 \sum_{n=0}^{\infty} \epsilon_n \Re\left(B_{1n} + B_{1n}B_{1n}^*\right), \tag{3.46}$$

This shows that the losses are simply a function of the amplitude of the reflected wave. To equation 3.46 the losses due to the scattering, L_s are added. L_s at a large distance from the scatterer is such that

$$L_s = \omega\rho_1 \sum_{n=0}^{\infty} \Re\left(\epsilon_n B_{1n}B_{1n}^*\right). \tag{3.47}$$

The total energy loss L_t is therefore

$$L_t = -\omega\rho_1 \sum_{n=0}^{\infty} \Re\left(\epsilon_n B_{1n}\right). \tag{3.48}$$

The average energy carried per unit time across a normal unit area by the compression wave is

$$E = \frac{1}{2} k_{1c} \omega \rho_1, \tag{3.49}$$

where k_{1c} is the wave number of the compression wave in the fluid [38]. Remembering that B_n is dependent on ψ, the attenuation due to a single scatterer for an angle ψ is

$$\alpha_\psi = \frac{L_t}{E} = \frac{-2}{k_{1c}} \sum_{n=0}^{\infty} \Re \left(B_{1n} \epsilon_n \right). \tag{3.50}$$

This is multiplied by the number of particles per unit length, N where

$$N = \frac{f_r}{\pi R^2} \tag{3.51}$$

and where f_r is the volume fraction. The cylindrical scatterers lie at different orientations to the oncoming wave, hence the average cosine of attenuation over the range of angles from $\psi = 0$ to $\psi = \frac{\pi}{2}$ is

$$\alpha = \frac{-2 f_r}{\pi R^2 k_{1c}} \Re \left(\int_0^{\frac{\pi}{2}} \epsilon_n B_{1n} \cos(\psi) d\psi \right). \tag{3.52}$$

To compensate, in some degree, for the assumption that viscosity effects are neglected (equation 3.46) the attenuation of the fluid is added in the calculated in equation (3.52). The expression for α is therefore,

$$\alpha = \frac{-2 f_r}{\pi R^2 k_{1c}} \Re \left(\int_0^{\frac{\pi}{2}} \epsilon_n B_{1n} \cos(\psi) d\psi \right) + \alpha_f, \tag{3.53}$$

where α_f is the attenuation due to the fluid.

A similar approach is taken by Hipp et al. [41] for low attenuating systems. In their approach they include a background attenuation term which is defined as

$$\alpha_{bg} = f_r \alpha' + (1 - f_r) \alpha'' \tag{3.54}$$

where α' intrinsic attenuation of the dispersed phase or scatterers and α'' is the intrinsic attenuation of the dispersant, or surrounding fluid. In their derivation, this term is added to the attenuation due to the interaction with the particles. For very dilute suspensions, $f_r \ll 1$ hence $\alpha_{bg} \approx \alpha''$ and hence adding this background term become the equivalent to equation 3.53.

In addition to being able to calculate the attenuation, the coefficients of expansions can also be used to calculated for the wave potentials in the area surrounding a single fibre. Figure 3.4 shows the effect of the fibre on the reflected wave potential field where the angle of incidence is 45°.

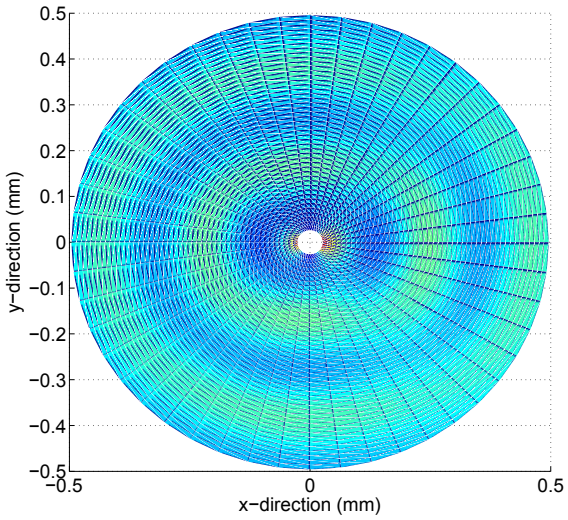

Figure 3.4: Amplitude of the reflected wave potential surrounding a fibre scattering a plane, ultrasonic wave of 10 MHz where $\psi = 45°$*. The fibre was nylon with* $c_2 = 2530\, ms^{-1}$*,* $\nu = 0.431$*, tan* δ*=0.2 and* $R = 26\,\mu m$

Chapter 4

Comparison to Spherical Scatters

The JED models are the cylindrical equivalence of the model of attenuation for spherical particles derived by Epstein and Carhart/ Allegra Hawley [38, 39]. It is therefore of interest to compare these models to show the similarities and the points at which they deviate. This is of particular interest when considering the possible applications of this model to modelling attenuation in pulp since pulp is made up of both fibres and fines. It is therefore possible that the fine proportion of the suspension could be modelled using the ECAH model if necessary.

The derivations of both models are very similar with the exception that, in the spherical case, the boundary conditions are expressed in terms of spherical coordinates and hence the wave potentials are expanded in terms of modified Bessel functions. In addition, in spherical coordinates, there is only one transverse wave as opposed to two for the cylindrical case [32, 46].

The derivation for the spherical model, as described by Epstein and Carhart [38], is taken up from the expression for the energy loss per unit time due to a single particle, W, where

$$W = -\frac{2\pi\omega\rho N}{k_c}\sum_{n=0}^{\infty}(2n-1)\Re(A_n + |A_n|^2) \tag{4.1}$$

and N is the number of particles, k_c is the wave number of the compression wave in the fluid, A_n are the coefficients associated with the reflected wave potential and n is an integer. ω is the angular frequency and ρ is the density of the fluid.

The energy of the incident wave carried per unit time across a normal unit area is defined as, [38],

$$E = \frac{1}{2}k_c\omega\rho \tag{4.2}$$

Hence

$$\alpha_s = -\frac{4\pi N}{k_c^2}\sum_{n=0}^{\infty}(2n+1)\Re(A_n + |A_n|^2) \tag{4.3}$$

For a unit volume, the number of spheres, N, is

$$N = f_r \frac{3}{4\pi R^3}, \tag{4.4}$$

where f_r is the volume fraction. Hence

$$\alpha_s = -f_r \frac{3}{R^3 k_c^2} \sum_{n=0}^{\infty} (2n+1) \Re(A_n + |A_n|^2). \tag{4.5}$$

Epstein and Carhart only considered the first two terms and neglected the $|A_n|^2$ term since it was the square of a small number. Hence their final expression was

$$\alpha_s = -f_r \frac{3}{R^3 k_c^2} \Re(A_0 + 3A_1). \tag{4.6}$$

In Allegra Hawley [39] the attenuation is given as:

$$\alpha_s = -f_r \frac{3}{2R^3 k_c^2} \sum_{n=0}^{\infty} (2n+1) \Re(A_n). \tag{4.7}$$

In their equation there is an additional factor of two in the denominator when compared to that of Epstein and Carhart (equation 4.5). The reason for this is not clear from the Allegra Hawley's article.

In a review of ultrasound techniques for characterizing colloidal dispersions [48], an expression for the complex wave number, β, in a scattering medium is given for dilute suspensions. This is based on the far field scattered or reflected wave potential, $\phi_1(\theta, r)$ for a single particle,

$$\phi(\theta, r) = \phi_o f(\theta) \frac{e^{ik_{1c}r}}{r}, \tag{4.8}$$

where ϕ_o is the incident wave potential and k_{1c} is the wave number of the fluid. $f(\theta)$ gives the scattering amplitude as a function of the angle with respect to the propagation axis [1]. $f(\theta)$ is defined as

$$f(\theta) = \frac{1}{ik_c} \sum_{n=0}^{\infty} (2n+1) A_n P_n \cos\theta. \tag{4.9}$$

The complex wave number can then be expressed as

$$\left(\frac{\beta}{k_c}\right)^2 = 1 + 4\pi N f(0). \tag{4.10}$$

[1] Note that for a spherical scatterer the incidence angle ψ, used for cylindrical particles, would have no relevance

where $f(0)$ is the forward scattering scattering amplitude. This is from a derivation for spherical particles by Foldy [49]. At low concentration, the assumption $\frac{\beta}{k_c} \approx 1$ can be made. Thus,

$$\beta = k_c + \frac{4\pi N}{2k_c^2}\sum_{n=0}^{\infty}(2n+1)\Im(A_n) - i\frac{4\pi N}{2k_c^2}\sum_{n=0}^{\infty}(2n+1)\Re(A_n). \tag{4.11}$$

The attenuation of the medium is the imaginary part of the above equation. Hence

$$\alpha_s = -\frac{4\pi N}{2k_c^2}\sum_{n=0}^{\infty}(2n+1)\Re(A_n). \tag{4.12}$$

Substituting for N,

$$\alpha_s = -\frac{3f_r}{2R^3k_c^2}\sum_{n=0}^{\infty}(2n+1)\Re(A_n), \tag{4.13}$$

which is the same expression as equation 4.7 derived by Allegra and Hawley [39] and supports the addition of the factor of two.

The JED model gives expression for the attenuation of cylindrical particles in suspension such that,

$$\alpha_c = \frac{-2f_r}{\pi R^2 k_{1c}}\Re\left(\int_0^{\frac{\pi}{2}}\epsilon_n B_{1n}\cos(\psi)d\psi\right). \tag{4.14}$$

where the expansion of coefficient of the reflected wave potential is B_{1n}.

As can be seen by comparing the spherical and cylindrical attenuations, the expressions are similar. However, without considering the differences in the expansion coefficients one sees that α_s is inversely proportional to R^3 and k_c^2 compared to α_c which is inversely proportional to R^2 and k_c. The R terms are simply a result of the volume concentration calculation and the effect of the assumption of infinitely long particles. It means that for a given f_r and R, there will be fewer spherical particles than cylindrical particles attenuating the ultrasound signal. The k_c terms show that as the frequency increases ($k_c = 2\pi f/c_{1c}$), this term will tend to lower α_s more than α_c.

Another difference is the influence of higher terms of the series expansion on the attenuation. In the spherical attenuation calculation, the terms in the series are multiplied by $(2n+1)$, hence greater weight is given to higher terms in the series that to the lower terms in the series. In the cylindrical case the only difference is between the first term in the series and the other terms of the series is a factor of two. However, in both the cylindrical and the spherical attenuation these higher terms quickly become small. Hence this should not make a significant impact on the attenuation.

A comparison of the model attenuation from a suspension of nylon particles in water, normalised with respect to concentration, between sphercial and cylindrical particles is shown in the figure 4.1. In this case, the cylindrical particles have been aligned so that

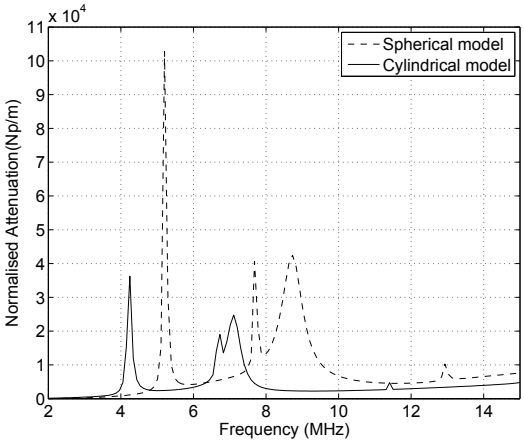

Figure 4.1: Plot of the modelled attenuation of spherical and cylindrical nylon particles in water. The angle of incidence and the loss tangent were set to zero. Neither the viscous properties of the water nor the thermal properties of either the particle material or the water are considered. The parameter values were $R = 22\,\mu m$, $c_2 = 1340 ms^{-1}$, $\rho_2 = 1131\,kgm^{-3}$, $tan\ \delta = 0$, $\nu = 0.3$, $c_1 = 1490 ms^{-1}$ *and* $\rho_1 = 996\,kgm^{-3}$.

the angle of incidence is zero. To allow a clearer comparison of the resonances between the two types of particles, the intrinsic loss in the particle material in both cases was removed.

The figure shows that there exists a similar resonance pattern between the cylindrical and spherical attenuation resonance maxima though they are not exactly aligned exists. The difference is thought to be due to solution to Bessel functions and to those of the modified Bessel functions. Physically, it relates to the differences in the geometry. These results, together with the results from Chapter 5 which show that the mode in a nylon cylinder at these frequencies can be approximated to modes excited when the angle of incidence is zero, suggests that the resonances are from the same cause in both the cylindrical case and the spherical case. A review article [50] discusses the different types of waves in spherical and cylindrical particles in general and describes the different waves that exist, for example quasi-Rayleigh waves (or rather leaky waves in this case since the scatterer is immersed in water), Franz waves for when the scatterer acts as an impenetrable object and Stonely waves, for when it behaves as an elastic object as well as whispering gallery waves. However, the latter were shown to exist where the wavelength is much smaller than the radius [51], which is not the case here. It should be possible using the descriptions of these waves to show that the resonance features shown in this example are from the same type of wave. However, this is not studied further in this thesis.

The addition of intrinsic loss in the particle material by increasing tan δ, has a damping effect on the resonance in both cases, as is shown in figure 4.2.

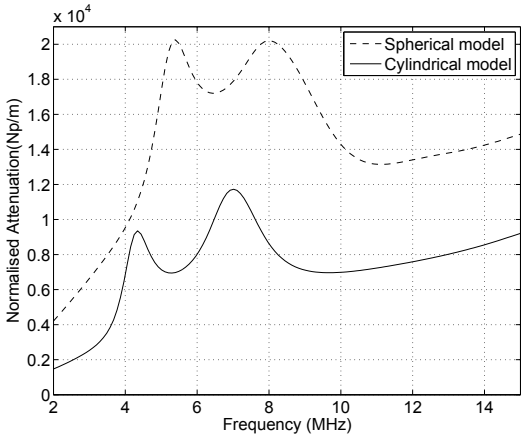

Figure 4.2: Plot of the modelled attenuation of spherical and cylindrical nylon particles in water. Here the intrinsic loss of the particle material has been included. The only parameter that differs from Fig. 4.1 is tan $\delta = 0.2$.

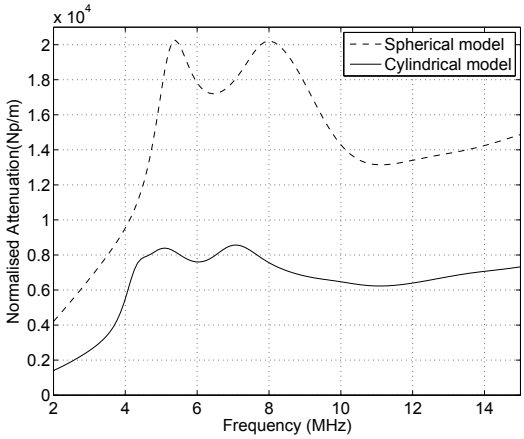

Figure 4.3: Plot of the modelled attenuation of spherical and cylindrical nylon particles in water. The attenuation is the average of the attenuation with incident angles ranging from 0 to $\frac{\pi}{2}$. The parameter values are the same as those in Fig. 4.2.

The orientation of the cylindrical particle affects the attenuation hence a comparison between randomly orientated particles and the spherical model is done and shown in figure 4.3. The effect of this is further damping of the resonances maxima of the cylindrical particles and a shift in frequencies. The reason for the damping and the shift in frequencies is described in more detail in chapter 5.

In conclusion, the comparison between the spherical and the cylindrical models shows

that the relationship to the frequency differs as well as the relationship to the volume concentration. The resonance frequencies between a cylindrical scatterer and a spherical scatterer have a similar shape, though to a lesser extent when the incident angle is varied. This suggests that the dominant resonance modes are the same type in both cases, for this material in this frequency-radius region. Finally, the comparison also shows that an increase in the intrinsic loss of the material has a damping effect on these resonances in both cases.

Chapter 5

Modes of Vibration

When an object is struck, it will vibrate. These vibrations are a superposition of numerous waves of certain velocities and frequencies propagating in specific directions. The modes of these vibrations are generally a function of the material properties and the geometry of the object. If the object is surrounded by another medium, e.g. the object is immersed in water, the frequencies and wave velocities of these modes are altered. The energy of the vibrations will be attenuated due to a number of processes e.g. internal friction in the solid which is quantified by the loss tangent (Chapter 3).

When an object is forced to vibrate at a certain frequency, the energy absorbed by the object depends on the frequencies of these modes of vibration. This is why the modes of vibration of particles in a suspension are important when studying the attenuation of ultrasound waves in suspensions of such particles.

Figure 5.1 is the attenuation calculated over a range of frequencies by the JED non-viscous model (Chapter 3) and shows a feature appearing to be resonance maximum. The assumption is that particular frequencies of the incident wave will match the frequencies of certain modes of vibration and this will affect the energy absorbed by the cylinder and hence the attenuation. By studying the modes of vibration of infinitely long cylinders surrounded by a fluid, the reason for the extrema in the attenuation spectra (hereto referred as attenuation) can be investigated. A greater understanding of these extrema could lead to a better understanding of the relationship between them and the material properties of the cylinders.

Modes of vibration even in simple geometries quickly become quite complex. An example of the simplest modes of vibration mentioned earlier in chapter 3, was the longitudinal wave propagating along the z axis of a narrow, unconstrained rod. An diagram of the geometry is given is Figure 5.2. This is the first mode of vibration of a longitudinal wave, L[0,1] (labelled 1 in figure 5.3). At low frequencies (shown in figure 5.3 as low values of a/Λ) this wave has a velocity, c_o, which equals $\sqrt{E/\rho_2}$, where E is the Young's modulus and ρ_2 is the density. As the frequency increases, the longitudinal wave starts to exhibit the behaviour of a surface wave and the wave velocity will asymptotically approach the velocity of a surface wave ($c_{\mathscr{S}}$ in figure 5.3). As discussed by Kolsky [28],

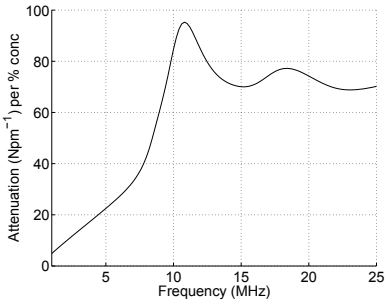

Figure 5.1: Attenuation calculated from the JED non-viscous model for a suspension of nylon fibres in water. The cylinder radius was 26 μm and the material properties used are given in Table 5.1.

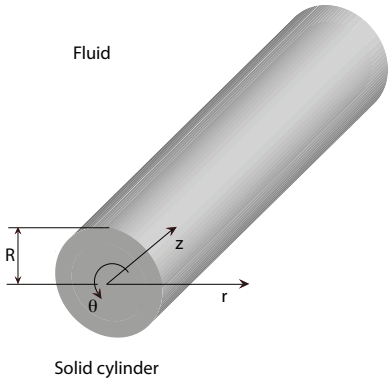

Figure 5.2: Diagram of the geometry of a rod.

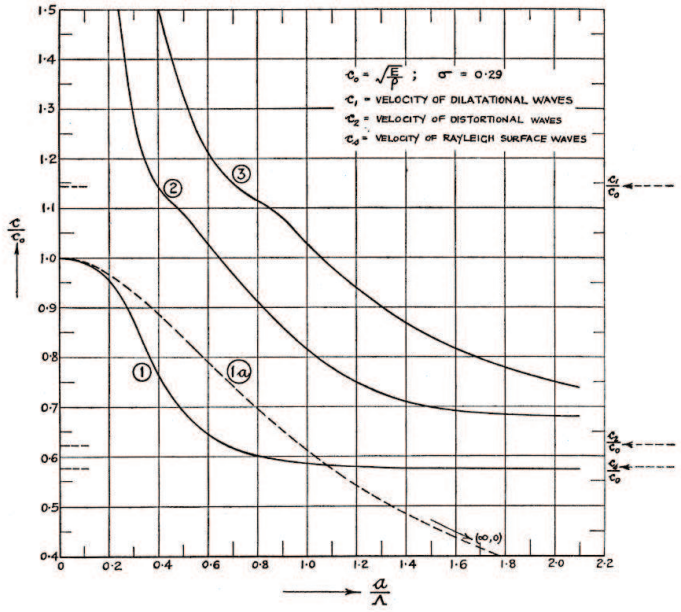

Figure 5.3: The normalised phase velocity c/c_o of longitudinal waves as a function of normalised frequency, a/Λ, in cylindrical steel bars of radius a and Poisson ratio, in the diagram given the term σ, where $\sigma = 0.20$. $c_0 = \sqrt{E/\rho}$ as explained in the text, c_1 and c_2 in the diagram refer to the compressional and the shear wave velocity in steel, repectively. $c_{\mathscr{S}}$ is the wave velocity of the surface or Rayleigh waves [52].

Pochhammer derived the frequency equation for infinitely long cylinders where the wave propagation is along the axis of the cylinder, z. These can be used to give expressions for longitudinal or extensional waves, torsional waves and flexural waves [28]. These waves have different modes of vibration, one of them being the L[0,1] discussed above. The velocities of the other modes of vibration of the longitudinal wave are shown in Figure 5.3 labelled 2 and 3.

$c_{\mathscr{S}}$, discussed above, is the velocity of a surface wave or Rayleigh wave and is a wave which travels along the free surface of a half space. The particle motion is in the plane of the surface and from being large at the surface, falls off rapidly as the depth into the medium increases. Their use in the determination of elastic properties in the thin surface layer of different materials discussed by Every [53].

The figure shows that above the normalised frequency of 0.2, according to Kolsky a second cylindrical mode appears on at the surface, L[0,2] labelled 2 in figure 5.3. Longitudinal waves are symmetrical in θ and hence are of the zeroth circumferential mode. Other waves such as flexural waves, have higher orders. These higher order circumferential modes give rise to dipolar $n = 1$ and quadrupole $n = 2$ radiation patterns

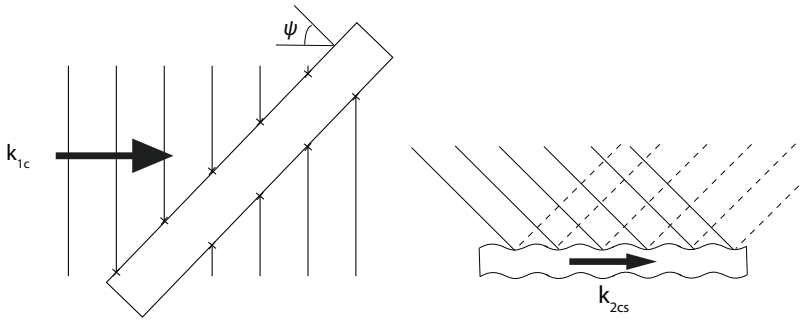

Figure 5.4: Diagram of the wave caused by an oblique angle between the incident plane wave and the z-axis of the cylinder.

in the medium surrounding the cylinders.

The aim in examining modes of vibration is to identify which mode of vibrations can be identified from the attenuation and with that information go on to relate the modes to the elastic constants involved. The solutions for the natural frequencies are complicated when shear waves are considered. This is the case when the incident wave propagates in the z-direction and when modes greater than $n > 0$ are considered. The complexity is increased when the cylinder is surrounded by a fluid as the effect of the fluid on the cylinder surface alters the oundary conditions. These effects are inertial and, if the fluid is viscous, the viscous boundary effects discussed in Chapter 3 also have to be considered. This means that the system is complex and analytical expressions for the modes of vibration are difficult to establish. A modern approach to calculating mode of vibrations of fluid load cylinders is through finding numerical solutions of the equations that govern the motion and satisfy the boundary conditions [54].

5.1 Effect of oblique incidence

Before studying the modes further it is of interest to investigate the effects of an oblique angle of incidence between the wave initiating the vibrations in the cylinder and the z-axis of the cylinder. A diagram of a cylinder surrounded by a fluid with an incident wave approaching the cylinder at an oblique angle, ψ, is shown in figure 5.4(a). This causes compression at points along the cylinder surface with the distance between the points equalling the projected incident wavelength, $\lambda_{1c} \sin \psi$, where λ_{1c} is the wavelength of the compression wave in the fluid. In effect, there now exists a wave in the solid propagating in z with a wave number, k_{2cs} (figure 5.4(b)), such that $k_{2cs} = k_{1c} \sin \psi$, where k_{1c} is the wave number of the compression wave in the fluid.

Table 5.1: Material Properties

Material Property	Value
Nylon: density, ρ_2 (kgm^{-3})	1140
Nylon: Compression velocity,c_2 (ms^{-1})	2531
Nylon: Poisson's ratio,ν,	0.433
Water: density ρ_1 (kgm^{-3})	1000
Water: Compression velocity,c_1 (ms^{-1})	1500

5.2 Comparison between Attenuation and Modes of Vibration

The modes of vibration of an immersed cylinder can be obtained using commercially available software based on the numerical solutions mentioned earlier. In this section a comparison between these modes and a JED model of attenuation is presented. The comparison is done for the specific case of the nylon fibres in suspension using the material properties given in table 5.1 and a fibre radius of 26 μm (as used in Paper D). The frequency range examined was 1-25 MHz. Since the JED non-viscous model has shown to adequately model nylon fibres in suspension (Paper D), this model is used in the comparison. In the calculation of the modes, the surrounding fluid is assumed to be non-viscous and the fibre material is assumed to be isotropic. The parameters used in the mode calculation were as for the JED non-viscous model.

The modes are calculated using the software, Disperse, developed by Lowe and Pavlakovic at the Imperial College London, UK. The software is designed for analysing of the modes in wave guides and is based on their work in this area [54]. The model used by Disperse for calculating the mode of cylindrical wave guides is based on the general solution for the propagation of waves in hollow cylinders [55, 56]. The modes are found by obtaining a global matrix (GM) made up of the partial waves in a similar way to the matrix of the system of equations used in the JED models for calculating the reflection coefficients, B_n. However, the objective when establishing wave guides modes, is to find the modal response of the GM and subsequently to find the guided waves that propagates along the axis of the cylinder. This is done by iteratively varying three parameters: frequency, wave number and attenuation until valid combinations of these three form guided waves [26]. The valid solutions are when the determinant of the GM is zero.

The exact details of the differences between the system of equations used in the JED models and the GM have not been examined. However, the assumption used by Palvakovic and Lowe is that the wave propagates in z direction [26], which is not necessarily the case in the JED model when the angle of incidence can be set to zero. For example, in Paper D normal incidence is used in the comparison between the JEDv1 model and the model used by Flax and Neubauer [57].

The partial waves in the global matrix used by Palvakovic and Lowe each have two directions, whereas in the JED models, only one direction of the partial waves is consid-

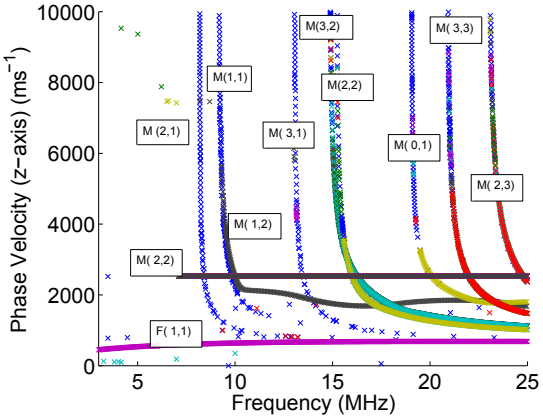

Figure 5.5: The GM solutions calculated for a nylon cylinder immersed in water with a radius of 26 μm with the material properties given in Table 5.1. The modes have been labelled with the first number indicating the circumferential mode. The second number is arbitrary. The wave with the prefix F, can be identified as a flexural wave. Note that the software was unable to link the modes in the above cases and hence each point is a modal solution to the GM. Difficulties in locating the modes of vibration meant that a search for minimum values was used as a starting point for the search the modes of vibration. These minimum values appear as extraneous points in the figure

.

ered. This suggests that one would find the system of equations used for calculating the attenuation to be a subset of the GM.

Figure 5.5 show the phase velocity, plotted again frequency, of the modes propagating in the z direction and calculated from the GM. The angle of incidence required to excite a mode, when the incident wave is propagated in water, can be calculated from phase velocity of the mode and the velocity of the wave in water.

The attenuation from the JED model is averaged over all angles of incidence. It is also the sum of n terms associated with θ (circumferential terms). To compare the features in the attenuation with the modes of vibration, the attenuation is calculated for one angle of incidence and for one of the series of the circumferential term. This is done since otherwise attenuation from each of the different n terms and each angle are superimposed on one another and the individual features of the attenuation due to each term and angle are lost.

Figures 5.6 are plots of the zeroth circumferential modes and the attenuation for the $n = 0$ circumferential terms for two different angles. The frequency at which a mode is excited in shown in figure 5.6(a) as the frequency at which the mode line intersects the 30° line. The corresponding attenuation ($\psi = 30°$, $n = 0$) is plotted in figure 5.6(c). At the frequency of mode excitation, it can be seen that the attenuation drops and immediately increases just after this point. Similar plots of the mode line and attenuation but with

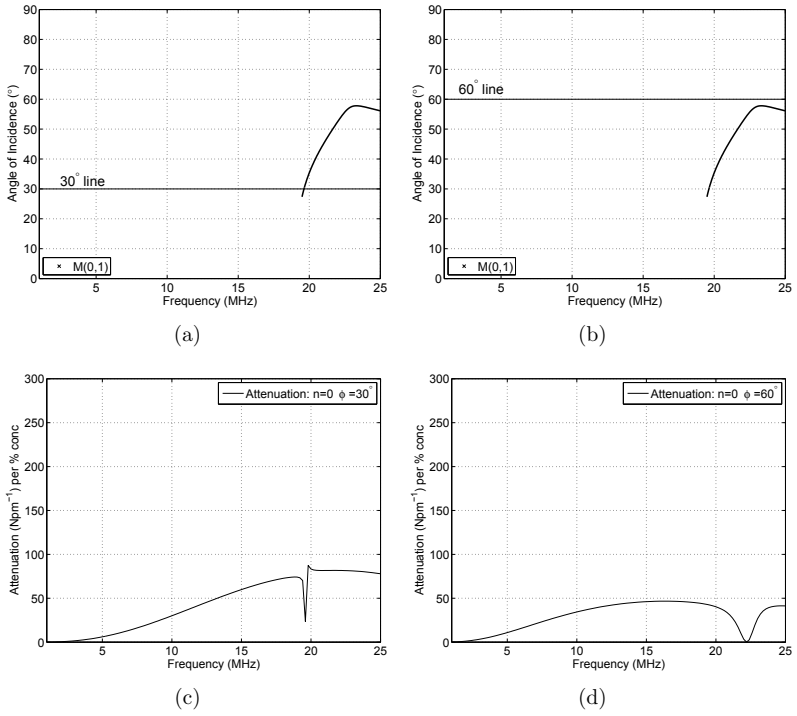

Figure 5.6: Comparison of modes of vibration (zeroth circumferential mode) and modelled attenuation, for the n=0 circumferential terms, for two different angles of incidence.

$\psi = 60°$, are plotted in figure 5.6(b) and 5.6(d). Figure 5.6(d) also shows that the attenuation drops despite the fact that the 60° line does not intersect with the mode line. The fact that the lines do not intersect implies that this wave mode could not be excited when $\psi = 60°$. It is uncertain if there are numerical differences that cause this mismatch of the results or if the effect of this mode coming close to being in existence at this point is sufficient to cause a minimum in the attenuation. Note that in the case for $\psi = 30°$, this minimum occurs just under 20 MHz and when $\psi = 60°$ the minimum is around 22 MHz.

The other maxima that can be seen in the attenuation in figure 5.6 are at 16 MHz where the angle of incidence is 30° and at 22 MHz where the angle of incidence is 60°. No mode excitation is found to correspond to this these maxima. However, it is possible that this is due to a failure of the iterative process used to find the mode. The modes are found using a search routine for finding the values of frequency, wave number (of the axially propagating mode of vibration) and attenuation that solve the GM. The first part of this is a coarse sweep of two of the parameters with the third held constant to find minima in the determinant. After this, a fine search is used to find the solution. It is

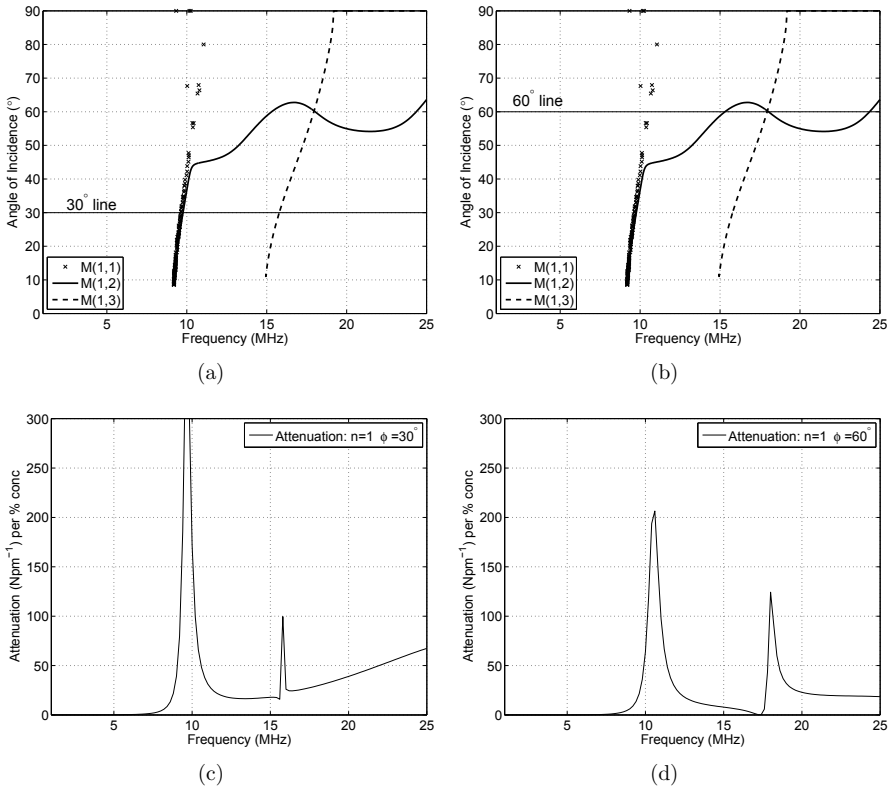

Figure 5.7: Comparison of modes of vibration (first circumferential mode) and modelled attenuation for the n=1 circumferential terms for two different angles of incidence.

possible that a coarse sweep was not done in the correct region to be able to locate this root. An alternative reason is that the software specifies that only modes propagation in the z are located [26]. It may, therefore, be possible that this maxima is caused by a purely circumferential mode and hence would not be detected by the software.

Similar plots are shown in figures 5.7 - 5.9 for $n = 1$ to $n = 3$. In all the figures where $n > 0$, the attenuation has a maximum at the frequency where the mode is excited. These maxima for $n > 0$ are caused by an increase in the radial displacement at the frequency at which a mode or modes are excited. This increase is radial displacement, suggested by Pavlakovic and Lowe [26], absorbs energy and hence the attenuation increases.

However at $n = 0$, there is a minimum in the attenuation. This is attributed to there being little radial displacement in this mode and hence little energy is leaked into the water [26].

Figure 5.7 shows the comparison of the first circumferential modes and the attenuation for the $n = 1$ circumferential terms. Figure 5.7(c) is a plot attenuation at $\psi = 30°$

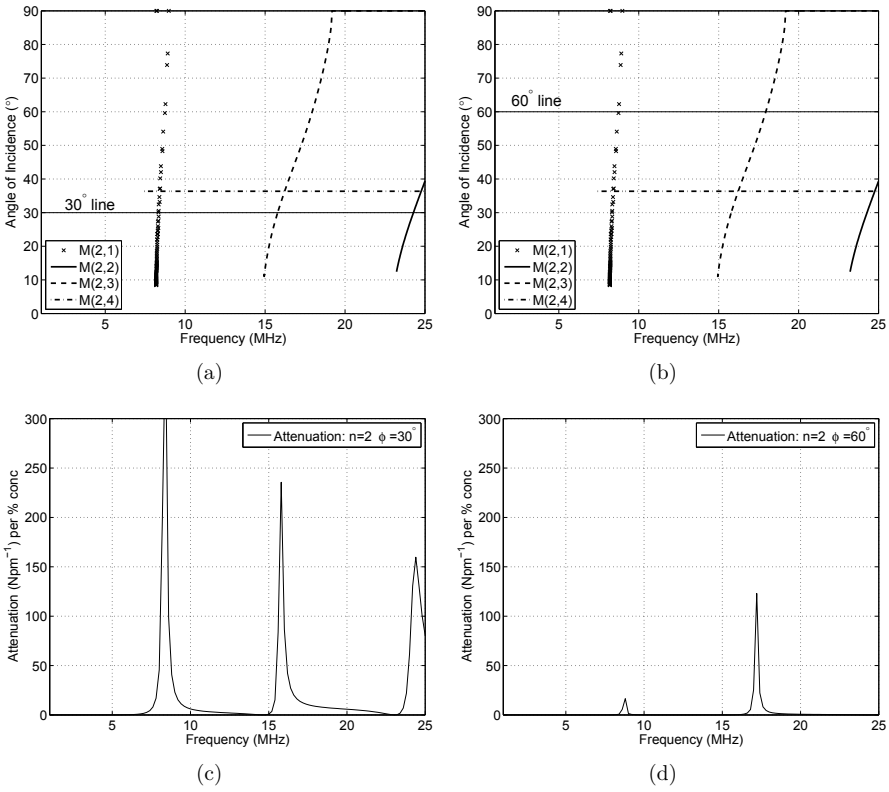

Figure 5.8: Comparison of modes of vibration (second circumferential mode) and modelled attenuation for the n=2 circumferential terms for two different angles.

(n=1). In figure 5.7(a) the intersect of the 30° line and the mode lines M[1,1] and M[1,3], are at the frequencies at which these modes are excited when $\psi = 30°$. These mode excitation correspond to obvious maxima occurring in the attenuation plotted in figure 5.7(c). However the impact of the excitation of M[1,2] on the attenuation is difficult to assess when $\psi = 30°$ as it crosses at the same point as M[1,1]. The match between the frequencies at which maxima occur in the attenuation and frequencies at which modes are excited is similar in the case of $\psi = 60°$ (shown in Figures 5.7(b) and 5.7(d)) except that the frequencies at which the modes are excited is higher. At $\psi = 60°$ there appears to be little or no effect of the M[1,2] mode on the attenuation.

Figure 5.8 shows the plots for the second circumferential modes and the attenuation for the $n = 2$ circumferential terms. As seen for both the incident angles plotted, there is a good match between frequencies at which the modes are excited and the frequencies at which maxima appear in the attenuation.

In figure 5.9 the comparison between the third circumferential modes and the attenu-

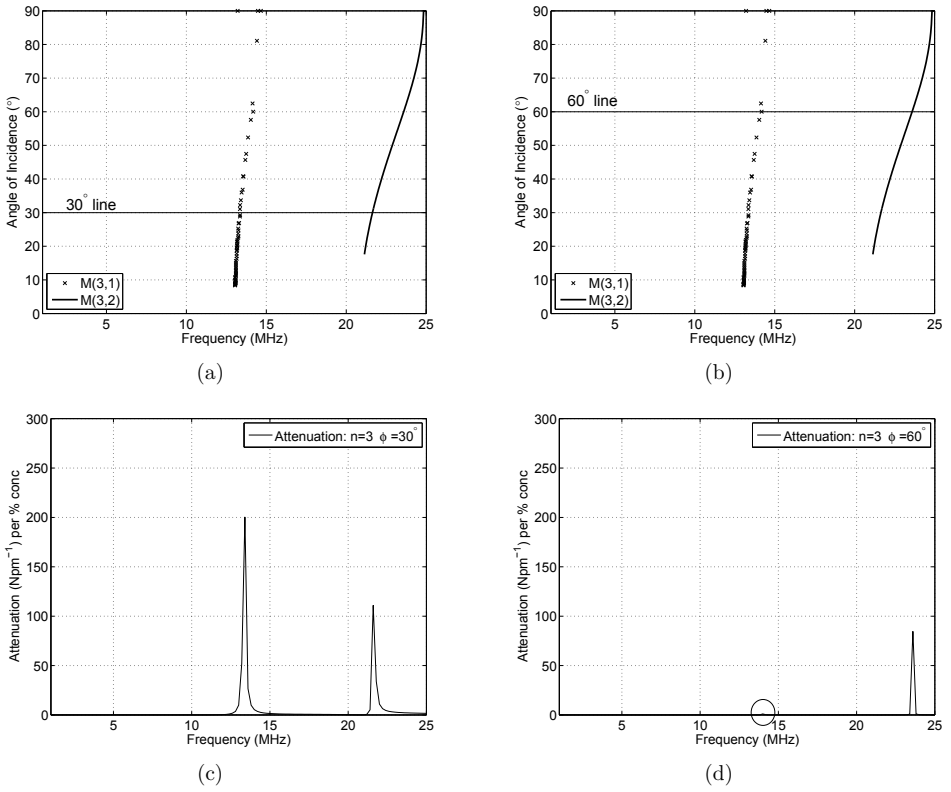

Figure 5.9: Comparison of modes of vibration (third circumferential mode) and modelled attenuation for the $n = 3$ circumferential terms for two different angles incidence.

ation for the $n = 3$ circumferential terms is shown. There is again a good match between the mode excitation frequencies and the frequencies of the maxima in the attenuation. Note the maximum in the attenuation, when $\psi = 60°$ for the mode M[3,1], is very small and hence is marked with a circle.

The good match between the mode excitations and the extrema in the attenuation aids in the validation of the JED models. This comparison can also be used to identify the modes causing the maxima in the experimentally derived attenuation. Examining a plot of the modelled attenuation for the nylon fibres in figure 5.10, the maxima are difficult to distinguish as the loss tangent is large. A plot of the attenuation using a lower loss tangent allows identification of the different modes as shown by the dashed line in figure 5.10.

As can be seen by comparing the maxima in Figure 5.10, with those in figures 5.7 - 5.9, the dominant maxima are those from the lower frequency modes, M[1,1], M[2,1] and M[3,1]. Interestingly, the other maxima from the other modes are not distinct despite

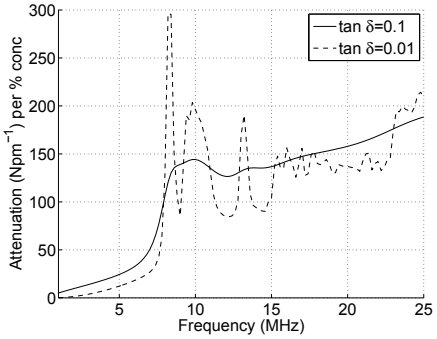

Figure 5.10: Modelled attenuation in a suspension of nylon fibres in water. The cylinder radius was 26 μm and the material properties used are given in Table 5.1.

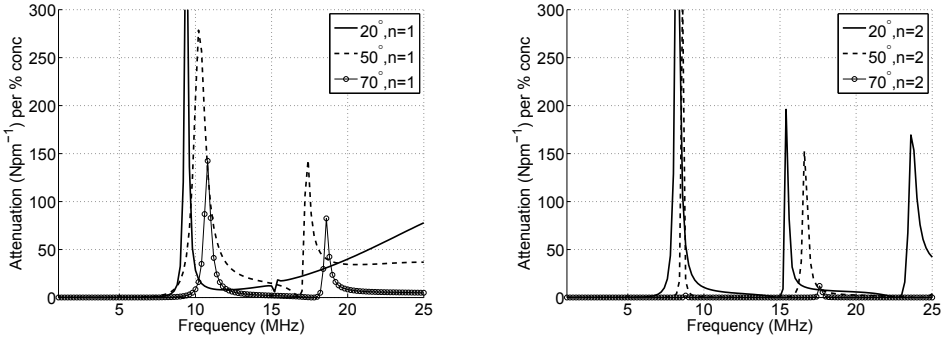

Figure 5.11: Plot of the attenuation of three different incidence angles. Figure 5.11(a) is the attenuation considering only $n = 1$ circumferential terms and figure 5.11(b) is the attenuation considering only $n = 2$ circumferential terms.

the fact that when examined individually the impact they have on the attenuation is considerable. The reason is because these latter modes show a stronger relationship between the angle of incidence and the frequency than the M[1,1], M[2,1] and M[3,1] modes. The M[1,1], M[2,1] and M[3,1] also have a strong relationships to the frequency but these appear at velocities below that for the fluid, c_1. Because the lowest velocity that can be excited is c_1 (1500 ms^{-1}) these relationships are not apparent. For these higher frequency modes, in general, a decrease in the wave velocity in the z direction (lower angle of incidence), increases the frequency at which the mode is excited (see figure 5.5). Since the attenuation is determined for randomly orientated fibres and hence is average of the attenuation of all angles of incidence, this shift in frequency with incident angle means that the effect of the excitation of these higher modes on the attenuation is effectively dampened out. This is shown in figures 5.11(a) and 5.11(b).

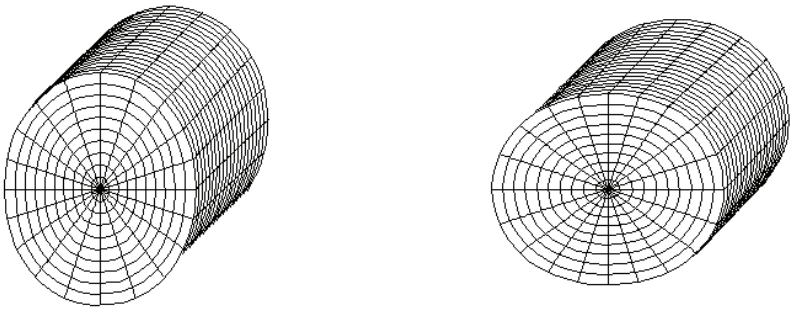

(a) (b)

Figure 5.12: Diagram of the mode shape of M[2,1] at two different instants of the motion

The result is that in the total attenuation in a suspension of randomly orientated fibres, the main source of the resonance features is due to the modes M[2,1] and M[1,1]. The mode M[3,1] also appears to have an effect when the loss tangent is low, but as can be seen in figure 5.10, when the loss tangent is higher, this is barely distinguishable.

5.3 Examining the major modes

Once the modes causing the maxima in the attenuation are identified, they can be examined more closely to gain information on which elastic properties affect them. Thus the elastic properties that can be expected to be determined from these attenuation measurements are identified.

Figure 5.12 shows the shape of the mode M[2,1] responsible for the first maximum seen in the attenuation at 9 MHz in figure 5.10. This mode would produce a quadrupole radiation pattern in the $r-\theta$ plane. The mode also has very little deformation along the z-axis. In both the JED models and the GM calculation of the modes used in this comparion, the material is assumed to be isotropic. In general, fibre materials can be more accurately described as transversely isotropic than isotropic, for example polyester and nylon fibres. A transversely isotropic (T-isotropic) material [53] can be defined by 5 elastic constants (as opposed to 2 in the isotropic case) and these are E_{rr}, E_{zz}, G_{rz},$G_{r\theta}$, and ν_{zr} (See Section 5.3.1). Assuming an isotropic material when the material is T-isotropic would definitely affect modes that have strain in both the $r-\theta$ plane and along the z axis. It is less certain that a mode with little or no z dependance would be affected, assuming that the motion is calculated based on the transverse properties. This implies that the mode illustrated in figure 5.12 is related to the transverse properties of the material rather than the longitudinal properties. Measurement of attenuation capturing this mode would then give estimates for the transverse properties of the material.

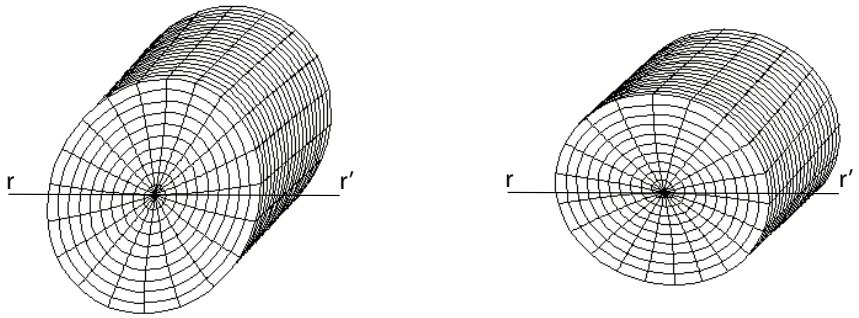

(a) (b)

Figure 5.13: Diagram of the mode shape of M[1,1] at two different instants of the motion

The next maximum in the attenuation, shown in figure 5.10, is at 11 MHz and is caused by the mode M[1,1]. The resulting motion is a tilting movement about the line r, r' as shown in figure 5.13. A view of the mode in the r, z plane is shown in figure 5.14. As can be seen this is a shearing motion in the r, z plane. Hence it would be expected that this mode would give estimates for the shear in the longitudinal direction, G_{rz}. This supports the findings in Papers D and Papers F. However unless $G_{rz} \approx G_{r\theta}$, the behaviour of this mode when the material is assumed to be isotropic instead of T-isotropic could be affected. It would be of interest to investigate further the difference between the modes of a cylinder of T-isotropic material and those of a cylinder of isotropic material. This can be done by using the GM to calculate the modes of a cylinder of T-isotropic material and of particularly interesting would be any changes to the M[1,1] mode.

The final mode that causes a maximum in the attenuation curve, though marginally when the loss tangent is high, is the M[3,1] mode. The behaviour of this mode is shown in figure 5.15. As can be seen from its shape, the greatest displacement is in the r, θ plane. Hence it is expected that the main properties governing this motion would be those in the transverse direction. As before, this suggests that inaccuracies due to the assumption of an isotropic material would not affect this mode significantly. This is, again, assuming that the motion is calculated based on the transverse properties.

There is an potential problem in estimating the elastic properties from these modes that is highlighted from their investigation. This is that the modes M[2,1] and M[3,1] are largely influenced by the transverse properties, $E_{\theta,r}$, $G_{\theta,r}$ of the material and the M[1,1] is largely influenced by the longitudinal shear, G_{rz}. If the fibre material is isotropic, the elastic property estimates will not be affected. If the material is T-isotropic but $G_{rz} \approx G_{\theta,r}$, again, there should be little problem in estimating elastic properties. However, if the material is T-isotropic, such that $G_{rz} \neq G_{\theta,r}$, then, at best, the transverse Young's modulus, $E_{\theta,r}$ and G_{rz} can be estimated but the isotropic condition that $-1 \leq \nu \leq 0.5$

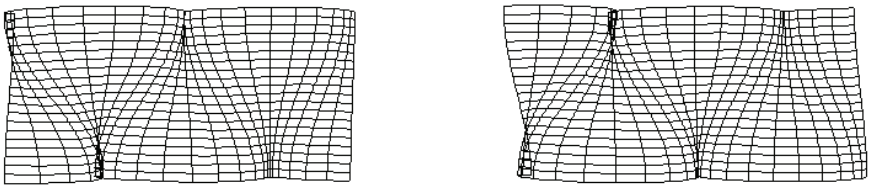

(a) (b)

Figure 5.14: Diagram of the mode shape of M[1,1] at two different instants of the motion in the r, z plane

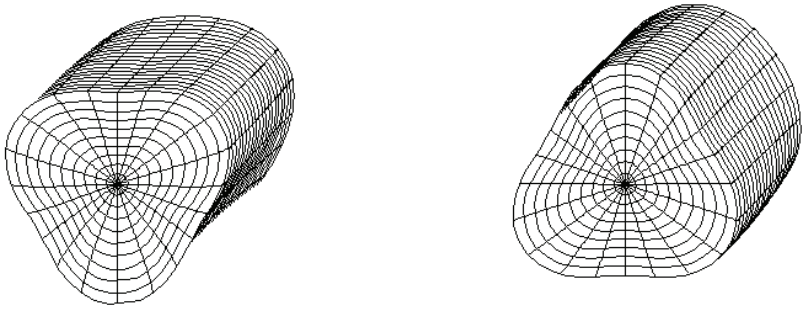

(a) (b)

Figure 5.15: Diagram of the mode shape M[3,1] at two different instants

will not hold hence neither will the relationships between the other elastic constants. However, the consequences of this are likely to be more serious since the modes M[2,1] and M[3,1] depend on both $E_{\theta,r}$ and $G_{\theta,r}$ which would not be compatible with value for G_{rz} estimated from the mode M[1,1]. A model based on T-isotropic material may have to be used, if the accuracy of the isotropic model is inadequate.

Since the angle of incidence makes little difference to the frequencies at which the modes M[1,1], M[2,1] and M[3,1] are excited, it is possible to study these modes under the condition that that the incident wave is perpendicular to the cylinder ($\psi = 0$). This simplifies the JED non-viscous model considerably to the models used by Faran [58] and

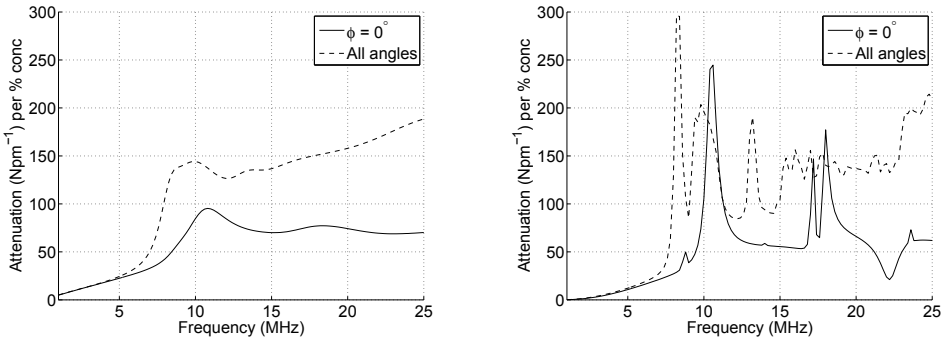

Figure 5.16: Comparison between the attenuation with a incidence angle of 0° and attenuation from randomly orientated fibres. Figure 5.16(a) is with a loss tangent of 0.2 and figure 5.16(b) is with no intrinsic loss in the fibres.

Flax et al. [59, 60] and use can be made of these authors interpretation of these modes of vibration. This was investigated to some extent in Paper C. The results of this paper showed that the resonance peaks in the back-scattering models [58–60] were at the same frequencies as the peaks in the attenuation ($\psi = 0$). However, in the derivation of the surface waves (Franz, Stoneley and Rayleigh waves) by Flax et al. [60] it was assumed that the wavelength was much smaller that the diameter. No such assumption can be made for fibre suspensions and hence it was concluded that it is difficult to establish which kind of waves cause the maxima in the attenuation. More work could be done in this area.

However, although normal incidence models can be used to analysis the type of modes that are excited, this does not mean the attenuation of randomly orientated fibres is the equivalent to attenuation of fibres lying normally to the incident wave. As can be seen in figure 5.16, although the first three maxima appear at approximately the same frequencies their effect on the amplitude of the attenuation at that frequency is different. Also, the modes at higher frequencies make a considerable difference to the level of attenuation at higher frequencies.

In conclusion, the wave modes that cause the maxima in the attenuation in a suspension of solid cylindrical scatterers have been identified. Their relation to material properties has been briefly investigated. This comparison also highlights a potential problem with the assumption of an isotropic material used in the JED models in their application to T-isotropic fibres. The possibilities of a more thorough investigation on the modes of vibration could be done by comparing to previous studies on mode of vibrations of cylinder with normal incidence excitation since the frequency of these modes causing the maxima do not have a strong relationship to ψ. However, when fitting the modelled attenuation to the experimental attenuation, all modes must be considered and not just the modes contributing to the maxima as there is a considerable difference between the

attenuation when $\psi = 0$ and the average attenuation of the all orientations.

5.3.1 Transversely Isotropic Material

In a material with cylindrical orthotropy, the relationship between the stress, τ_{ij}, and the strain ϵ_{ij} in terms of compliance is

$$\begin{Bmatrix} \epsilon_{rr} \\ \epsilon_{\theta\theta} \\ \epsilon_{zz} \\ \epsilon_{\theta z} \\ \epsilon_{rz} \\ \epsilon_{r\theta} \end{Bmatrix} = \begin{bmatrix} S_{11} & S_{12} & S_{13} & 0 & 0 & 0 \\ & S_{22} & S_{23} & 0 & 0 & 0 \\ & & S_{33} & 0 & 0 & 0 \\ & & & S_{44} & 0 & 0 \\ & & & & S_{55} & 0 \\ & & & & & S_{66} \end{bmatrix} \begin{Bmatrix} \tau_{rr} \\ \tau_{\theta\theta} \\ \tau_{zz} \\ \tau_{\theta z} \\ \tau_{rz} \\ \tau_{r\theta} \end{Bmatrix} \tag{5.1}$$

Where

$$S_{11} = \frac{1}{E_{rr}}; S_{22} = \frac{1}{E_{\theta\theta}}; S_{33} = \frac{1}{E_{zz}};$$

$$S_{12} = S_{21} = -\frac{\nu_{\theta r}}{E_{\theta\theta}} = -\frac{\nu_{r\theta}}{E_{rr}};$$

$$S_{13} = S_{31} = -\frac{\nu_{zr}}{E_{zz}} = -\frac{\nu_{rz}}{E_{rr}};$$

$$S_{23} = S_{32} = -\frac{\nu_{z\theta}}{E_{zz}} = -\frac{\nu_{\theta z}}{E_{\theta\theta}};$$

$$S_{44} = \frac{1}{G_{\theta z}}; S_{55} = \frac{1}{G_{rz}}; S_{66} = \frac{1}{G_{r\theta}};$$

and the compliance relation is describe by 9 independent elastic constants [61].

A transversely isotropic materials is a special class of the orthotropic material which have the same properties in one plane (r,θ) and different properties in the direction normal to this plane (z). Hence

$$S_{11} = \frac{1}{E_{rr}} = S_{22} = \frac{1}{E_{\theta\theta}};$$

So $E_{rr} = E_{\theta\theta}$ and $\nu_{\theta r} = \nu_{r\theta}$

$$S_{44} = \frac{1}{G_{\theta z}} = S_{55} = \frac{1}{G_{rz}};$$

So $G_{\theta z} = G_{rz}$ and

$$S_{11} - S_{12} = S_{66}; \frac{1 + \nu_{\theta r}}{E_{rr}} = \frac{1}{G_{r\theta}};$$

hence $E_{rr} = (1 + \nu_{\theta r})G_{r\theta}$ so $\nu_{\theta r}$ does not need to be estimated. This leave E_{rr}, E_{zz}, G_{rz}, $G_{r\theta}$ and ν_{zr}

Chapter 6

Parameter Estimation

The earlier chapters have dealt with the modelling of attenuation in suspensions of cylindrical scatterers. Assuming that the attenuation can be modelled, the next step is to use the model to solve the inverse problem. What is an inverse problem? The inverse problem is where a model is used to establish the inputs to the system from a known output.

There are some obvious issues with the inverse problem. To illustrate, the result of a sum is 10 and is the result of 2 numbers added together thus model is established. The problem is that 5 and 5 and 3 and 7 are equally valid solutions. So unless a better model is available, the solution will be non-unique. This is an example of an ill-posed problem.

A well-posed problem is one where a solution: exists, it is unique, and that the solution depends continuously on the data. Even if a problem is well-posed, it is not necessarily well-conditioned. A well-conditioned problem in non-mathematical terms, is when errors in the solution are related to errors of approximately the same magnitude in the dependent variables [62]. An example of an ill-conditioned problem is if there were a small error in the attenuation, it would result in large errors in the estimation of the shear wave speed.

Parameter sensitivity is also an important aspect in solving the inverse problem. This is where changes in the parameters of the model or in the physical properties of the system do not result in changes in the output. For example, a change in the compression wave velocity of the fibre does not result in changes in the attenuation.

The lack of sensitivity of the output to the parameter of interest classes the system as an ill-posed problem as the solutions are non-unique and since there is more than one value that gives the same output.

The method of establishing values of the parameter is done by optimizing the fit between the modelled output and the measured output. This is generally done using a search algorithm. This algorithm will have certain criteria that it should meet before returning a result. For example a change in the parameters, for which the values are being searched, causes a change in the output that is below a certain tolerance. Once these criteria are met, the results are returned. The results are a single value for each of

the parameters. As there is only one value returned for each parameter, a single value is returned for parameters that would theoretically give non-unique solutions. A small error in the attenuation or a different initial starting point would give a different value for the parameter. The result is that a small error in the attenuation gives large errors in the parameter of interest and the problem can be seen as being ill-conditioned. Hence, the parameter sensitivity can be related to the degree of ill-conditioning.

The parameters estimated from the JED models were all properties of the suspension. In all cases, the properties of water were assumed to be known as was the density of the fibre material. The three main properties estimated were the compression wave velocity, c_{2c}, Poisson's ratio, ν, the loss tangent, $\tan\delta$. In Papers F & G, in addition to these three properties, the volume fraction was also estimated within narrow boundaries to allow for errors in the measurement.

Establishing values for these properties is done by optimizing the fit between the modelled attenuation and the measured attenuation. This is done by minimizing the difference between the modelled and the measured attenuation. The difference is quantified by a cost function, V. This cost function is defined to suit the problem. The cost function used in all cases was

$$V = \sum_{n=1}^{N} |\alpha_{mn} - \alpha_{en}|^2 \tag{6.1}$$

where α_m, is the attenuation of the model at the n^{th} frequency interval and α_e is the attenuation calculated from experimental measurements at the n^{th} frequency interval. N is the maximum number of frequency intervals used. The frequency intervals used were a subsample of the measured signal. The subsample start value and end value was set by the amplitude of the attenuation i.e. by the energy in the reflected signal. The subsample rate was chosen so that the main features of α_e were represented. This subsample rate was lower than the sample rate of the signal because of the computational time taken to calculate at higher rates. The points on the experimental attenuation curves shown in the papers where a comparison is done between the model and the experiments are marked with the subsample intervals.

6.1 Search Algorithm

To minimise V, a search algorithm is used. The algorithm used was an interior trust region and that can be subject to bounds on the parameters [63]. It is based on the trust region method for unconstrained minimisation which can be expressed as

$$min\{\psi_k(s) \stackrel{\text{def}}{=} g_k^T s + \frac{1}{2} s^T B_k s : ||\bar{D}_k s|| \leq \Delta_k\} \tag{6.2}$$

Where $g_k \stackrel{\text{def}}{=} \nabla f(x_k)$. B_k is the symmetric approximation to the Hessian matrix $\nabla^2 f(x_k)$. $\bar{D}_k$ is the scaling matrix and Δ_k is a positive scalar representing the trust region size. The symbols $||\cdot||$ denote the 2-norm. More details are given in the article.

Table 6.1: Parameter values

Parameter	Symbol	Value
Frequency	f	1-15 MHz
Radius	R	20 μm
Density	ρ	1390 kgm^{-3}
Loss tangent	$\tan\delta$	0.3
wave velocity (water)	c_1	1498 ms^{-1}
Density	ρ_1	1093 kgm^{-3}
Volume Fraction	f_r	0.13%.

Equation 6.2 is given to show the basis of the algorithm used. Neither the choice of algorithm nor the details of its function are dealt with in this thesis. However the method of estimating material properties from attenuation measurements would benefit from further work.

6.2 Parameter Sensitivity of the JED Model

To asses the influence of a specific parameter (in this case a material property) has on the JED modelled attenuation, this paramater is changed and the effect this has on the attenuation is calculated.

The influence of the shear and compression wave velocity in the solid (c_{2s} and c_{2c} respectively) are investigated since it is from these values the elastic moduli can be obtained assuming the density, ρ_2 is known.

The attenuation over a range of values for c_{2c} and c_{2s} for a range of frequencies was calculated. The difference between these attenuation curves and the attenuation curve at a fixed value of c_{2c} and c_{2s} was calculated using equations 6.1 and 6.2. The fixed value or reference point was $c_{2c} = 2000\,\mathrm{ms}^{-1}$ and $c_{2s} = 750\,\mathrm{ms}^{-1}$. The other parameters were kept constant and their values are given in Table 6.2.

Plotting V against the range of values of c_{2c} and c_{2s} shows the degree by which the attenuation changes with changes in c_{2c} and c_{2s}. Note that since the material is assumed to be isotropic and Poisson's ratio, ν is set such that $\nu \geq 0$, this puts the limit on c_{2c} as $c_{2c} > \sqrt{2}c_{2s}$. The isotropic condition sets the upper bound on ν as $\nu \leq 0.5$. Contours of the level of V over c_{2c} and c_{2s} are plotted in figure 6.1(a). The different colours represent different values of V. The values of c_{2c} and c_{2s} that correspond to areas of blue have low V and hence there is little difference between the attenuation at the reference point and the attenuation calculated using these values of c_{2c} and c_{2s}. The plot shows deep troughs, where c_{2s} is constant, but c_{2c} varies. The presence of the three troughs, seen more clearly in the surface version of the same plot (Fig. 6.1(b)), implies that the model is sensitive to c_{2s} in that it only gives three distinct values for c_{2s} but it is less sensitive to the value of c_{2c}. This is because values of c_{2c}, which vary along the base of the trough shown in figure 6.1(b), give approximately the same value of attenuation.

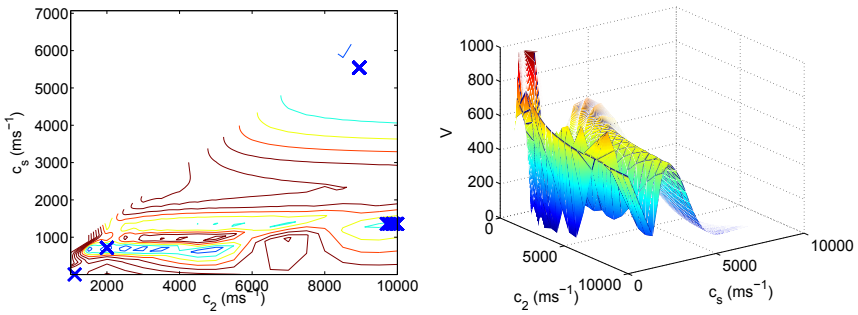

(a) (b)

Figure 6.1: Fig. 6.1(a) is a contour plot of V against c_{2c} and c_{2s}. Fig. 6.1(b) is a 3D surface of V against c_{2c} and c_{2s}. The crosses mark the convergence points of the search function.

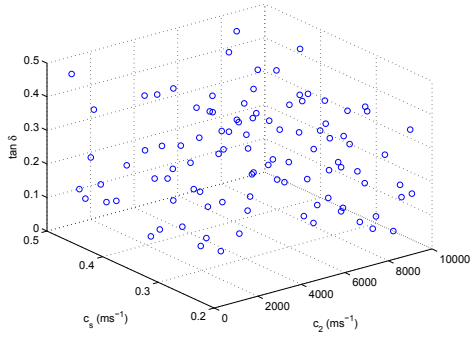

Figure 6.2: Plot of the randomised starting point used to investigate the sensitivity and in papers D and E

Although these troughs exist, the lowest point is only at the fixed point which shows that there is only one global minima. This means that it should be possible to correctly identify the material properties of c_{2c} and c_{2s} assuming the values of $\tan\delta$ and ρ were known.

Since the existence of a global minima has been established for this case, the ability of the trust-region reflective Newton algorithm to locate the global minimum is then tested. This is done because being able to locate the global minimum from any starting point means that the method of estimating the elastic properties will not be dependent on the starting point. For the method to be robust, an algorithm that converges to the global minimum is required.

The random starting points used in Papers E and F were used in this test and are plotted in figure 6.2. The resulting converging points of the algorithm are plotted as crosses on figure 6.1(a). 17% of the starting points sucessfully converge on the reference

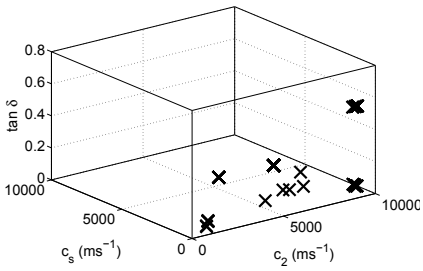

(a)

Figure 6.3: Points of convergence of the randomised starting points when $\tan\delta$ is also optimised by the trust-region reflective Newton algorithm.

point. The majority of the other starting points converge at or very close to the boundaries of the parameters. A more sophisticated cost function which penalised values lying close to the boundary would prevent the initial values converging on the edges of the boundaries and increase the number of points converging on the reference value.

The above analysis assumes that ρ and $\tan\delta$ are known. The likelihood of knowing the density of the fibres material of the fibre in suspension is high since this can often be obtained by other measurements. However, knowing the loss tangent is unlikely if one does not know c_{2c} or c_{2s}. Hence the influence $\tan\delta$ has on the sensitivity should also be considered.

If the algorithm is used to optimise $\tan\delta$ as well as c_{2c} or c_{2s} the points converge as shown in figure 6.3(a). This is using the same randomised starting points as used above.

These convergence points match with local minima in V. This is illustrated for two cases: in figure 6.4(a) with $\tan\delta = 0$ and in figure 6.4(b) with $\tan\delta = 0.03$. The points marked with a circle are the convergence points with a value of $\tan\delta$ that equals the contour plot. Hence it can be seen that the convergence points are where V is local minimum.

When $\tan\delta$ is not fixed, it can be seen that there is a convergence point that is in the centre of the range of c_{2c} and c_{2s}. So, even penalising the values close to the boundaries would not remove this local minimum. However, at this convergence point the attenuation curve does not contain the resonance features as shown in figure 6.5. It may, therefore, be possible to modify the cost function such that if a resonance feature, i.e. a point of zero gradient, exists in the attenuation curve to which the comparison is being made, then it should also exist in the optimised curve, or at least weighted so that values causing a resonance feature would have a lower cost function.

Studying the sensitivity plot, it can be seen that at $c_{2s} > 4000$ the contours are flatter, showing the cost function does not vary in this region. This suggests that it would be difficult to identify materials with properties in this region due to the low sensitivity of the cost function to c_{2c} and c_{2s}.

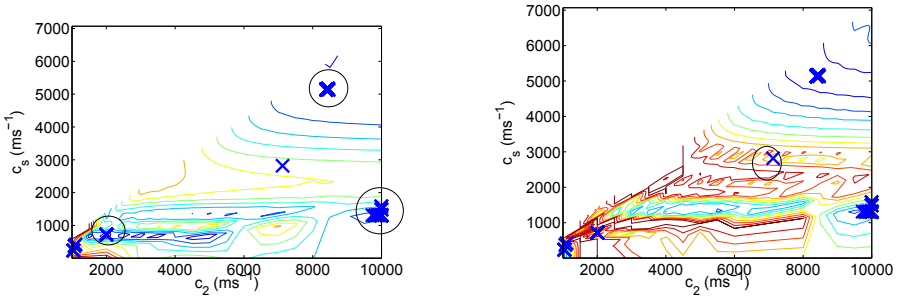

(a) (b)

Figure 6.4: Two examples of plots of V over a range of values of c_{2c} and c_{2s} and a specific value of tan δ. In figure 6.4(a)), $\tan\delta = 0$. The point of convergence that also have tan $\delta = 0$ are marked with a circle. In figure 6.4(b)) $\tan\delta = 0.03$ hence the point marked with a circle is that with tan $\delta = 0.03$

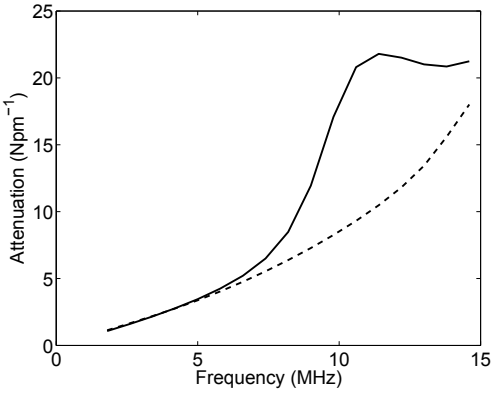

Figure 6.5: Plot of the attenuation at the convergence point, $c_{2c} = 7100$, c_{2s}=2800. The solid line is the reference attenuation and the dashed line is the attenuation calculated using the aforementioned values of c_{2c} and c_{2s}.

In conclusion, the sensitivity study shows that the model is more sensitive to c_{2s} than c_{2c} but that there is a global minimum, hence if the model accurately predicts the attenuation and there is low noise, it is possible for c_{2c}, c_{2s} and $\tan\delta$ to be identified, if the solution lies at or near the reference point tested. A more sophisticated cost function reduces the dependency of the method of estimating elastic properties on the starting point.

Chapter 7

Online Considerations

The objective is to make the measurement method an online system. The implications of this should then be considered. The following is a brief discussion of these considerations.

To be an online system the three parts of the measurement method should be considered. These are the measurements of the attenuation, the model used and the estimation of the elastic properties from the model and measurement data.

7.1 Measurements

Affecting the measurements are the transducers, the working frequency range and any disturbances to the signal that are not modelled.

The transducers used in the experiments were standard, commercially available ones. It should therefore not be a problem basing an online system on these transducers.

The frequencies used should be those which excite wave modes, to increase the accuracy of the estimation process. However high frequencies are more difficult to implement in a measurement system as they attenuate more than lower frequencies and hence the distance travelled by the pulse must be reduced in order that the signal to noise ratio is sufficiently high. The experimental results used a frequency range of 2-30 MHz and a distance travelled by the pulse of 20 mm. A system based on these dimensions would be desirable.

The signal is potentially disturbed by a number of factors that should be investigated. These are

1. temperature
2. pressure
3. fines
4. air bubbles
5. additives (e.g. fillers)
6. dirt

7.2 Model and Estimation Process

The model and the estimation process are treated together since it is their combined effect that has an impact on whether or not the system can be implemented as an online one.

In addition to the attenuation measurement, the model requires the cross-sectional geometry of the fibres. In the experiments carried out on pulp, these measurement were obtained from the PulpEye pulp analyser system [64] and laboratory measurements of the fibre wall thickness. Online fibre wall thickness measurements are currently being developed [65]. Systems for obtaining this information should be available presently.

Speed of Computation

The objective for an online measurement system is that the results be available within the time taken for a control loop to be executed.

The current speed of computation varies from 40 minutes to several hours depending on the starting values. This is running on a single 2.5 GHz processor and no work has yet been done on the speed of the computation of the elastic fibre property measurements.

The following are suggests for improving the speed of the computation and have not been tested.

Cost function 1

The minimisation of the error between the measured and modelled attenuation uses a search algorithm. This searches the entire valid space, with different initial values. Once the first values have been established, these could be used as the starting point for the next estimation. Hence greatly reducing the time taken for the estimation.

Cost function 2

Alternatively, the cost function can be modified using the suggestion in Chapter 6, which would reduce the dependancy on the initial values. This would reduce the number of different starting points required to locate the global minimum and hence reduce the search time. Once first results for a pulp are established they could then be used as the start for the next iteration which again would reduce the search time.

Discrete values of the estimate

Given the discrepancies between the shapes of the fibres and the regular shapes used in the model and the variation in the fibre properties, the accuracy of the method will not very be high. Therefore it is unnecessary to search for slight changes in properties. This point has not been used in the estimation process and would be likely to contribute significantly to the speed of the process.

Integration

The integration over all angles is done based on a gradient estimation procedure. Whilst this increases the speed of the estimation in the current implementation, it is not conducive to making the code parallelised. Using trapezoidal numerical integration, although slower would allows the process to be more easily distributed over a number of processors and hence the speed would be proportional to the number of processors.

Distributed radii

Calculation for the different radii is also a calculation that can be easily parallelised since one result is not dependent on the other. This is another part of the process where the speed would be proportional to the number of processors used.

Programming language

The code is written in Matlab, Mathworks Inc. This is an excellent tool for evaluation different methods and testing different algorithms. However, it is slow so once an algorithm for the search part of the estimation process has been evaluated and decided on, the code can be written in a lower level language, such as 'C'.

A commercial optical pulp analyser takes typically 15 minutes from the time the pulp enter the system before the results are analysed. This means that the method for determining elastic properties has a maximum of 15 minutes before any loss of data will occur.

Chapter 8

Summary of the Papers

This section give a summary of each paper included in the thesis. It includes a comment for each paper on my personal contributions and the involvement of the other authors. Torbjörn Löfqvist has been my supervisor throughout and his was the original idea of characterizing paper pulp using ultrasound.

8.1 Paper A - Estimating Suspended Fibre Material Properties by Modelling Ultrasound Attenuation

Authors: Yvonne Aitomäki and Torbjörn Löfqvist
Reproduced from: Proceedings of International Conference of Mathematical Modelling of Wave Phenomena 2005

Summary
The JED model v1 (see Chapter 3) is described in detail. This is compared to the model that includes thermal and viscous shear effects in the fluid derived by Habeger [32]. Experimentally derived attenuation for a suspension of nylon fibres cut from fishing line in water is compared to the predicted attenuation from the model. The nylon used in the fishing line is a polyamide copolymer so the exact material properties of the fibre were difficult to establish since the type of the copolymer was not known. The results lay between those expected for nylon 66 and nylon 6. Resonance peaks in the attenuation were both predicted and found experimentally. The conclusion was that the model appears to be sufficiently sensitive to material properties. Thus estimations of these properties from the attenuation may be possible.

Personal contribution
Work was carried out by Aitomäki with consultation with Löfqvist. The paper was written by Aitomäki and Löfqvist.

8.2 Paper B - Ultrasonic Measurements and Modelling of Attenuation and Phase Velocity in Pulp Suspensions

Authors: Jan Niemi, Yvonne Aitomäki and Torbjörn Löfqvist
Reproduced from: Proceeding of IEEE Ultrasonic Symposium, Rotterdam, Holland 2005

Summary

This paper introduces a method of performing phase unwrapping that minimises discontinuities in the phase shift. This is used to calculate the phase velocity in pulps of different consistency. The results show that dispersion is caused by fibres and correlates with mass fraction. Attenuation measurements of pulp are also made, with the aim of finding resonance peaks in the frequency response of the attenuation predicted by the model. Clear peaks are not found. This is thought to be due to the effect of the distributed radii of the pulp fibres. Estimations of the properties are made from these curves but comparison with known values was not done. This is due to the difficulties in carrying out single fibre tests on saturated wood fibres.

Personal contribution

The experiments and the phase velocity work was carried out by Niemi and Löfqvist. The attenuation theory and calculations was carried out by Aitomäki. The paper was written by Niemi and Aitomäki and Löfqvist.

8.3 Paper C - Inverse Estimation of Material Properties from Ultrasound Attenuation in Fibre suspensions

Authors: Yvonne Aitomäki and Torbjörn Löfqvist
Reproduced from: Elsevier Ultrasonics, Volume 49, Issues 4-5, May 2009, Pages 432-437

Summary

In this paper experiments on nylon 66 give evidence for the effect different fibre radii have on the attenuation. This supports the JED model. An estimation process is implemented which estimates material properties that give the best fit between the model and the measurement attenuation. The results show that the shear modulus is within the expected range based on previous studies. The Young's Modulus is underestimated even when compared to transverse values for the material.

Personal contribution

Work was carried out by Aitomäki with consultation with Löfqvist. The paper was written by Aitomäki with considerable comments and corrections provided Löfqvist and the journal reviewer.

8.4 Paper D - Sounding Out Paper Pulp: Ultrasound Spectroscopy of Dilute Viscoelastic Fibre Suspensions

Authors:Yvonne Aitomäki and Torbjörn Löfqvist
Presented at Acoustics and Ultrasonics in the Processing of Industrial Soft Solids Conference, held in Leeds, February 2005. The proceedings were sent but as yet have not been published.
Summary
The reason why the resonance peaks appear in the frequency response of the attenuation is explored in this paper. The influence of the shear wave velocity and the fibre radius on the resonance of the first peaks is shown. Hence, experimentally determining the location of the first resonance peak would help establish the value of the shear modulus. This supports the results in Paper D, which showed that the shear modulus was estimated to within a previously established range. The reason that the first resonance peaks are associated with shear waves is because shear wave velocity is lower than compression wave velocity. The exact nature of the wave that causes this resonance is not yet established, since the proof that they are Rayleigh waves relies on asymptotic values for the Bessel functions, which are only valid for $ka \gg 1$, where a is the radius and k the wave number of the wave in the fluid. Since this is not the case with the fibre suspension used, the conclusion that the peaks in attenuation are also caused by Rayleigh waves cannot be drawn.
Personal contribution
Work was carried out by Aitomäki with consultation with Löfqvist. The paper was written by Aitomäki. Feedback and comments were provided by Löfqvist.

8.5 Paper E - Damping mechanisms of ultrasound scattering in suspension of cylindrical particles: Numerical analysis

Authors: Yvonne Aitomäki, Jan Niemi and Torbjörn Löfqvist
To be submitted to: Journal of the Acoustical Society of America
Summary
The addition of viscosity to the ultrasound scattering models increase complexity. This paper investigates whether or not the addition of viscosity is necessary in a suspension of cylindrical scatterers when their radii is of the order of the wavelength and is not close to the viscous skin depth. The modelled attenuation of a scatterer surrounded by a viscous fluid is compared to that where the fluid is non viscous. The results show that the intrinsic loss in the scatterer and the viscosity both have a damping effect on the attenuation. Hence, with high intrinsic loss ($\tan\delta \geq 0.1$), the effects of viscosity is negligible. This holds if the frequency is not in the region where the viscous skin depth

equals the radius.

The conclusion is that a simpler model where the fluid is assumed to be non-viscous can be used to model attenuation in suspensions of fibres with $\tan\delta \geq 0.1$.

Personal contribution
The original idea was that of Löfqvist. Work was carried out by Aitomäki with consultation with Löfqvist. The paper was written by Aitomäki. Feedback and comments were provided by Löfqvist and Carlson, whose help is gratefully acknowledged.

8.6 Paper F - Estimating material properties of solid and hollow fibres in suspension using ultrasonic attenuation

Authors: Yvonne Aitomäki and Torbjörn Löfqvist
To be submitted to: IEEE Transactions on Ultrasonics, Ferroelectrics, and Frequency Control

Summary
This study firstly investigates the difference in attenuation measurements between solid and hollow fibres in suspension. Secondly, it tests whether a solid model (JED non viscous distributed radii) is sufficient for modelling hollow fibres or whether a hollow model (JED hollow distributed radii) should be used. The measured attenuation in suspensions of hollow and solid fibres of the same material, polyester, are compared. A comparison is then done between the estimated material properties obtained from using these different models on the different measurements of attenuation. The results show that the solid model gives good results with solid fibres in suspension and the hollow model gives reasonable results with the hollow fibres in suspension. Both of these results compare well with reference values for block polyester. However the solid model with the hollow fibres suspension gives poor estimates of elastic properties despite giving the best match to the modelled attenuation and the measured attenuation.

On a more general scientific note, this paper highlights the point that a good fit between data and the model does not necessarily mean the model gives a correct interpretation of the behaviour of the system. It may simply mean there are sufficient degrees of freedom in the model to allow a good fit to be achieved.

Personal contribution
Work was carried out by Aitomäki with consultation with Löfqvist. The paper was written by Aitomäki. Feedback and comments were provided by Löfqvist and Carlson, whose help is gratefully acknowledged.

8.7 Paper G -Comparison of softwood and hardwood pulp fibre elasticity using ultrasound

Authors: Yvonne Aitomäki and Torbjörn Löfqvist
To be submitted
Summary
This paper is a preliminary test of the model on fibres in pulp. A comparison is done between the estimated values for elastic moduli between softwood and hardwood fibres after refining. The estimates are obtained from fitting attenuation measurements from these pulps to modelled attenuation. The model used is a layered cylinder model, where the surrounding fluid is assumed to be non-viscous and the distribution of the fibre radii is also considered (JED hollow distributed radii). The measurements are made on pulps with negligible fine content and at pressures of approximately 5 bars. This high pressure reduces the size of the air bubbles in the suspensions, that otherwise could significantly attenuate the ultrasound. An optical measurement device is used to measure the fibre geometry with the exception fibre wall thickness. The wall thickness and the mass fraction were both established by laboratory measurements of the pulp samples. The results show that there is little difference between the estimates of the elastic moduli for the hardwood and the softwood pulp fibres. The results for softwood are 1.6 GPa well to individual fibre test from other work.

The results show that either the due to the processing these fibres undergo, they both have similar values for their elastic moduli or that method is not sufficiently accurate to detect differences between hardwood and softwood fibres. Based on the assumption that the fibres are better described as transversely isotropic than isotropic, the results of previous studies and the work done in chapter 5, the estimated value for the Young's modulus is likely to be that of the transverse plane ($E_{\theta,r}$) of the fibres than of the axial direction, E_z.
Personal contribution
The original idea was that of Löfqvist and Aitomäki. The measurements were carried out by Niemi and Aitomäki and Löfqvist. The estimates of the elastic properties was carried out by Aitomäki. The method was written by Niemi and the rest of the paper was written by Aitomäki. Feedback and comments were provided by Löfqvist.

Chapter 9

Conclusion

The hypothesis set out in the introduction was: The measurement of the ultrasound attenuation can be used to estimate the elastic properties of wood fibres in pulp online. This was divided into three research question. These questions were investigated in the thesis and are answered as follows:

1. Can elastic properties be estimated from ultrasound attenuation?

   Concluding the work done in Papers D and F, the method can give estimates for shear modulus and the transverse Young's modulus of fibres. This is supported by the investigation of the modes of vibration in Chapter 5. The aforementioned papers also highlight the importance of the outer fibre radius (or radii) and the radius (radii) of the lumen on the attenuation. Consequently, this geometric information is required in order to extract elastic properties from the ultrasonic signals. Optical systems such as PulpEye [64] can provide values for the outer fibre radii and methods of obtaining the fibre wall thickness are currently being implemented [65]. The radii of the lumen can be determined from these values. This provides sufficient geometric detail to estimate the elastic properties of fibres.

2. Can the method be applied to wood fibres in pulp?

   In the introduction it was stated that a model is required which captures only the wood fibre properties that are important to attenuation. Concluding the work in this thesis, the wood fibre can be assumed to be an infinitely long cylinder. It cannot be assumed to be solid and hence a hollow model is required (Papers F & G). The material of the fibre does not necessarily need to be modelled as transversely isotropic. The method can give good estimates from assuming the material to be isotropic (Papers D & F). In addition, the fluid in the model can be treated as non-viscous, as wood fibres are viscoelastic [19] (Paper E).

   The exact shape of the cross section of the fibres is assumed to not have an important impact on the attenuation. In addition, the dependency of attenuation on the elastic properties is assumed to have symmetric distribution about the average of

the elastic properties. Given these assumptions the conclusion can be drawn that the method can be applied to wood fibres in pulp (Paper G). Obviously, these assumptions need to be verified. The further work section contains a discussion of how this can be done.

3. Can the measurement method be used online?

   Using a simple model in the method, decreases the computation time taken to estimate the elastic properties. Based on the work done, the simplest model that could be used would be the layered cylindrical model that treats distribution radii distribution (JED distributed radii). Implementation of the suggestions for reducing the computational time (Chapter 7) should allow the results to be available in a time comparative to that of the optical results from current pulp analysers. The computational time is, however, dependent on the number of processors used.

   The measurement system used in Paper G was attached to as a module in a PulpEye system. PulpEye is a pulp analyser and is available as an online version. Hence it should be straightforward to make the measuring system itself online. Making a standalone system would, however, require more work. The addition of fines has not been addressed in this thesis. The impact of fines on attenuation and the necessity of including a model for such particles would need addressing in an online version of a system based on this method.

From these answers it can be seen that all the evidence so far supports the hypothesis that the measurement of the ultrasound attenuation can be used to estimate the elastic properties of wood fibres in pulp online and hence continued testing is justified.

There are certain conditions that need to be fulfilled for the method to have application in the paper and pulp industry and it is these that should be tested. These conditions are:

1. The diameter distribution of the fibres is required as are estimates of the radii of lumen.
2. The elliptical cross-section of the fibres can be treated appropriately.
3. A suspension of fibres with different elastic properties can be treated appropriately.

With these conditions fulfilled the shear modulus and the transverse Young's modulus of the pulp fibres can be measured. Thus a system with sensors based on this method can be implemented.

With such a system, process efficiency and paper quality could be improved through:

1. Improvement in the refining process based on fibre flexibility calculation obtained from the geometry and the elastic properties.
2. Early detection of inappropriate fibre stiffness in the paper manufacturing process.
3. Improvement in pulp fractionation allowing pulp to be better suited to the end product.

These all contribute not only to economic gains for the paper industry but are of benefit to the wider community in terms of the reduced environmental impact that increased energy efficiency produces and the increase in availability of energy by-products from this industry.

So as you drive around in your biofuel car, using the ethanol produced from black liquor that would otherwise have been burned to cook the pulp more than was necessary, you can reflect on the role played by Online Fibre Properties Measurements: Foundations for a method based on ultrasound attenuation!

Chapter 10

Further Work

10.1 Further work

Modelling

For completeness, this method should be tested on isotropic fibres. This would provide more confidence in the results. Glass is one of the few fibres that is isotropic and is readily available hence is the obvious choice in such a test. An initial test was attempted with chopped glass fibres with a diameter of 20 μm and a length of 12.7 mm. This proved unsuccessful, as the fibres could not be easily separated. Attempts to separate the fibres included baking in oven and boiling with sulphuric acid. Neither attempt was successful. With hindsight, experience and a little patience, this is not a difficult test and could be performed on longer, larger diameter glass fibres that could be cut to length in the laboratory.

The assumption that the exact shape of the layered scatterer has little impact on the attenuation requires validation before the method can be applied to wood pulp with confidence. This can be investigated by examining the differences in attenuation between ellipsoidal scatterers and regular cylindrical scatterers. However, ellipsoidal geometry is considerably more challenging. It could be tested using simulations to some extent by a comparison between the cylindrical model and the model developed by Hasheminejad and Sanaei [66]. However, this would require the assumption of zero or negligible shear as the theory only applies to fluid cylinders. The reason is that the equivalent function to Bessel functions for ellipsoidal geometries are Mathieu functions as used by Harumi [67] in expressions for an elastic ribbon (the extreme case of an ellipse). However, these functions are not orthogonal hence one cannot solve for each series of n as one can for the Bessel functions, unless there are special conditions. The implications of this are that if it were necessary to model fibres as ellipses, using Mathieu functions the model would become very large and complex. Alternatively, a model based on the T-matrix approach would perhaps be more appropriate [68].

Perhaps an easier approach is to investigate experimentally ellipsoidal geometry by

scaling the problem and using a much larger scatterer and low frequencies. This would allow the geometry of the scatterer to be more easily controlled. A comparison between the modes of a cylinder and an ellipse could be done and the effects on the amplitude of the scattered wave after averaging over the surface at a distance from the scatterer and over different incident angles. This would in fact be a similar experiment to that done very early on by Faran in 1951 [58] on cylinders and spheres. The basis of the experiment is that the attenuation is proportional to the reflection coefficient from a single scatterer. It may also be possible to extrude elliptical fibres and test these directly in suspension under the assumption that extruding to a different geometry has little effect on the material properties of the fibre.

The next assumption that should be investigated before the method can be applied to wood pulp with confidence is that the dependency of attenuation on the elastic properties has symmetric distribution about the average of the elastic properties. This should be simple to test and can be done by simulation. The model can be used to simulate the attenuation from a mixture of fibres with different elastic properties. This attenuation can then be compared to the attenuation from an average of the elastic properties. If these two attenuations do not differ significantly, then the assumption is correct.

However, considering the modal behaviour of the attenuation this is unlikely and hence it may be necessary to modify the model to allocate different fractions of the suspension to different elastic moduli. It is difficult to predict whether there is sufficient information in the attenuation signal to provide estimates for the elastic moduli of the different fibres. The accuracy of the assumption that the dependency of attenuation on the elastic properties has symmetric distribution about the average of the elastic properties will depend on the distribution of these properties. Hence it will depend on the type of pulp that is being tested.

Comparison to other methods

Alternatively, other methods of measuring the transverse elastic properties of fibres and the longitudinal shear modulus could be investigated. For example an atomic force microscope (AFM) could be used to measure these properties but differences in scale and frequency make the comparison of these results difficult. Another method is to build a composite of the fibres and from testing and modelling, derive the transverse fibre properties. This would be of great value in validating the results for polymer fibres, in particular fibres that are not affected by their immersion in water such as polyester. However, the elastic properties of wood fibre when wet are known to differ from their properties when dry [22] so it would be difficult to validate the estimation from the ultrasound method using this technique.

Error Analysis

A basic attempt to test the sensitivity of the estimations to noise in the attenuation measurement was carried out in Papers D, F & G by estimating the values from the experimentally measured attenuation, $\alpha_e \pm 2\sigma$ where σ is the standard deviation of the

mean. A more thorough analysis of the stability of the model in general to noise in the parameters could establish which parameters and to what degree, they influence the attenuation.

Fines

As mentioned in the conclusion, the fine content will also attenuate the ultrasound. The percentage of fines in the pulp will be the deciding factor in whether they have to be taken into account or not. The attenuation due to fines can be predicted using a scattering model for spherical particles such as those discussed in Chapter 4. Further work on how such a model could be included in the method would be necessary if it were found that fines have a significant impact on the attenuation. However, previous studies have shown that fine concentration in pulp does not have a large impact on ultrasound attenuation [69].

References

[1] A. Crevecoeur and E. Kilby, *Key Statistics 2007*. Confederation of European Paper Industries, Brussels, 2007.

[2] Södra, "Södra annual report 2008," Feb. 2008.

[3] W. Birk, Personal communication, Apr. 2009.

[4] A. Hagedorn, J. Orccotoma, P. Schueler, B. Snow, and J. Jarvinen, "Optimizing machine efficiency through fibre quality management," in *2006 TAPPI Papermaker's Conference*. Technical Association of the Pulp and Paper Industry, 2006.

[5] A. Kaw, *Mechanics of composite materials*. Taylor & Francis, 2006.

[6] Lorentzen-Wettre, "L&W STFI Fibermaster." [Online]. Available: http://www.lorentzen-wettre.com/bprod/prod.cfm?prodid=9100

[7] D. Krotz, "Laser ultrasonic sensor streamlines papermaking process," http://www.lbl.gov/Science-Articles/Archive/EETD-papersensor-Ridgway.html, 2006-04-04.

[8] (2006, 08) New evidence suggest longer paper making history in china. [Online]. Available: http://news.xinhuanet.com/english/2006-08/08/content_4937457.htm

[9] S. Anttilainen, "Metso supplied sc paper machine line sets a new world speed record at stora enso kvarnsveden," 2007. [Online]. Available: http://www.metsoautomation.com/News/newsdocuments.nsf/Web2NewsDoc/CAC7C79ED6B6E117C22572A00048448C?OpenDocument&ch=ChMetsoPaperWebEng&id=CAC7C79ED6B6E117C22572A00048448C&

[10] D. McIntosh, *Handbook of Pulp and Paper Technology*. Van Nostrand Reinhold Company, 1970, ch. 1-5, pp. 37–46.

[11] J. Yang and R. Evans, "Prediction of moe of eucalypt wood from microfibril angle and density," *Holz als Roh- und Werkstoff*, vol. 61, no. 6, pp. 449–452, 2003.

[12] J. Tchepel, J. Provan, A. Nishida, and C. Biggs, "A procedure for measuring the flexilibity of single wood-pulp fibres," *Mechanics of Composite Materials*, vol. 42, no. 1, pp. 83–92, 2006.

[13] H. Karlsson, *Fibre Guide*. Lorentzen & Wettre, Kista, Sweden, 2006.

[14] K. K. Piteå, "Välkommen till en rundvandring in kappa kraftliner piteå," 2006.

[15] T. Wikström, "Flow and rheology of pulp suspensions at medium consistency," PhD Thesis, Chalmers University of Technology, 2002.

[16] P. Brodeur and J. Gerhardstein, "Overview of applications of ultrasonics in the pulp and paper industry," in *1998 IEEE Ultrasonics Symposium*, 1998, pp. 809–815.

[17] A. Heikkurinen and L. L., *Mechanical pulping*, ser. Papermaking Science and Technology. Fapet Oy, 1999, no. 5, ch. The character and properties of mechanical pulp, pp. 395–413.

[18] E. Avallone, T. Baumeister, A. Sadegh, and L. Marks, *Marks' Standard Handbook for Mechanical Engineers*, 11st ed. McGraw-Hill Book Company, Inc, 2006, ch. Cylinders and Spheres, pp. 5:45–5:57.

[19] L. Salmen, "Viscoelastic properties of in situ lignin under water-saturated conditions," *Journal of material science*, vol. 19, no. 9, pp. 3090–3096, Sept. 1984.

[20] J. Levlin and L. Söderhjelm, *Pulp and Paper Testing*. Fapet Oy, 1999.

[21] H. Karlsson and P. Fransson, "STFI FiberMaster fives the papermaker new muscles," *Sv. Papperstidning*, vol. 10, no. 26, 1997.

[22] E. Ehrnrooth, "Softening and mechanical behaviour of single wood pulp fibres - the influence of matrix composition and chemical and physical characteristics," PhD Thesis, Department of Wood and Polymer Chemistry, University of Helsinki, 1982.

[23] L. Kinsler, A. Frey, A. Coppens, and J. Sanders, *Fundamentals of Acoustics*, 4th ed. John Wiley and Sons Inc., 2000.

[24] L. Hall, "The origin of ultrasonic absorption in water," *Phys. Rev.*, vol. 73, no. 7, pp. 775–781, Apr 1948.

[25] A. D. Pierce, *Acoustics: An introduction to its physical principles and applications*. American Institute of Physics, 1994, ch. The wave theory of sound, pp. 1–53.

[26] B. Palvakovic and M. Lowe, *User's Manual: Disperse- A system for generating dispersion curves*, 2nd ed., Imperial College London, London, UK, July 2003.

[27] L. Kinsler, A. Frey, A. Coppens, and J. Sanders, *Fundamentals of Acoustics*, 4th ed. John Wiley and Sons Inc., 2000, ch. Chapter3 Vibrations of bars, p. 218.

[28] Kolsky, *Stress Waves in Solids*. Dover, 1963.

[29] A. Bhatia, *Ultrasonic Absorption*. Dover, 1968, ch. 11, p. 272.

[30] W. M. Ewing, W. Jardetzky, and F. Press, *Elastic Waves in Layered Media*. McGraw-Hill Book Company, Inc, 1957, ch. Homogeneous and isotropic half space, pp. 24–73.

[31] D. McClements and M. Povey, "Scattering of ultrasound by emulsions," *Journal of Physics D: Applied Physics*, vol. 22, pp. 38–47, 1989.

[32] C. Habeger, "The attenuation of ultrsound in dilute polymeric fiber suspensions," *Journal of Acoustical Society of America*, vol. 72, pp. 870–878, sep 1982.

[33] M. Morse, P and K. Ingard, *Theoretical Acoustics*. Princetown University Press, 1986, ch. 6, p. 401.

[34] N. Herrmann and D.J.McClements, "Influence of visco-inertial effect on the ultrasonic properties of mondisperse silican suspensions," *Journal of the Acoustical Society of America*, vol. 106, p. 1178, 1999.

[35] Rayleigh, *The Theory of Sound*. Macmillan, 1926.

[36] V. Knudsen, J. Wilson, and N. Anderson, "The attenuation of audible sound in fog and smoke," *The Journal fo the Acoustical Society of America*, vol. 20, no. 6, pp. 849–857, Nov 1948.

[37] C. J. T. Sewell, "The extinction of sound in a viscous atmosphere by small obstacles of cylindrical and spherical form," *Philosophical Transactions of the Royal Society of London. Series A, Containing Papers of a Mathematical or Physical Character*, vol. 210, pp. 239–270, 1911. [Online]. Available: http://www.jstor.org/stable/90992

[38] P. Epstein and R. Carhart, "The absorption of sound in suspensions and emulsions. i. water fog in air," *The Journal of the Acoustical Society of America*, vol. 25, no. 3, pp. 553–565, May 1953.

[39] J. Allegra and S. Hawley, "Attenation of sound in suspension and emulsions: Theory and experiments," *The Journal of the Acoustical Society of America*, vol. 51, no. 5, pp. 1545–1564, 2 1972.

[40] M. Povey, *Ultrasonic Techniques for Fluid Characterization*. Academic Press, 1997, ch. A.4, p. 179.

[41] A. K. Hipp, G. Storti, and M. Morbidelli, "Acoustic characterization of concentrated suspensions and emulsions. 1. model analysis," *Langmuir*, vol. 18, no. 2, pp. 391–404, 2002. [Online]. Available: http://pubs.acs.org/doi/abs/10.1021/la015538c

[42] P. Lloyd and M. Berry, "Wave propagations through an assembly of spheres iv. relations between different multiple scattering theories," *Proc. Phys. Soc.*, vol. 91, pp. 678–688, 1967.

[43] D. Adams, "Ultrasonic propagation in paper fibre suspensions," in *3rd IFAC conference on instrumentation and automation in paper*, 1776.

[44] C. Habeger and G. Baum, "Ultrasonic characterizations of fibre suspension," The Institue of Paper Chemistry, Appleton, Wisconsin, IPC Technical Paper series 118, Nov 1981.

[45] M. Morse, P and K. Ingard, *Theoretical Acoustics*. Princetown University Press, 1986, ch. 8, p. 401.

[46] P. Morse and H. Feshbach, *Method of Theoretical Physics*. McGraw-Hill Book Company, Inc, 1953, vol. II, ch. 13.

[47] G. Strang, *Linear Algebra and Its Applications*. Brooks Cole, February 1988.

[48] R. Challis, M. Povey, M. Mather, and A. Holmes, "Ultrasound techniques for characterizing colliodal dispersions," *Reports in Progress in Physics*, vol. 68, pp. 1541–1637, 2005.

[49] L. L. Foldy, "The multiple scattering of waves. I. General theory of isotropic scattering by randomly distributed scatterersisotropic scattering by randomly distributed scatterers," *Phys. Rev. (2)*, vol. 67, pp. 107–119, 1945.

[50] S. K. Numrich and H. Uberall, *Physical Acoustics Vol. XXI*. Academic Press, 1992, ch. Scattering of sound pulses and the ringing of target resonances, p. 235.

[51] J. Dickey, G. Frisk, and H. Uberall, "Whispering gallery wave modes on elastic cylinders," *Journal of the Acoustical Society of America*, vol. 59, no. 6, pp. 1339–1346, June 1976.

[52] R. M. Davies, "A critical study of the hopkinson pressure bar," *Philosophical Transactions of the Royal Society of London. Series A, Mathematical and Physical Sciences*, vol. 240, no. 821, pp. 375–457, 1948. [Online]. Available: http://www.jstor.org/stable/91440

[53] Every, *Dynamic methods for measuring the elastic properties of solids*, ser. Handbook of elastic properties of solids, liquids and gases. Academic Press, 2001, vol. 1, ch. Introduction, p. 25.

[54] B. N. Pavlakovic and M. Lowe, "A general purpose apporach to calculating the longitudinal and flexural modes of mulit-layered, embedded, transversely isotropic cylinders," *Review of Progress in Quantitative NDE*, vol. 18, pp. 239–246, 1999.

[55] D. C. Gazis, "Three-dimensional investigation of the propagation of waves in hollow circular cylinders. i. analytical foundation," *The Journal of the Acoustical Society of America*, vol. 31, no. 5, pp. 568–573, 1959. [Online]. Available: http://link.aip.org/link/?JAS/31/568/1

[56] ——, "Three-dimensional investigation of the propagation of waves in hollow circular cylinders. ii. numerical results," *The Journal of the Acoustical Society of America*, vol. 31, no. 5, pp. 573–578, 1959. [Online]. Available: http://link.aip.org/link/?JAS/31/573/1

[57] L. Flax and W. Neubauer, "Acoustic reflection from layered elastic absorptive cylinders," *Journal of the Acoustical Society of America*, vol. 61, no. 2, pp. 307–312, Feb 1977.

[58] J. Faran, "Sound scattering by solid cylinders and spheres," *Journal of the Acoustical Society of America*, vol. 23, no. 4, pp. 405–418, July 1951.

[59] L. Flax, L. Dragonette, and H. Uberall, "Theory of elastic resonance excitation by sound scattering," *Journal of the Acoustical Society of America*, vol. 63, no. 3, pp. 723–730, Mar 1978.

[60] G. Frisk, J. Dickey, and H. Uberall, "Surface wave modes on elastic cylinders," *Journal of the Acoustical Society of America*, vol. 58, no. 5, pp. 996–1008, Nov 1975.

[61] P. Sinha, *Composite materials and structures*. The Department of Aerospace Engineering, Indian Institute of Technology, Kharagpur, 1995, ch. Macromechanical behaviour. [Online]. Available: http://www.ae.iitkgp.ernet.in/ebooks/index.html

[62] E. E. Kalu and A. Kaw, *Numerical Methods with Applications*. Kalu, E. E. and Kaw, A., 2008.

[63] T. Coleman and Y. Li, "An interior trust region approach for nonlinear minimization subject to bounds," *SIAM Journal on Optimization*, vol. 6, pp. 418–445, 1996.

[64] Eurocon, "Pulpeye pulp analyser." [Online]. Available: http://www.pulpeye.com/

[65] Ö. Sundvall, Personal communication, Nov 2008.

[66] S. Hasheminejad and R. Sanaei, "Ultrasonic scattering by a fluid cylinder of elliptic cross section, including viscous effects," *Ultrasonics, Ferroelectrics and Frequency Control, IEEE Transactions on*, vol. 55, no. 2, pp. 391–404, February 2008.

[67] K. Harumi, "Scattering of plane waves by a rigid ribbon in a solid," *Journal of Applied Physics*, vol. 32, no. 8, pp. 1488–1497, 1961. [Online]. Available: http://link.aip.org/link/?JAP/32/1488/1

[68] T. A. K. Pillai, V. V. Varadan, and V. K. Varadan, "Sound scattering by rigid and elastic infinite elliptical cylinders in water," *The Journal of the Acoustical Society of America*, vol. 72, no. 3, pp. 1032–1037, 1982. [Online]. Available: http://link.aip.org/link/?JAS/72/1032/1

[69] M. Tormanen, J. Niemi, T. Lofqvist, and R. Myllyla, "Pulp consistency determined by a combination of optical and acoustical measurement techniques," *Measurement Science and Technology*, vol. 17, no. 4, pp. 695–702, 2006. [Online]. Available: http://stacks.iop.org/0957-0233/17/695

Part II

Paper A

Estimating Suspended Fibre Material Properties by Modelling Ultrasound Attenuation

Authors:
Yvonne Aitomäki and Torbjörn Löfqvist

Reformatted version of paper originally published in:
Proceedings of International Conference of Mathematical Modelling of Wave Phenomena 2005

Estimating Suspended Fibre Material Properties by modelling Ultrasound Attenuation

Yvonne Aitomäki and Torbjörn Löfqvist

Abstract

An analytical model for use in the inverse problem of estimating material properties of suspended fibres from ultrasonic attenuation has been developed. The ultrasound attenuation is derived theoretically from the energy losses arising when a plane wave is scattered and absorbed off an infinitely long, isotropic, viscoelastic cylinder. By neglecting thermal considerations and assuming low viscosity in the suspending fluid, we can make additional assumptions that provide us with a tractable set of equations that can be solved analytically. The model can then be to used in inverse methods of estimating material properties. We verify the model with experimentally obtained values of attenuation for saturated Nylon fibres. The experimental results from Nylon fibres show local peaks in the attenuation which are thought to be due to the resonant absorption at the eigenfrequencies of the fibres. The results of the experiments show that the model is sufficiently sensitive to detect differences in different types of Nylon. Applications for suspended fibre characterization can be found in the paper manufacturing industry.

List of Symbols

Unless otherwise indicated subscript 1 refers to the fluid medium and subscript 2 refers to the solid medium.

$\mathbf{A_1}$,$\mathbf{A_2}$	transverse vector potentials	$\mathbf{M}, \mathbf{N}$	transverse vector potential
a_c	$R \times k_c$	M	elastic modulus
a_s	$R \times k_s$	R	radius of the fibre
a_{cc}	$R \times k_{cc}$	r , θ, z	cylindrical coordinates
a_{sc}	$R \times k_{sc}$	V	velocity
a_{cs}	$R \times k_{cs}$	α	acoustic attenuation
B_n, D_n, E_n	coefficients of expansion	α_1	acoustic attenuation ín water
C_p	heat capacity in the fluid	β	thermal expansivity
c	velocity of sound	$\tan\delta_2$	loss tangent of the viscoelastic solid
$\mathbf{c}$	complex speed of sound in the sound	ϵ_{ij}	strain
f_r	volume fraction of fibres	η_1	viscosity of the fluid
$H_n^{(1)}$	nth order Hankel function of the first kind	Γ_{ij}^l	Christoffel symbol
J_n	nth order Bessel function of the first kind	λ	wavelength
K	heat conductivity coefficient	ω	angular frequency

$\hat{\mathbf{k}}$	unit vector along the z-axis in cylindrical co-ordinates	ρ	density
		λ_2, μ_2	Lamê's 1st and 2nd constants
k_c	wave number of the compressional wave	υ_2	Poisson's ratio
k_s	wave number of the transverse wave	ψ	the angle between the incident wave and the longitudinal axis of the cylinder
k_{cc}	wave number of the compressional wave along the r-axis	ϕ_c	compressional wave scalar potential
k_{cs}	wave number component of the compressional wave along the z-axis	ϕ_o	incident compressional wave scalar potential
k_{sc}	wave numbers of the transverse wave along the r-axis	ϕ_r	reflected compressional wave scalar potential
		χ, ξ	transverse wave scalar potentials

1 Introduction

Our research is aimed at the on-line estimation of the characteristics of pulp fibres suspended in water. An application is in the paper manufacturing industry where estimating fibre characteristics can potentially improve the quality control of the finished paper. The measurement method used is based on ultrasound as it is rapid, inexpensive, non-destructive and non-intrusive.

The focus of our investigation is on establishing the material properties of the suspended, fluid-saturated fibres from ultrasonic attenuation measurements. To do this we need to solve the inverse problem of deriving these properties from the attenuation. We therefore require a model that relates attenuation to material properties and one that is analytical since this is more amenable than numerical solutions for solving the inverse problem. Habeger established a model related attenuation to material properties, where the equations are solved numerically [1]. We have developed an analytical solution based on the same equations.

Habeger's model is a cylindrical extension of the Epstein-Carhart [2]/Allegra-Hawley [3] model. In the calculation of attenuation, the set of equations are solved numerically and are based on a number of different material properties. By neglecting thermal effects and assuming low viscosity in the suspending fluid, we can make additional assumptions that provide us with a more tractable set of equations that can then be solved analytically.

In this paper we describe the simplified model used to relate the attenuation to the material properties of the fluid saturated fibres. We compare the analytical solution with that obtained by a numerical solution of the non-simplified equation system [1], to verify the validity of the additional assumptions that are made. We then verify the model with experimentally obtained values of attenuation for saturated Nylon fibres. We go on to discuss the results, draw conclusions and outline the next steps in our investigations.

2 Theory

The attenuation is derived from calculating the energy losses arising when a plane wave is incident upon an infinitely long, straight cylinder. The cylinder material is assumed to be isotropic and viscoelastic. The energy losses taken into account are from the wave being partially reflected, partially transmitted at the solid/fluid interface and from the generation of damped, transverse waves in the solid medium at the boundary. The highly damped thermal skin layer, that is generated by the acoustically induced pulsations of the solid is shown by [1] to have the greatest effect where the thermal wavelength is of the order of the radius. We, therefore, consider frequencies above this region and hence the thermal effects are neglected in the derivation of attenuation. The advantage is that the thermal material properties of the fibre and fluid can then be neglected, reducing the number of material properties in the solution and hence increasing the feasibility of estimating the remaining material properties from attenuation measurements. A viscous wave in the fluid (as defined by [2]) is also generated but again this is highly damped and is neglected in the final stages of the derivation.

Expressions for the wave potentials from the conservation of mass, energy and momentum were derived by [2] and are expressed for the fluid as:

$$\nabla \cdot \mathbf{A_1} = 0 \tag{1}$$

$$\nabla^2 \phi_{c_1} = -k_{c_1}^2 \phi_{c_1} \tag{2}$$

$$\nabla \times \nabla \times \mathbf{A_1} = k_{s_1}^2 \mathbf{A_1} \tag{3}$$

$$\mathbf{V_1} = -\nabla \phi_{c_1} + \nabla \times \mathbf{A_1} \tag{4}$$

where, $k_{c_1} = \omega / c_1$ and $k_{s_1} = \sqrt{i\omega\rho_1/\eta_1}$.

In the solid, the displacement potentials are used instead of the velocity potentials. Hence,

$$\nabla \cdot \mathbf{A_2} = 0 \tag{5}$$

$$\nabla^2 \phi_{c_2} = -k_{c_2}^2 \phi_{c_2} \tag{6}$$

$$\nabla \times \nabla \times \mathbf{A_2} = k_{s_2}^2 \mathbf{A_2} \tag{7}$$

$$\mathbf{V_2} = i\omega \left(\nabla \phi_{c_2} - \nabla \times \mathbf{A_2} \right) \tag{8}$$

where $k_{c_2} = \omega / (c_2 (1 - i \tan \delta_2 / 2))$ and $k_{s_2} = \sqrt{i\omega\rho_2/\mu_2}$. Further details of the definition for the wave number in a viscoelastic solid and the complex shear modulus, μ_2, are described in the Appendix.

The stress tensor can be expressed in terms of the wave potentials:

$$\tau_{ij_1} = \eta_1 \left[(k_{s_1}^2 - 2k_{c_1}^2) \phi_{c_1} \right] \delta_{ij} + 2\eta_1 \dot{\epsilon}_{ij} \tag{9}$$

$$\tau_{ij_2} = \left[(\omega^2 \rho_2 - 2\mu_2 k_{c_2}^2) \phi_{c_2} \right] \delta_{ij} + 2\mu_2 \epsilon_{ij} \tag{10}$$

Where the strain is

$$\epsilon_{ij} = \frac{1}{2}(V_{i,j} + V_{j,i} - 2\Gamma^l_{ij}V_l) \tag{11}$$

The fluid wave potential is divided into an incident part and a reflected part, $\phi_{c_1} = \phi_{o_1} + \phi_{r_1}$. The incident plane wave potential, ϕ_{o_1}, is expressed in cylindrical coordinates and we let this equal $e^{i(k_{cc_1}r + k_{cs_1}z - \omega t)}$ as in [1].

Since the plane of the cylinder lies at an angle ψ to the incident wave, the wave numbers are expressed in terms of their components along the cylindrical coordinate axes.

$$k_{cc_1} = k_{c_1}\cos(\psi) \tag{12}$$

$$k_{cs_1} = k_{c_1}\sin(\psi) \tag{13}$$

The inicident wave potential is expanded using Bessel functions of the first kind [4] as

$$\phi_{o_1} = \left(J_0(k_{cc_1}r) + 2\sum_{n=1}^{\infty} i^n \cos n\theta J_n(k_{cc_1}r)\right) e^{i(k_{cs_1}z - \omega t)} \tag{14}$$

And the reflected wave potential in the fluid expanded using Hankel functions of the first kind:

$$\phi_{r_1} = \left(B_{0_1}H_0^{(1)}(k_{cc_1}r) + 2\sum_{n=1}^{\infty} i^n \cos n\theta B_{n_1}H_n^{(1)}(k_{cc_1}r)\right) e^{i(k_{cs_1}z - \omega t)} \tag{15}$$

The combination of the equations (14) and (15) give us an expression for ϕ_{o_1} expanded in terms of Bessel and Hankel functions. To meet the boundary conditions for all values of z and t, the time and z dependence of the potentials must be the same as ϕ_{o_1}. The equivalent expression for the compressional wave potential in the solid is

$$\phi_{c_2} = \left(B_{0_2}J_0(k_{cc_2}r) + 2\sum_{n=1}^{\infty} i^n \cos n\theta B_{n_2}J_n(k_{cc_2}r)\right) e^{i(k_{cs_1}z - \omega t)} \tag{16}$$

where, $k_{cc_2} = \sqrt{(k_{c_2}^2 - k_{cs_1}^2)}$.

To meet the boundary conditions in cylindrical coordinates, the transverse potential can be expanded in terms of two independent scalar potentials, see [5] such that, $\mathbf{M} = \nabla \times \chi\hat{\mathbf{k}}$, $\mathbf{N} = \nabla \times \nabla \times \xi\hat{\mathbf{k}}$ and $\mathbf{A} = \mathbf{M} + \mathbf{N}$. Where χ and ξ are solutions to the scalar Helmholtz equation so, $\nabla^2\chi = -k_{s_2}^2\chi$ and $\nabla^2\xi = -k_{s_2}^2\xi$. The energy dissipated by the transverse waves in the fluid are however very small when the viscosity is low hence these are neglected. Expanding the transverse waves in solid in terms of Bessel and Hankel functions we get

$$k_{s_2}^2\xi_2 = \left(D_{0_2}J_0(k_{sc_2}r) + 2\sum_{n=1}^{\infty} i^n \frac{\partial \cos n\theta}{\partial\theta} D_{n_2}J_n(k_{sc_2}r)\right) e^{i(k_{cs_1}z - \omega t)} \tag{17}$$

$$ik_{cs_1}\chi_2 = \left(E_{0_2}J_0(k_{sc_2}r) + 2\sum_{n=1}^{\infty} i^n \cos n\theta E_{n_2}J_n(k_{sc_2}r)\right) e^{i(k_{cs_1}z - \omega t)} \tag{18}$$

where, $k_{sc_2} = \sqrt{k_{s_2}^2 - k_{cs_2}^2}$.

The boundary conditions are that the velocity along the surface normal and the stresses in all directions are continuous at the solid-fluid interface. So at $r = R_2$, $V_{r_1} = V_{r_2}$, $\tau_{rr_1} = \tau_{rr_2}$, $\tau_{r\theta_1} = \tau_{r\theta_2}$ and $\tau_{rz_1} = \tau_{rz_2}$. Since we neglect the velocity of the viscous wave in the fluid we do not consider the boundary conditions of continuous velocity at the solid/fluid interface in the θ and z directions. The boundary conditions are expressed in terms of the potentials using (4), (8) and (9)-(11) and then expanded according to (14)-(18). The angular dependencies of the functions are orthogonal so the coefficients can be determined by applying the boundary condition to each order of expansion separately.

For $n \neq 0$,

$$a_{cc_1}J'(a_{cc_1}) + B_{n_1}a_{cc_1}H_n^{(1)\prime}(a_{cc_1}) = -i\omega\big[B_{n_2}a_{cc_2}J_n'(a_{cc_2}) - E_{n_2}a_{sc_2}J_n'(a_{sc_2}) + n^2D_{n_2}J_n(a_{sc_2})\big] \quad (19)$$

$$\eta_1\big\{[(a_{s_1}^2 - 2a_{c_1}^2)J_n(a_{cc_1}) - 2a_{cc_1}^2J_n''(a_{cc_1})] + B_{n_1}[(a_{s_1}^2 - 2a_{c_1}^2)H_n^{(1)}(a_{cc_1}) - 2a_{cc_1}^2H_n^{(1)\prime\prime}(a_{cc_1})]\big\} = \mu_2\big\{B_{n_2}[(a_{s_2}^2 - 2a_{c_2}^2)J_n(a_{cc_2}) - 2a_{cc_2}^2J_n''(a_{cc_2})] + 2D_{n_2}n^2[J_n(a_{sc_2}) - a_{sc_2}J_n'(a_{sc_2})] + 2E_{n_2}a_{sc_2}^2J_n''(a_{sc_2})\big\} \quad (20)$$

$$\eta_1\big\{a_{cc_1}J_n'(a_{cc_1}) - J_n(a_{cc_1}) + B_{n_1}[a_{cc_1}H_n^{(1)\prime}(a_{cc_1}) - H_n^{(1)}(a_{cc_1})]\big\} = \mu_2\big\{B_{n_2}[a_{cc_2}J_n'(a_{cc_2}) - J_n(a_{cc_2})] + \frac{1}{2}D_{n_2}[n^2J_n(a_{sc_2}) - a_{sc_2}J_n'(a_{sc_2}) + a_{sc_2}^2J_n''(a_{sc_2})] + E_{n_2}[J_n(a_{sc_2}) - a_{sc_2}J_n'(a_{sc_2})]\big\} \quad (21)$$

$$\eta_1\big\{2a_{cs_1}[a_{cc_1}J_n'(a_{cc_1}) + a_{cc_1}B_{n_1}H_n^{(1)\prime}(a_{cc_1})]\big\} = \mu_2\big\{2a_{cs_1}a_{cc_2}B_{n_2}J_n'(a_{cc_2}) + D_{n_2}n^2a_{cs_1}J_n(a_{sc_2}) + E_{n_2}a_{sc_2}J_n'(a_{sc_2})\frac{(a_{sc_2}^2 - a_{cs_1}^2)}{a_{cs_1}}\big\} \quad (22)$$

For $n = 0$, D_{n_2} is only present (21) hence the solution in this case is that $D_{n_2} = 0$. Hence for $n = 0$ there are 3 equations and 3 unknowns and for $n \neq 0$ there are 4 equations and 4 unknowns. The expression for the coefficients $B_{n_1}, B_{n_2}, D_{n_2}, E_{n_2}$ was then found for $n = 0$ and $n \neq 0$ using Maple ©,Maplesoft, Waterloo, Canada.

This gives us the solution to the conservation equations. The subsequent derivation of the loss in energy due to the the scattering and absorption by the cylinder follows that of [1]. The resulting expression for the attenuation, α is:

$$\alpha = \frac{-2f_r}{\pi R^2 k_{c_1}}\Re\left(\int_0^{\frac{\pi}{2}}\cos(\psi)(B_{0_1} + 2B_{1_1} + 2B_{2_1})d\psi\right) \quad (23)$$

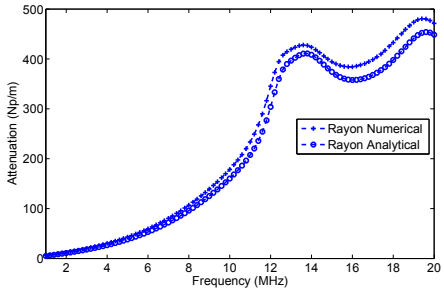

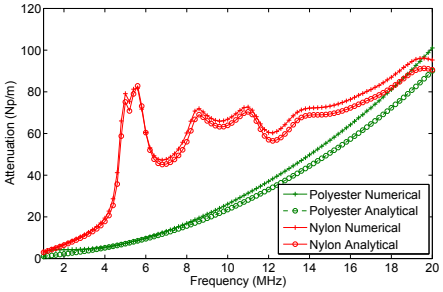

Figure 1: test

Figure 2: Attenuation as a function of frequency for different fibres. The attenuation is expressed in nepers per meter (Np/m),where neper (Np) is a dimensionless unit [6]. $\eta_1 = 9.4 \times 10^{-4}\, Nsm^{-2}$, $\rho_1 = 996\, kgm^{-3}$, $c_1 = 1490\, ms^{-1}$, $K_1 = 0.59\, Wm^{-1}K^{-1}$, $C_{p_1} = 4.14 \times 10^3\, Jkg^{-1}K^{-1}$, $\beta_2 = 2.36 \times 10^{-4}\, K^{-1}$. *The parameter values for the fibres are shown in table 2*

	Rayon	Nylon	Polyester
R (m)	13×10^{-6}	30×10^{-6}	13×10^{-6}
$\tan\delta_2$	0.125	0.2	0.1
υ_2	0.3	0.4	0.4
$\rho_2(\mathrm{kgm}^{-3})$	1400	1140	1340
$c_2(\mathrm{ms}^{-1})$	1090	1340	5860
$K_2(\mathrm{Wm}^{-1}\mathrm{K}^{-1})$	0.15	0.36	0.038
$C_{p2}(\mathrm{Jkg}^{-1}\mathrm{K}^{-1})$	1.5×10^3	1.42×10^3	1.02×10^3
$\beta_2(\mathrm{K}^{-1})$	36×10^{-5}	6×10^{-5}	1.7×10^{-5}

Table 2: Parameter values of the different fibres used in the numerical and analytical models

Note that in the insertion of asymptotic values for the Bessel and Hankel function as $r \to \infty$, Habeger's [1] expression appears to be missing a factor of 2. The attenuation is the sum to infinity of a series of B_{n_1} where n is an integer. However, when calculating the attenuation, the energy associated with the the higher order was assumed to be negligible and the series was truncated at $n = 2$. The attenuation calculated does not take into account the attenuation of the compressional wave through the water itself. This is, therefore, added to the attenuation of the fibres calculated above and is assumed to be $\alpha_1 = 25 \times 10^{-15} f^2$ taken from [6], where f is the frequency.

The effects of the additional assumptions that were made to derive the analytical model can be assessed by comparing the attenuation predicted by the analytical solution presented here and the numerical solution presented by [1]. These assumptions are that the acoustic attenuation from thermal processes are negligible and that the viscous wave generated in the fluid is also negligible. The results of the differences between the predicted attenuation are shown in figure 2 for three different types of polymer fibres:

Rayon, Nylon and Polyester. In general the discrepancy in the results is proportional to the attenuation. The two curves for each fibre have a similar shapes, with the exception of Polyester at low frequencies. This exception is not further examined here. The effect the assumptions have depends on the frequency range and radius used as well as the fluid properties and the thermal properties of the fibre. In the cases examined here, the discrepancies are not large, although the effect these errors have on the parameter estimation needs to be assessed when the model is used in solving the inverse problem.

We have, therefore, a simplified expression for α that can be used in solving the inverse problem. It is a function of the material properties of the saturated fibre and the suspending fluid, the radius of the fibre and fibre volume fraction. The next step is then to verify the model with experimentally obtained values of attenuation from suspension of fibre with known material properties and uniform radius.

3 Experimental

The experimental setup consists of a broadband transducer with a centre frequency of 10 MHz (V311), manufactured by Panametrics, Waltham, MA, USA. A pulser/receiver 5072PR from Panametrics was used to excite the transducer and amplify the received signal. The signal was then digitized using a CompuScope 14100 oscilloscope card, by Gage Applied Technologies Inc., Lachine, QC, Canada, with 14-bit resolution and a sampling rate of 100 MHz. All data was stored in a computer for off-line analysis. The resulting time-domain waveforms were calculated using the average of 100 sampled waveforms to reduce random noise. Before the averaging, the sampled waveforms are aligned to reduce timing jitter by using a method proposed by [7]. A digital thermometer F250, by Automatic Systems Laboratories LTD, England, monitored the temperature both in the suspension under test and in the room. The temperature was used to calculate the speed of sound in the water [8]. The fibre suspension was carefully poured into the measurement cell and then stirred until the majority of the air bubbles were removed. The measurement cell is described in detail in [9]. The attenuation of the sample was calculated according to [10].

The fibre suspension was made of Nylon fishing line, (STROFT™ GTM) with a nominal diameter of 60 μm,[1] chopped to a length of approximately 4 mm. The Nylon was a polyamide copolymer tempered to improve its tensile strength. The fibres were weighed and mixed with water to a concentration of 0.5% by weight. They were then left in water for 3 days to stabilise the temperature and to allow the fibres to become fully saturated. To prevent the fibres from settling during the test the suspension was stirred gently. A set of 30 runs were taken each with an average of 100 pulses.

[1] Permissbile diameter fluctuation $\pm 1\,\mu$m, Permissible norminal size deviation $+38\,\mu$m

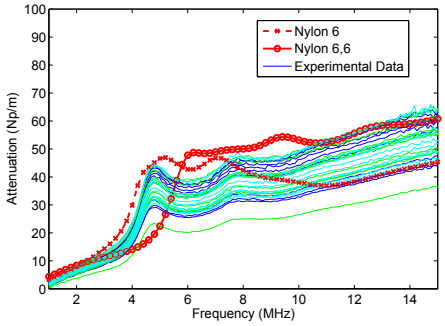

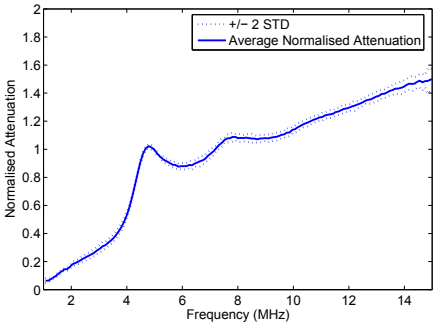

Figure 3: test

Figure 4: Attenuation as a function of frequency for a suspension of Nylon fibres in water at 0.5% concentration. Modelled and experimental attenuation values. Parameters for the saturated fibres are in shown in table 3. Right-hand figure is the Average of the Attenuation normalised by the value of the attenuation at 5MHz to remove the variance directly proportional to the attenuation.

4 Results

Figure 4 show the results from the 0.5% concentration of suspended Nylon fibres. As we can see there is a large variation in the level of attenuation although the shape of the curve is similar in all the measurement with local peaks in the attenuation at 4.8 MHz and at 7.7 MHz.

In the right-hand figure 4, the attenuation has been normalised by the value of the attenuation at 5MHz to remove the effect of variance directly proportional to the attenuation. Attenuation proportional variance is thought to be due to the inherent inhomogeneity of the suspension as the attenuation is proportional to the volume fraction. The fibres form flocs and through a combination of stirring and settling each time an ultrasonic pulse is emitted it travels through a different arrangement of fibres resulting in a different volume concentration and hence a different attenuation. The remaining variance, shown in the normalised attenuation graph increases with increasing attenuation and this is thought to be due to an decrease in the signal to noise ratio at the higher levels of attenuation found at higher frequencies.

The modelled attenuation is plotted in figure 4 with two possible set of parameters which are listed in table 3. The material properties are however, difficult to establish. The density was taken from the manufacturer data sheet, and adjusted for 5% water absorption. The speed of sound in Nylon 6 was taken from Habeger [1], whereas for Nylon 6,6 although the rod velocity was taken from his measurements in saturated fibres, Poisson's ratio in Nylon 6,6 was taken as 0.39 [11]. This means the speed of sound in Nylon 6,6 was calculated as 2345 ms^{-1}. Poisson's ratio for Nylon 6 was taken as the value that gave the best fit in Habeger [1] experiments. The exact value of the loss tangent was

	Nylon 6	Nylon 6,6
R (μm)	46.8 ± 0.4	46.8 ± 0.4
$c_2(\mathrm{ms}^{-1})$	1340	2345
$\rho_2(\mathrm{kgm}^{-3})$	1131	1131
υ_2	0.3	0.39
$\tan\delta_2$	0.2	0.15

Table 3: Parameter values used for Nylon

adjusted to best fit the experimental data as it can vary from very low, 0.01, in lightly crossed amorphous polymer to 3 depending on the molecular structure [12].

As the plots show, neither Nylon 6 or Nylon 6,6 fits the whole range. Nylon 6, gives a good fit for the low frequencies and Nylon 6,6 for the higher frequencies. The wide margin of error in the elastic constants and hence the speed of sound and the fact that the Nylon used was a polyamide copolymer, tempered to improve its tensile strength, could explain some of the discrepancies between the model results and the experimental results. Other explanations are that the values of the material parameters are not constant across the frequency range we are examining or that some of the fibres are not freely suspended but interact with one another which results in unpredictable ultrasonic attenuation. Multiple scattering would also cause differences between predicted and experimental results.

The peaks are thought to correspond to the resonant absorption at the eigenfrequencies of the cylinder, possibly of the shear wave, as opposed to reflections of internal waves from the ends of the fibres. This is because the peaks appear in both the experimental and the modelled values of attenuation and the modelled values are based on cylinders of infinite length.

5 Conclusions

In conclusion, we have established an analytical model relating the attenuation of ultrasound, in a suspension of fibres in a low viscosity fluid, to the material properties of the fibres. This model is amenable for use in solving the inverse problem of determining material properties of saturated fibres from measurements of attenuation. The results of the experiments indicate that the Nylon tested, a polyamide copolymer, has properties between that of Nylon 6 and Nylon 6,6. The material properties of saturated fibres are difficult to assess and hence have large margin of error. The results suggests that the model is sufficiently sensitive to material properties to detect differences in different types of Nylon.

The additional assumptions made that allow the analytical solution to be derived causes some discrepancies in the calculation of attenuation. However, the large variations in attenuation thought to be due to the inherent inhomogeneity, is likely to mask these differences.

6 Further Work

The elastic properties of the saturated Nylon fibres need to be investigated with an alternative method to verify that they do indeed lie between that of Nylon 6 and Nylon 6,6. Investigations at different concentrations need to be carried out to test if the inhomogeneity of the attenuation is the cause of the attenuation proportional variation.

Further work needs to be done to establish the cause of the local peaks in the frequency response of the attenuation. By testing other materials and different diameters of fibres the accuracy of the model can be assessed further.

The next step is then to use this model in solving the inverse problem in suspensions of greater complexity such as paper pulp where online data on the material properties of wood fibre in suspension is required. For this, a method for optimising the fitting of the modelled attenuation to the experimental values needs to be developed. The effects of non-uniform diameters and anisotropic nature of the pulp fibres also need to be assessed.

A Appendix

Here, we have defined the elastic modulus involved in the vibratory motion as complex and equal to:

$$M_2(\omega) = M_2' - iM_2'', \quad \text{where} \quad M_2(\omega) = \lambda_2(\omega) + 2\mu_2(\omega) \tag{A.24}$$

$\tan\delta_2$ is then defined as the phase difference between the real and imaginary part of the elastic modulus:

$$\tan\delta_2 \quad = \quad -\frac{M_2''}{M_2'} \tag{A.25}$$

Denoting the compressional speed of sound in the solid as complex where $\mathbf{c_2} = c_2' - ic_2''$ we get

$$c_2'^2 - c_2''^2 = \frac{M_2'}{\rho_2}, \qquad 2c_2'c_2'' = \frac{M_2'\tan\delta_2}{\rho_2} \tag{A.26}$$

As $\tan\delta_2$ is small at the limit $\tan\delta \to 0$, which is the equivalent of assuming $c_2' \gg c_2''$ we get,

$$\mathbf{c_2} \quad \approx \quad c_2'\left(1 - i\frac{\tan\delta_2}{2}\right) \tag{A.27}$$

With the additional assumption that $k_{c_2}' \gg k_{c_2}''$ we get the same expression as derived by [13]. For ease of readability in the main text, the prime that distinguishes the real from the imaginary part has been dropped. So, in the main text, $c_2 = c_2'$.

μ_2 can be expression in terms of Poisson's ratio, υ_2 and the complex speed of sound using (A.24) and (A.27), if we assume that Poisson's ratio is real at these frequencies.

$$\mu_2 \quad = \quad \left(\frac{0.5 - \upsilon_2}{1 - \upsilon_2}\right) c'^2\rho_2(1 - i\tan\delta_2) \tag{A.28}$$

References

[1] C. Habeger, "The attenuation of ultrsound in dilute polymeric fiber suspensions," *Journal of Acoustical Society of America*, vol. 72, pp. 870–878, sep 1982.

[2] P. Epstein and R. Carhart, "The absorption of sound in suspensions and emulsions. i. water fog in air," *The Journal of the Acoustical Society of America*, vol. 25, no. 3, pp. 553–565, May 1953.

[3] J. Allegra and S. Hawley, "Attenation of sound in suspension and emulsions: Theory and experiments," *The Journal of the Acoustical Society of America*, vol. 51, no. 5, pp. 1545–1564, 2 1972.

[4] M. Morse, P and K. Ingard, *Theoretical Acoustics*. Princetown University Press, 1986, ch. 8, p. 13.

[5] P. Morse and H. Feshbach, *Method of Theoretical Physics*. McGraw-Hill Book Company, Inc, 1953, vol. II, ch. 13.

[6] L. Kinsler, A. Frey, A. Coppens, and J. Sanders, *Fundamentals of Acoustics*, 4th ed. Wiley, 1999, ch. 8.

[7] A. Grennberg and M. Sandell, "Estimation of subsample time delay differences in narrowband ultrasonic echoes using the hilbert transform correlation," *IEEE Transactions on Ultrasonics, Ferroelectrics, and Frequency Control*, vol. 41, no. 5, pp. 588–595, 1994.

[8] N. Bilaniuk and G. S. K. Wong, "Speed of sound in pure water as a function of temperature," *The Journal of the Acoustical Society of America*, vol. 93, no. 4, pp. 2306–2306, 1993.

[9] T. Löfqvist, "Ultrasonic wave attenuation and phase velocity in a paper-fibre suspension," in *Proc.IEEE Ultrasonics Symposium*, vol. 1, Oct 1997, pp. 841–844.

[10] D. McClements and P. Fairley, "Frequency scanning ultrasonic pulse echo reflectometer," *Ultrasonics*, vol. 30, pp. 403–405, 1992.

[11] L. Pedersen. (2002) Tables of acoustic properties of materials. [Online]. Available: http://www.ondacorp.com/tecref_acoustictable.html

[12] J. Ferry, *Viscoelastic Properties of Polymers*, 3rd ed. John Wiley & Sons Inc, 1980, ch. 2, pp. 46–47.

[13] M. Povey, *Ultrasonic Techniques for Fluid Characterization*. Academic Press, 1997, ch. A.4, p. 179.

Paper B

Ultrasonic Measurements and Modelling of Attenuation and Phase Velocity in Pulp Suspensions

Authors:
Jan Niemi, Yvonne Aitomäki and Torbjörn Löfqvist

Reformatted version of paper originally published in:
Proceedings of IEEE Ultrasonic Symposium, pp.775-779 (Rotterdam, Holland),2005

Ultrasonic Measurements and Modelling of Attenuation and Phase Velocity in Pulp Suspensions

Jan Niemi, Yvonne Aitomäki and Torbjörn Löfqvist

Abstract

In the manufacturing process of paper the mass fraction and material properties of the fibres in the pulp suspension are important for the quality of the finished product. This study presents two different methods of pulp characterisation. The first is based on phase velocity, which we use to investigate the composition of the pulp. Here a method is presented where the optimal number of circular shifts within the sampling window of the signal is determined which gives, in a weakly dispersive medium, a continuous phase spectrum and minimizes the likelihood of discontinuities within the bandwidth. Hence, the ambiguity in phase unwrapping is avoided. The results from phase velocity measurements show that the phase velocity weakly increases with increasing amount of fines in the suspension. The dispersion is caused by the fibres and it correlates with fibre mass fraction. The second method is based on attenuation and is used to characterise the wood fibres. The results of the attenuation experiments show that it is possible to inversely calculate wood fibre properties by fitting the model to the experimental data, if the fibre diameter distribution is known. However, the accuracy of these calculation is difficult to determined and more work in this area is required.

1 Introduction

In the manufacturing process of paper the mass fraction and material properties of the fibres in the pulp suspension are important for the quality of the finished product. When using recycled paper, fibres with unknown and varying material properties enter the process. Therefore, there is an increasing demand for methods of on-line characterisation of the pulp suspension as well as the fibres in suspension.

This study presents two different methods of pulp characterisation. The first is based on phase velocity, which we use to investigate the composition of the pulp. The second is based on attenuation and is used to characterise the wood fibres.

In the first method, we investigate how the phase velocity changes with different mass fractions of fibres and fines. To determine the phase velocity, a method is proposed based on a method by [1], where the an echo is circularly shifted an optimal number of samples.

In the second method, to be able to characterise the wood fibres, we use an analytical model which relates the material properties of saturated fibres to the attenuation. We then aim to solve the inverse problem of identifying which values result in the best fit of the model to the attenuation values calculated from experiments.

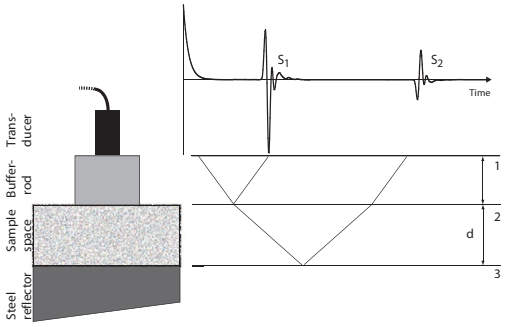

Figure 1: Lattice diagram of the pulse-echo measurement system used this study

2 Phase Velocity

2.1 Theory and experiments

When determining the phase velocity from pulse-echo measurements, one encounters the problem of performing a correct phase unwrapping. The problem is well known and has been addressed in earlier investigations, for instance [2]. The problem arises when the phase velocity is calculated from the phase spectra of a the Fourier transform of each of the two echoes. In this study, we propose a method, termed Minimum Phase Angle (MPA), that determines an optimal number of circular shifts to the windowed signal which results in a continuous phase spectrum and minimizes the likelihood of discontinuities within the bandwidth. Therefore the ambiguity in the phase unwrapping is avoided. To experimentally test the method experiments were performed in pulp fibre suspensions, which are weakly dispersive. The experiments were carried out using the pulse-echo technique in a custom designed test cell. A schematical view of the measurement cell used in this study is shown in Fig. 1.

The echoes from the interfaces depend on the initial pulse pressure amplitude $p_0(t)$ emitted from the transducer and the reflection and transmission coefficients of the different interfaces. For simplicity, we omit the reflection and transmission coefficients and the attenuation. With these assumptions, the echoes from the interfaces between the buffer rod/suspension and suspension/steel reflector are

$$P_1(\omega) = P_0(\omega)e^{-2j\frac{\omega}{c_1}d_1} = P_0(\omega)e^{-j\varphi_1(\omega)} \quad (1)$$

$$P_2(\omega) = P_0(\omega)e^{-2j\omega(\frac{d_1}{c_1}+\frac{d_2}{c_2})} = P_0(\omega)e^{-j\varphi_2(\omega)} \quad (2)$$

where $P_1(\omega)$ and $P_2(\omega)$ are the Fourier transform of the echoes $p_1(t)$ and $p_2(t)$, respectively. d_1 and d_2 are the distance in respective medium. The factor 2 above comes from that the fact the pulse is travelling back and forth through the medium. c_1 and c_2 are the velocities in the buffer rod and pulp suspension, respectively. $P_0(\omega)$ is the Fourier

transform of the initial emitted pulse from the transducer. Note that echo $p_1(t)$ has an extra phase shift of π compared to $p_2(t)$.

2.2 The method of minimum phase angle

To reduce the ambiguity in the phase unwrapping the following method is proposed.

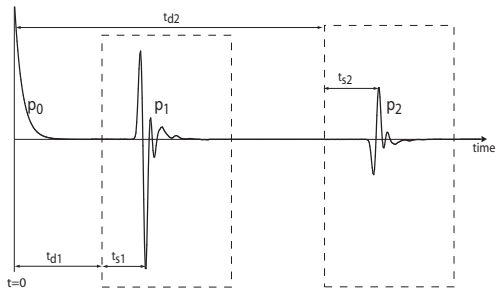

Figure 2: The received signal with illustrations of the time delays and time shifts

The sampled signal is divided into two sampling windows with time delays $t_d = n_d/f_s$ shown in Fig. 2 where n_d is the number of samples that the sampling window is delayed and f_s is the sampling frequency. Within each sampling window the signal is circularly shifted sample by sample. At each shift, a calculation of the phase angle is carried out as

$$PA = \frac{1}{f_2 - f_1} \sum_{m=f_1}^{f_2} \varphi_m^2 \tag{3}$$

where φ_m is the phase spectrum within the frequency bandwidth of $f_1 < m < f_2$ of the shifted sample. Thereafter a sign shift of the echo is carried out, representing a phase shift of π, and again circularly shifted and calculated with the same method. The results are compared and the circularly shifted sample that gives a phase spectrum without discontinuities and minimum value of PA is then chosen. The outcome is then the optimal time shift of $t_s = n_s/f_s$ where n_s is the number of samples the signal is shifted.

This results in two time delays, the time delay from the sampling window and time delay from the circular shift within the window. This gives the phase spectrum for the respective echoes as

$$\varphi_1(\omega) = \phi_1(\omega) + \omega(t_{d1} + t_{s1}) \tag{4}$$

$$\varphi_2(\omega) = \phi_2(\omega) + \omega(t_{d2} + t_{s2}) \tag{5}$$

where ϕ_1 and ϕ_2 are the respective phase spectra of the circularly shifted signal. t_{d1} and t_{d2} are the time delay for respective sampling window. t_{s1} and t_{s2} are the circular shift within respective sampling window. An illustration of how PA changes when echo $p_1(t)$ is circularly shifted within the sampling window is shown in Fig. 3. In this example, the minimum of PA is found when $p_1(t)$ is shifted 100 samples to the left and inverted. Fig.2.3(c) shows the phase spectrum at the minimum of PA for $p_1(t)$ and $-p_1(t)$. We can see that the inverted signal has a phase spectrum with the minimum likelihood of a discontinuity being present in the spectrum.

The phase velocity for a pulp suspension sample can be expressed using (1)-(2) and (4)-(5) as

$$c_2(\omega) = \frac{\omega 2 d_2}{\omega(t_2 - t_1) + \theta(\omega) - \theta_d(\omega) + m\pi} \tag{6}$$

where $t_1 = t_{d1} + t_{s1}$, $t_2 = t_{d2} + t_{s2}$, $\theta(\omega) = \phi_2(\omega) - \phi_1(\omega)$, $\theta_d(\omega)$ is the phase difference due to diffraction [3] and m is a correction term if a phase shift of π is added by the proposed method. In this study $m = 0$ if the proposed method inverts $p_1(t)$ to compensate for the extra phase shift that occurred, $m = 1$ if $p_1(t)$ and $p_2(t)$ are not inverted and $m = -1$ if both $p_1(t)$ and $p_2(t)$ are inverted.

2.3 Experiment

The experimental setup consists of a broadband transducer with a centre frequency of 10 MHz (V311), manufactured by Panametrics, Waltham, MA, USA. A pulser/receiver 5072PR from Panametrics was used to excite the transducer and amplify the received signal. The signal was then digitized using a CompuScope 14100 oscilloscope card, by Gage Applied Technologies Inc., Lachine, QC Canada, with 14-bit resolution and a sampling rate of 100 MHz. All data was stored in a computer for off-line analysis. The resulting time-domain waveforms were calculated off-line using the average of 100 sampled waveforms to reduce random noise. Before the averaging process, the sampled waveforms are aligned to reduce timing jitter by employing a method proposed by [4]. A digital thermometer F250, by Automatic Systems Laboratories LTD, England, monitored the temperature both in the suspension under test and in the room. The temperature in the pulp suspensions under test was $20.0 \pm 0.2°C$. The pulp suspensions was carefully poured into the measurement cell and thereafter stirred slowly to remove air bubbles from the suspension. An illustration of the measurement cell is shown in Fig. 1 and is described in detail in [5]. To accurately determine the distance d_2 in the cell, pure, distilled water was used as a reference since it has a well known relationship between speed of sound and temperature, see [6]. Using the temperature of the calibration fluid and a cross-correlation technique to determine the time-of-flight for an ultrasonic pulse, the distance d_2 was found to be 0.03010 ± 0.00004 m.

The pulp samples used in this study were produced from thermo-mechanical pulp (TMP). The TMP was fractionated by Bauer-McNett fractionator according to SCAN-standard 6:69 [7]. This process separated the pulp into two fractions; a fibre fraction

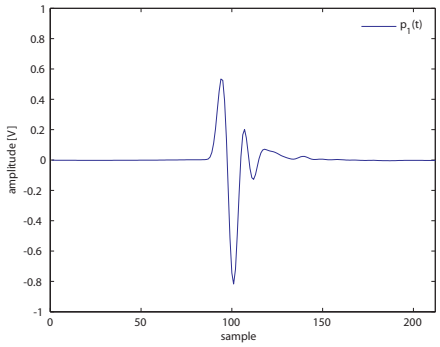

(a)

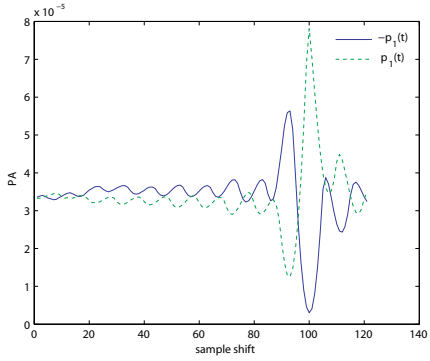

(b)

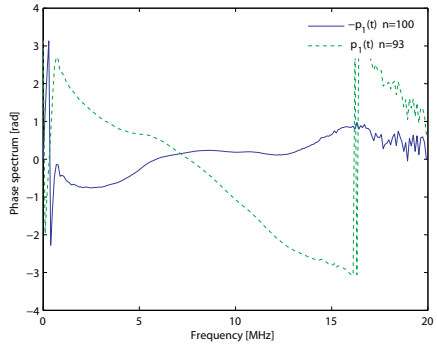

(c)

Figure 3: (a) shows echo $p_1(t)$. (b) shows the results of $pa(m)$ from $p_1(t)$ and when $p_1(t)$ is inverted. (c) shows the phase spectrum of $p_1(t)$ and $-p_1(t)$ when the echoes are shifted 93 and 100 samples respectively, i.e at respective minimum of pa

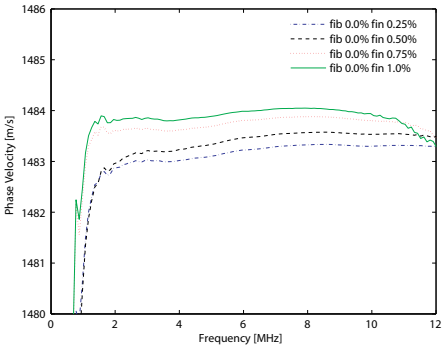

Figure 4: Phase velocity in pulp suspension containing fines and no fibres

and a fines fraction. The fibre fraction consists of fibres that passed the 48 wire mesh, resulting in fibre lengths that vary between 1-3 mm and diameter of 20-50 μm. The fines were obtained by passing the pulp through the 200 wire mesh and then subsequently filtered through 400 wire mesh. They have a length of 30-74 μm and a diameter of a few μm. Both the fines and fibre size distributions were analyzed using a Kajaani Fiberlab instrument, Metso Corporation, Finland. From these fractions, a set of samples were made by mixing fibres and fines at predetermined ratios between 0-1.0% by mass.

2.4 Results

The results from the phase velocity measurement for suspensions containing only fines is shown in Fig.4. The figure shows that the velocity dispersion is small within the bandwidth of the ultrasonic pulse, 1.8-10 MHz, and that the phase velocity increases with increasing amount of fines in the suspension.The uncertainty in the measurement is ± 0.3 m/s based on ± 2 standard deviations.

Fig. 5, shows measurements of phase velocity for samples where the mass faction of fibres are the same as for fines. In this case, the velocity dispersion is noticeable and it is seen to correlate well with mass fraction, giving higher velocity dispersion with higher mass fraction. As an example, the velocity for 1.0% mass fraction changes from the lowest below 4 MHz to be the highest above.

3 Attenuation

3.1 Theory

The model is based on calculating the energy loss in the scatter wave from an infinitely long, viscoelastic, isotropic, cylindrical fibre. It is described in full in [8]. In [8], the modelled attenuation agrees well with experimental results of synthetic fibres such as

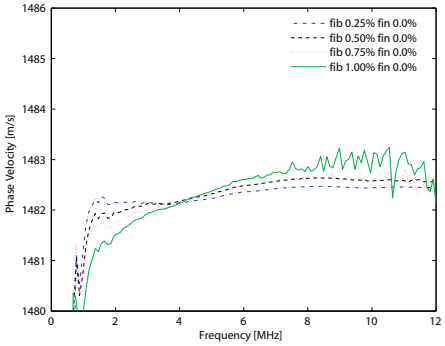

Figure 5: Phase velocity in pulp suspension containing fibres and no fines

nylon and shows localised extrema in the frequency response of attenuation. These peaks in frequency response of the attenuation are thought to be at the vibrational modes of the fibres. Although the locations of these peaks depend largely on the diameter of the saturated fibres, they also depend on their material properties.

In nylon, the locations of the peaks are more repeatable and hence more reliable than the measurement of the attenuation itself which varies due to the inhomogeneous nature of the suspension. The repeatability of the frequency at which these peaks occur and the fact that changes in diameter, Poisson's Ratio, Young's Modulus and the density of the fibre produce different effects on the shape of the modelled frequency response of the attenuation, means that the suspension can be better characterised if these extrema can be located.

The aim is, therefore, to determine if localised extrema also exist in the frequency response of the attenuation of wood fibres. This would allow us to solve the inverse problem with less ambiguity than attempting to solve the inverse problem from a simple curve.

The model shows the attenuation in the frequency range 1Mhz to 25 MHz to be very sensitive to fibre diameter. Using an average fibre diameter of 40 μm localised maxima in attenuation were predicted to be between 5 MHz to 10 MHz. However, the wood fibres in paper pulp have different diameters hence the diameter distribution of the wood samples is required to produce expected attenuation.

3.2 Experiment

The same measurement cell and paper pulp samples were used as in the phase velocity experiments. As the diameter of wood fibres are smaller than nylon the peaks are expected to appear at a higher frequency. Hence a 30 MHz transducer (Panametric V333) was used and the signal digitised by a CompuScope 102G oscilloscope card (Gage Applied Technologies, Inc Lachine QC Canada) with a 10-bit resolution and a sample rate

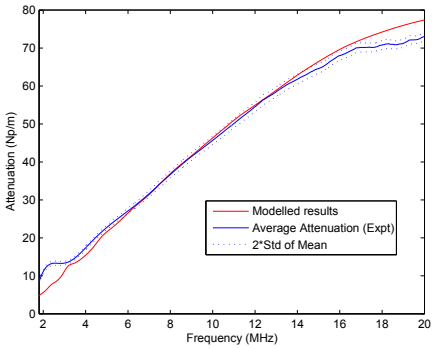

Figure 6: Comparison of the modelled attenuation to the measured attenuation for 0.5% concentration of wood fibres. Plot of the mean and 2x STD of the mean for 300 readings. The following material properties for saturated wood fibres were used in the model: density=1500 kg/m^3, Poisson ratio = 0.45, speed of sound= 1050 m/s and loss tangent=0.2. The properties of water were assumed to be: density=996 kg/m^3, speed of sound=1490 m/s, and viscosity=$9.4 \cdot 10^{-4} Pa \cdot s$

of 2GHz. The distance the signal travelled was calculated using the method previously described. Since the initial echo from the buffer rod could not be easily identified, the attenuation in the sample was obtained using pure, distilled water as reference giving,

$$\alpha_s(f) \quad = \quad \alpha_w(f) + \frac{1}{2d_2} ln \left(\frac{|P_w(f)|}{|P_s(f)|} \right) \tag{7}$$

where α_s is the attenuation in the sample, d_2 is the distance travelled by the signal, $P_s(f)$ is the amplitude in the frequency domain of the second echo in the sample and $P_w(f)$ is the amplitude in the frequency domain of the second echo in water. $\alpha_w(f)$ is the attenuation of water [9] and is assumed to be

$$\alpha_w(f) \quad = \quad 25 \cdot 10^{-15} f^2 \tag{8}$$

3.3 Results

Figure 6 is a comparison of the experimentally calculated average attenuation and the modelled attenuation. Good agreement has been obtained by adjusting the saturated wood fibre properties. The maximum at 2.2 MHz in the experimental results is not reflected in the model results though a small maximum does exists at 2.4 MHz and a slightly large one at 3.2 MHz, corresponding to fibres with diameters of 60 μm and 40μm respectively. This lack of agreement could be because the model is for a fibre that is continuous over its cross section. As wood fibres are hollow the vibrational modes, which are believed to be causing the maxima, will not occur at the frequencies predicted by the model. However, it may also be due differences between the distribution of the diameters in this particular sample and that used in the size analysis. The peak could also be an

experimental artifact. The sensitivity of the modelled attenuation on the fibre diameter, means the distribution of the diameters is the dominant factor in determining the material properties of the suspended fibres. With unknown fibre diameter distributions, there is a greater possibility of determining the diameters of the fibres if the local extrema in the frequency response of the attenuation are clear. However, the superposition of maxima and minima of one wood fibre diameter with other fibres of a different diameters results in a the smoothing of the signal, masking the effects of the individual fibres. The featurelessness of the curve means that the calculation of the material properties from the experimental measured attenuation is ambiguous. Combinations of different values can give similar results.

4 Conclusion

In this study we have considered measurements of phase velocity and attenuation in pulp suspensions. The proposed method to calculate phase velocity avoids the ambiguity with phase unwrapping if the medium is weakly dispersive. The result shows that the phase velocity increases with increasing amount of fines in the suspension. The dispersion is caused by the fibres and it correlates with fibre mass fraction.

The results of the attenuation experiments show that it is possible to inversely calculate wood fibre properties by fitting the model to the experimental data, if the fibre diameter distribution is known. However, the accuracy of these calculation is difficult to determined and more work in this area is required.

5 Further Work

The proposed minimum phase angle, or MPA, method has to be tested in cases when the phase velocity is highly dispersive.

The peak in the experimental results of the frequency response of attenuation at 2.2 MHz needs further investigation. Experiments on synthetic fibres are being carried out to explore the effect of hollow compared to solid fibres. If these effects are significant, further development of the model is required to take this into account.

References

[1] P. He, "Experimental verification of models for determining dispersion from attenuation," *IEEE Transactions on Ultrasonics, Ferroelectrics, and Frequency Control*, vol. 46, no. 3, pp. 706–714, 1999.

[2] J. Tribolet, "A new phase unwrapping algorithm," *IEEE Transactions on Acoustics, Speech, and Signal Processing*, vol. 25, no. 2, pp. 170–177, 1977.

[3] P. Rogers and A. Van Buren, "An exact expression for the lommel diffraction correction integral," *Journal of the Acoustical Society of America*, vol. 55, no. 4, pp. 724 – 8, 1974.

[4] A. Grennberg and M. Sandell, "Estimation of subsample time delay differences in narrowband ultrasonic echoes using the hilbert transform correlation," *IEEE Transactions on Ultrasonics, Ferroelectrics, and Frequency Control*, vol. 41, no. 5, pp. 588–595, 1994.

[5] T. Löfqvist, "Ultrasonic wave attenuation and phase velocity in a paper-fibre suspension," in *Proc.IEEE Ultrasonics Symposium*, vol. 1, Oct 1997, pp. 841–844.

[6] N. Bilaniuk and G. S. K. Wong, "Speed of sound in pure water as a function of temperature," *The Journal of the Acoustical Society of America*, vol. 93, no. 4, pp. 2306–2306, 1993.

[7] *SCAN-M 6:69, Fibre fractionation of mechanical pulp in the McNett apparatus*, Scandinavian Pulp, Paper and Board Testing Committee, Stockholm.

[8] Y. Aitomäki and T. Löfqvist, "Estimating suspended fibre material properties by modelling ultrasound attenuation," in *Mathematical modeling of wave phenomena: 2nd Conference on Mathematical Modeling of Wave Phenomena*, B. Nilsson and L. Fishman, Eds., vol. 834:1. AIP, 2006, pp. 250–259.

[9] L. Kinsler, A. Frey, A. Coppens, and J. Sanders, *Fundamentals of Acoustics*, 4th ed. John Wiley and Sons Inc., 2000.

,

Paper C

Sounding Out Paper Pulp: Ultrasound Spectroscopy of Dilute Viscoelastic Fibre Suspensions

Authors:
Yvonne Aitomäki and Torbjörn Löfqvist

Presented at:
Proceedings from the Acoustics and ultrasonics in the processing of industrial soft solids

Sounding out Paper Pulp: Ultrasound Spectroscopy of Dilute Viscoelastic Fibre Suspensions

Yvonne Aitomäki and Torbjörn Löfqvist

Abstract

A model of attenuation of ultrasound in fibre suspensions is compared to a model of backscattering pressure from submersed cylinders subjected to a sound wave. This analysis is carried out in the region where the wavelength is of the same order as that of the diameter of the fibre. In addition we assume the cylinder scatterer to have no intrinsic attenuation and the longitudinal axis of the scatterer is assumed to be perpendicular to the direction of propagation of the incident wave. Peaks in the frequency response of both the backscattering pressure, expressed in the form of a form function, and the attenuation are shown to correspond. Similarities between the models are discussed. Since the peaks in the form function are due to resonance of the cylinder, we infer that the peaks in the attenuation are also due to resonance. The exact nature of the waves causing the resonance are still unclear however the first resonance peaks are related to the shear wave and hence the shear modulus of the material. The aim is to use the attenuation model for solving the inverse problem of calculating paper pulp material properties from attenuation measurements. The implications of these findings for paper pulp property estimation is that the supporting fluid could, if possible, be matched to density of that of pulp fibres and that the estimation of material properties should be improved by selecting a frequency range that in the region of the first resonance peaks.

1 Introduction

This study is part of a project aimed at the on-line characterisation of pulp fibres suspended in water, as used in the paper manufacturing industry. An analytical model was developed to relate ultrasound attenuation to the material properties of the fibre and the supporting fluid. This model was presented in [1]. This has then been used this to solve the inverse problem of estimating material properties from measurements of ultrasonic attenuation in dilute suspensions of viscoelastic fibres [2].

Experiments from these studies showed local peaks in the frequency response of the attenuation [1, 2]. The focus of the study is on the cause of these peaks. A large body of work exists on attenuation due to suspended spherical particles, as reviewed in [3]. However, for cylindrical scatterers, much of the work has been based on backscattering and in the regime where the ratio of the wavelength to the diameter of the scatterer is small [4–9]. One of the theories arising from these works is the Resonance Scattering Theory (RST) [5]. This study compares the backscattering from theory developed for a

submersed cylinder [10] to a model of ultrasonic attenuation in a suspension of fibres in a fluid [1]. The theory developed by [10] is essentially the same as the nuclear scattering theory introduced in the derivation of the RST theory [5]. In this study we will use the rewritten version of [10] found in [11] since this matches the propagation direction of the wave used in the attenuation model.

Once a comparison of the resonance peaks is made, the explanation for the peaks in the backscattering is investigated to see if it is valid for the peaks found in the attenuation.

2 Theory

The attenuation is calculated from the simple cylinder scattering, (SCS), model [1]. The derivation of this model follows Habeger [12] cylindrical extension of the Epstein and Carhart [13]/Allegra Hawley [14] model. The resulting expression for the attenuation, α, of a suspension of fibres in a fluid of low viscosity, such as water is

$$\alpha = \frac{-2f_r}{\pi R^2 k}\Re\left(\int_0^{\frac{\pi}{2}}(\epsilon_n^2 B_n)\cos(\psi)d\psi\right), \tag{1}$$

where f_r is the volume fraction; R is the radius of the fibre; k is the wave number of the wave in water; ψ is the angle of the fibre to the direction of the oncoming plane ultrasound wave; $\epsilon_n = 1$, if $n = 0$, otherwise $\epsilon_n = 2$, and n is a positive integer. B_n are the n^{th} expansion coefficients of the wave potential of the reflected wave. The coefficients, B_n, are a function of the fluid properties: viscosity, density and speed of the compression wave and the fibre properties: shear modulus, density, loss tangent and speed of both the compression and the shear wave. The speed of the shear wave is a function of the shear modulus and the density and is related to the compression wave speed by Poisson's ratio.

For the purpose of the comparison between the attenuation and backscattering we assume that the axial plane of the fibres is perpendicular to the direction of propagation of the wave. Since we are focusing on the frequency at which the peaks occur we also assume that there is no intrinsic attenuation in the cylinder. This is done by setting the loss tangent to zero.

The expression for backscattering pressure from a cylinder at a large distance from the cylinder is

$$P_s \approx \sqrt{\frac{2a}{2r}}e^{ikr}f_\infty(\pi) \tag{2}$$

where P_s is the scattering pressure; a is the size of the scatterer and in this case equals R; r is the distance to the scatterer centre, k is the wave number of the wave in the fluid and $f_\infty(\pi)$ is the form function [5, 10].

The form function can be expressed using a phase shift expression, where the phase shift is that between the incident and reflected wave such that:

$$f_\infty(\pi) = \frac{2}{\sqrt{\pi ka}}\sum_{n=0}^{\infty}(-1)^n\epsilon_n\sin(\eta_n)e^{-i(\eta_n+\frac{3\pi}{4})} \tag{3}$$

where η_n is the phase shift [11] and is defined as,

$$\eta_n = \arctan\left[\tan\delta_n(ka)\frac{\tan\alpha_n(ka)+\tan\phi_n(k_La,k_Ta)}{\tan\beta_n(ka)+\tan\phi_n(k_La,k_Ta)}\right] \tag{4}$$

The following functions were used in the above equation:

$$\tan\alpha_n(x) = -x\frac{J_n'(x)}{J_n(x)}, \tag{5}$$

$$\tan\beta_n(x) = -x\frac{N_n'(x)}{N_n(x)}, \tag{6}$$

$$\tan\delta_n(x) = -x\frac{J_n(x)}{N_n(x)}, \tag{7}$$

$$\begin{aligned}\tan\phi_n(k_La,k_Ta) &= \frac{\rho_1(k_Ta)^2}{2\rho_2} \\ &\times \frac{\dfrac{\tan\alpha_n(k_La)}{\tan\alpha_n(k_La)+1}-\dfrac{n^2}{n^2-\dfrac{(k_Ta)^2}{2}+\tan\alpha_n(k_Ta)}}{\dfrac{n^2-\dfrac{(k_Ta)^2}{2}+\tan\alpha_n(k_La)}{\tan\alpha_n(k_La)+1}-\dfrac{n^2\cdot(\tan\alpha_n(k_Ta)+1)}{n^2-\dfrac{(k_Ta)^2}{2}+\tan\alpha_n(k_Ta)}}.\end{aligned} \tag{8}$$

Here, ρ_1 is the density of the water; ρ_2 is the density of the solid, k_T is the wave number of the shear wave in the solid; k_L is the wave number of the compression wave in the solid and n is a positive integer. J_n and N_n are Bessel function of the 1st kind and 2nd kind respectively, to the order n and J_n' and N_n' are the derivatives of the Bessel functions of the 1st kind and 2nd kind respectively, to the order n.

The frequency range is expressed in terms of normalised frequency $F_n = ka$, and we consider the range F_n from 0.2 to 5. The series expansion is truncated after eleven terms.

3 Results

The parameters in the models are set based on the material properties of Nylon 66 and water. However, as previously stated we are focusing on the frequency at which the peaks occur, so the loss tangent of the cylinder material is set to zero. To ease the comparison between the peaks in both backscattering and the attenuation, the amplitude of the attenuation is scaled and offset by 2 units. The results are presented in Figure 1.

Under these conditions there is a good match between the backscattering form function, $f_\infty(\pi)$ and the attenuation, α. The match between these two functions has two

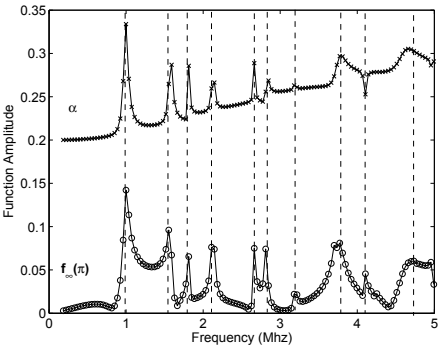

Figure 1: Plot of the acoustic attenuation, α, and the form function, $f_\infty(\pi)$, against normalised frequency for nylon fibres suspended in water. To ease the comparison between the peaks in both functions, the amplitude of the attenuation is scaled and offset by 2 units.

consequences. Firstly, the solution for the expansion coefficients used by Faran [10] can be used in the calculation of attenuation -equation (2) -instead of the solution for the expansion coefficient used in the attenuation. This results in a simpler solution as that used by Faran [10] uses slip boundary conditions. We can then compare the amplitudes of the attenuation calculated using the two different solutions for the expansion coefficients and hence the effects of the different boundary conditions. Work on this continues.

The second consequence of the match between the form function and the attenuation is that the resonance peaks in the form function have been well discussed, in both [10] and [6]. Faran [10] states that the normal modes of the cylinder are found when the normal component of the stress and the tangential component of the shear stress at the solid boundary are zero gives a condition which is identical to setting the denominator of Equation (8) to zero. Using this condition the normal modes can be calculated from Equation (8). Faran [10] also discusses that a shift in the resonance frequency of an immersed cylinder due to the reactive component of the acoustic impedance acting on the scatterer by the surrounding fluid. Although in his study this shift was small as the metal cylinders that were used had much greater densities than the surrounding fluid, in our case, where the density of nylon is close to that of water, the effect will be considerable. When calculating the normal mode for nylon, the first mode occurs at a normalised frequency of 1.4 (R = 44 μm, 7.8 MHz), however, the effect of the surrounding fluid moves this peak to a normalised frequency of 1.0 (R = 44 μm, 5.3 MHz). The frequency can be found by setting the denominator in equation 4 to zero. Also discussed is the fact that the since the speed of the shear waves is much lower than the speed of the compression wave. The first modes to appear are from the shear wave. Since the $n = 0$ does not support shear waves, the frequency of this mode depends on the speed of the wave and hence occurs at a normalised frequency of 3.57 (R = 44 μm, 19.3 MHz). These calculations are for a cylinder with no loss.

Resonances in backscattering are explained as being caused by creeping waves in the fluid and in the solid [6]. However, the assumption used in these explanations is that the normalised frequency is much greater than 1, which is not the case here. Hence the actual wave propagation modes in this region of normalised frequency are still not clear.

4 Conclusion

From the results so far it appears that the coefficient derived by Faran [10] for backscattering can be used to derive attenuation. From this model, the resonance modes of a cylinder and a cylinder in water can be obtained. They confirm that the peaks in the attenuation curves are due to resonance. It appears as if the shear waves are causing first peaks in the ultrasound attenuation although the exact nature of these waves has not been established. These calculations have been done under the conditions of no loss.

The implication of these findings for the use of estimating material properties of paper pulp from ultrasound attenuation are that, if possible, the density of the surrounding fluid should be as close as possible to that of the suspended fibre. This increases the phase shift in the suspension and increases the dependency of the attenuation on the material properties of the fibre. The frequency range should also be set, if possible, so that resonance peaks exists within the range. Since the frequencies of the peaks depend on the material properties of the fibre, identifying these frequencies should aid in estimating material properties.

References

[1] Y. Aitomäki and T. Löfqvist, "Estimating suspended fibre material properties by modelling ultrasound attenuation," in *Mathematical modeling of wave phenomena: 2nd Conference on Mathematical Modeling of Wave Phenomena*, B. Nilsson and L. Fishman, Eds., vol. 834:1. AIP, 2006, pp. 250–259.

[2] Y. Aitomäki, "Towards a measurement of paper pulp quality: ultrasonic spectroscopy of fibre suspensions," Licentiate Thesis, Luleøa University of Technology, 2005.

[3] R. Challis, M. Povey, M. Mather, and A. Holmes, "Ultrasound techniques for characterizing colliodal dispersions," *Reports in Progress in Physics*, vol. 68, pp. 1541–1637, 2005.

[4] H. Uberall, G. Gaunaurd, and J. Diarmuid Murphy, "Acoustic surface wave pulses and the ringing of resonances," *Journal of the Acoustical Society of America*, vol. 72, no. 3, pp. 1014–1017, Sept 1982.

[5] J. Diarmuid-Murphy, J. George, A. Nagl, and H. Uberall, "Isolation of the resonant component in acoustic scattering from fluid-loaded elastic spherical shells," *Journal of the Acoustical Society of America*, vol. 65, no. 2, pp. 368–373, Feb 1979.

[6] L. Flax, L. Dragonette, and H. Uberall, "Theory of elastic resonance excitation by sound scattering," *Journal of the Acoustical Society of America*, vol. 63, no. 3, pp. 723–730, Mar 1978.

[7] H. Uberall, L. Dragonette, and L. Flax, "Relation between the creeping waves and the normal modes of vibration of a curved body," *Journal of the Acoustical Society of America*, vol. 61, no. 3, pp. 711–715, Mar 1977.

[8] J. Dickey, G. Frisk, and H. Uberall, "Whispering gallery wave modes on elastic cylinders," *Journal of the Acoustical Society of America*, vol. 59, no. 6, pp. 1339–1346, June 1976.

[9] G. Frisk, J. Dickey, and H. Uberall, "Surface wave modes on elastic cylinders," *Journal of the Acoustical Society of America*, vol. 58, no. 5, pp. 996–1008, Nov 1975.

[10] J. Faran, "Sound scattering by solid cylinders and spheres," *Journal of the Acoustical Society of America*, vol. 23, no. 4, pp. 405–418, July 1951.

[11] J. Mathieu and P. Schweitzer, "Measurement of liquid density by ultrasound backscattering analysis," *Meausurement Science and Technology*, vol. 15, pp. 869–876, 2004.

[12] C. Habeger, "The attenuation of ultrsound in dilute polymeric fiber suspensions," *Journal of Acoustical Society of America*, vol. 72, pp. 870–878, sep 1982.

[13] P. Epstein and R. Carhart, "The absorption of sound in suspensions and emulsions. i. water fog in air," *The Journal of the Acoustical Society of America*, vol. 25, no. 3, pp. 553–565, May 1953.

[14] J. Allegra and S. Hawley, "Attenation of sound in suspension and emulsions: Theory and experiments," *The Journal of the Acoustical Society of America*, vol. 51, no. 5, pp. 1545–1564, 2 1972.

,

Paper D

Inverse Estimation of Material Properties from Ultrasound Attenuation in Fibre Suspensions

Authors:
Yvonne Aitomäki and Torbjörn Löfqvist

Reformatted version of paper originally published in:
Elsevier Ultrasonics, Volume 49, Issues 4-5, May 2009, Pages 432-437

Inverse Estimation of Material Properties from Ultrasound Attenuation in Fibre Suspensions

Yvonne Aitomäki and Torbjörn Löfqvist

Abstract

An investigation of a new method for measuring fibre material properties from ultrasonic attenuation in a dilute suspension of synthetic fibres of uniform geometry is presented. The method is based on inversely solving an ultrasound scattering and absorption model of suspended fibres in water for the material properties of the fibres. Experimental results were obtained from three suspensions of nylon 66 fibres each with different fibre diameters. A forward solution to the model with reference material values is compared to experimental data to verify the model's behaviour. Estimates of the shear and Young's modulus, the compressional wave velocity, Poisson's ratio and loss tangent from nylon 66 fibres are compared to data available from other sources. Experimental data confirms that the model successfully predicts that the resonance features in the frequency response of the attenuation are a function of diameter. Consistent estimated values for the compressional wave velocity and the Poisson's ratio were found to be difficult to obtain but in combination gave values of shear modulus within previously reported values and with low sensitivity to noise. Young's modulus was underestimated by 54% but was consistent and had low sensitivity to noise. The underestimation is believed to be caused by the assumption of isotropic material used in the model. Additional tests on isotropic fibre would confirm this. Further analysis of the model sensitivity and the reasons for the resonance features are required.

1 Introduction

The quality of paper pulp depends on a large number of factors and some of these are the properties of the pulp fibre itself [1]. Measuring pulp fibre characteristics has therefore the potential to provide paper manufacturers with increased control over their pulp production. The measurement method being investigated here is based on ultrasound, as it is rapid, inexpensive, non-destructive and non-intrusive. Consequently, such measurements could be done online. As an initial step on the way to online measurement of pulp fibre properties, the aim of this measurement method is to provide ultrasonic based measurements of the material properties of finite length, uniform fibres in suspension. Two approaches that can be used to model ultrasound propagation in fibre suspensions are to model it either as a solid porous media or as cylindrical scatters suspended in a fluid. The solid porous media approach has been applied to paper pulp using Biot's model of the attenuation and velocity of ultrasound [2]. However, the structural and solid/fluid

interaction parameters are many and difficult to establish. Using dilute solutions and higher frequencies than the Biot model, scattering models can be considered. Epstein-Carhart/Allegra-Hawley [3, 4], (ECAH), model and the Harker and Temple model [5] have been developed for spherical-like particles in suspension. A review of these and other theories mainly based on spherical particles and their application to determining particle size distribution is found in [6]. Studies of cylindrical particles have concentrated on large scatterers, where the product of the wave number and the radius, kR, is large and hence asymptotic assumptions can be made. In these studies, back-scattering rather than attenuation is considered [7, 8].

A scattering model for a suspension of fibres in water was developed by Habeger [9]. This is a cylindrical extension of the ECAH model and relates the attenuation to the properties of water, the properties of the fibre, and the fibre concentration. In the calculation of attenuation, the model equations are based on a number of different material properties and are solved numerically. Since the model is to be used to solve the inverse problem, i.e. determining the material properties from attenuation measurements, a simpler, analytical version of this model was sought which would have less unknown parameters and would have a quicker and more stable solution. By neglecting thermal effects and assuming low viscosity in the suspending fluid, a more tractable set of equations is reached that can be solved analytically [10]. This simplified cylinder scattering (SCS) model is the basis for the measurement method described here.

Firstly we test the model's forward, predictive accuracy and behaviour and secondly, its suitability for providing inverse solutions. In the predictive part we experimentally verify the model's response to changes in fibre diameter given reference data for the fibre properties. In the inverse testing, we investigate whether the SCS model can be used to estimate material properties of fibres in suspension from the attenuation of ultrasound across a range of frequencies.

We start by describing the SCS model and the experimental procedure used to obtain the frequency response of attenuation of a suspension of nylon fibres in water. We discuss the results from the predictive and inverse tests and draw conclusions about the measurement methods as well make some suggestions for further work.

2 Theory

In the SCS model, the attenuation is calculated from the energy losses arising when a plane wave is incident upon an infinitely long, straight cylinder. The cylinder material is assumed to be isotropic and viscoelastic. The energy losses taken into account are from the wave being partially reflected, partially transmitted at the solid-fluid interface and from the generation of damped, transverse waves in the solid medium at the boundary. The highly damped thermal skin layer, that is generated by the acoustically induced pulsations of the solid has been shown to have the greatest effect at frequencies where the thermal wavelength is of the order of the radius [9]. To simplified the model we neglect these thermal effects but to reduce the impact this has on the model's accuracy we only consider frequencies above this thermally sensitive region. A viscous wave in the

fluid (as defined by [3]) is also generated but due to the low viscosity, the energy loss due to this wave is small and is also neglected. In the model the waves are expressed in terms of the wave potentials of the incident and reflected wave in the fluid and the compressional and shear wave potentials in the fibre. The derivation is presented in [10] and the resulting equation for the attenuation α is

$$\alpha = \frac{-2f_r}{\pi R^2 k_{c_1}} \sum_{n=0}^{\infty} \Re \left(\int_0^{\frac{\pi}{2}} \epsilon_n B_n \cos(\psi) d\psi \right) \quad (1)$$

where f_r is the volume fraction; R is the radius of the fibre; k_{c_1} is the wave number of the compressional wave in water; $\Re$ denotes the real part of the expression, ψ is the angle of between the axial plane of the fibre and the direction of the oncoming ultrasound wave; n is a positive real integer; $\epsilon_n = 1$ if $n = 0$, otherwise $\epsilon_n = 2$ and where B_n is the n^{th} expansion coefficient of the wave potential of the reflected wave. With the assumptions stated above, the solution for the coefficients B_n, comes from using the boundary condition of continuous velocity in the radial direction and continuous stress in radial, tangential and axial directions at the fluid-solid interface. The actual expression for B_n is solved analytically using Maple© (Maplesoft, Waterloo, Canada). The result is an expression for B_n as a function of the fluid properties: viscosity, ν_1, density, ρ_1 and velocity of the compressional wave, c_1 and the fibre properties: radius, R, density, ρ_2, velocity of the compressional wave, c_2, shear wave, cs_2 and the loss tangent, $\tan\delta$. $\operatorname{Tan}\delta$ is the tangent of the angle by which the strain in a solid lags the stress causing it and is often taken as the elastic energy losses in solids [11]. B_n is also an explicit function of the shear modulus, G. The model assumes the material to be isotropic hence the elastic properties are set by only two parameters, in this case the Poisson's ratio, ν and c_2. Details of the relationship between these two parameters and the properties: Young's modulus, E, G and cs_2, referred to later in the paper are given in the appendix.

As can be seen in equation 2, the attenuation is a function of the sum of B_n. In our experiments on nylon in water, the series was truncated at n =3, as higher terms did not have any significant effect on the attenuation in the frequency range we are considering.

3 Experiment

The experiments were carried out using the pulse-echo technique. A diagram of the measurement cell used in this study is shown in figure. 1. Three fibre suspensions were made up using different diameters of nylon 66 fibres (Swissflock, Emmenbrücke, Switzerland). The fibre dimensions are given in table 1. The fibres were weighed and mixed with distilled water to a concentration of 0.5% by weight. The broadband transducer (V319, Panametrics, Waltham, MA, USA) used had a centre frequency of 15 MHz. The transducer was excited and the received signal amplified by a pulser/receiver (Model 5073PR, Panametrics). The signal was then digitized using an oscilloscope card (CompuScope 12400, Gage Applied Technologies Inc., Lachine, QC, Canada) with a 12-bit resolution and a sampling rate of 400 MHz. All data were stored in a computer for off-line analysis.

Table 1: Fibre dimensions

Diameter		Length
Dry	Saturated	
(10^{-6} m)	(10^{-6} m)	(10^{-3} m)
14.8	14.9 ±1.5	1.2
43.6	45.9 ±7.2	1.5
49.6	51.9 ±2.0	1.5

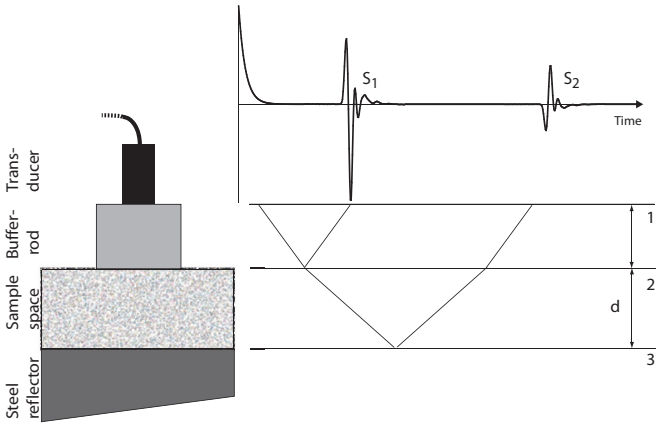

Figure 1: Diagram of the pulse-echo measurement system

The cell was calibrated using water, emptied and carefully filled with the fibre suspension. Each measurement set consisted of a sequence of 100 pulses and their echoes. Five sets were taken and the sample was stirred after each set. The cell was emptied and rinsed with temperature-controlled water, before the cell was filled with the next sample and the process repeated. Once all three samples were measured, the whole procedure was repeated twice more but with the samples measured in a different order. This resulted in 1500 pulse echoes for each sample

A digital thermometer (Model F250, Automatic Systems Laboratories LTD, England) monitored the temperature in the sample under test. During the whole process the temperature of the suspension varied from a minimum of 20.75±0.2 °C to a maximum of 21.47±0.2 °C. The temperature of the water during calibration was taken and used to calculate the velocity of the wave in the water. The distance d in figure 1 is the distance between the buffer rod and steel reflector. This was found using this wave velocity and the time-of-flight for an ultrasonic pulse to travel that distance. The latter was determined from a cross-correlation technique.

A fast Fourier transform was applied to each echo. The echoes were then averaged

and the attenuation calculated from

$$\alpha_E(f) = \frac{1}{2d} \ln \left(\frac{S_2 A_1}{S_1 A_2} \right) + \alpha_w, \tag{2}$$

where f is the frequency, $S_1 = S_1(f)$ and $S_2 = S_2(f)$ are the frequency dependent amplitudes of the first and second echoes in the sample, $A_1 = A_1(f)$ and $A_2 = A_2(f)$ are the frequency dependent amplitudes of the first and second echoes in water. α_w is the theoretical attenuation of water and equals $25 \cdot 10^{-15} f^2$ [12]. The addition of the expression

$$\frac{1}{2d} \ln \left(\frac{A_1}{A_2} \right) + \alpha_w, \tag{3}$$

in equation 2 serves to calibrate the sample signals with the signals from water to compensate for losses at the interfaces, transducer alignment and possible diffraction effects. The variance of the attenuation was calculated by first order approximations of the attenuation which is described particularly for the pulse-echo model by [13] in their comparison of parametric to non-parametric techniques for calculating ultrasound attenuation and phase velocity. Note that the noise in the signal from the distilled water sample is assumed to be insignificant as the signal in water has a high signal to noise ratio due to its low attenuation.

Lack of homogeneity of the fibre suspension is reduced by taking a large number of readings. On average the mass fraction of the measured suspension is equal to that of the whole sample. The volume fraction, f_r, used in the model, is calculated as,

$$f_r = \frac{\rho_1 m_f}{\rho_2 + (\rho_1 - \rho_2) m_f} \tag{4}$$

where m_f is the mass fraction, ρ_1 is the density of the water and ρ_2 is the density of the fibre.

Method for Parameter Estimation

The second part of the study tested the inverse solution of the model. An iterative search was used to find the values of the material properties that minimises the difference between the model attenuation and the average measured attenuation, over a range of frequencies with a known fibre diameter. After initial trial runs with four material properties being estimated i.e. ρ_2, c_2, ν and $\tan\delta$, it was decided that the known value of the density should be used in the model. The density was fixed to improve the accuracy of the other three material properties and is a property that in general can be measured using alternative methods. Additionally, work done by [14] on fibres in pulp indicates that the density of fibre material does not vary significantly. Elastic properties such as the G and E were calculated using the formula set out in the appendix, as mentioned earlier.

Table 2: Limits used in the parameter estimation procedure.

Material Property	Upper Value	Lower Value
c_2	500 ms^{-1}	7000 ms^{-1}
ν	0.2	0.5
$\tan\delta$	0	1

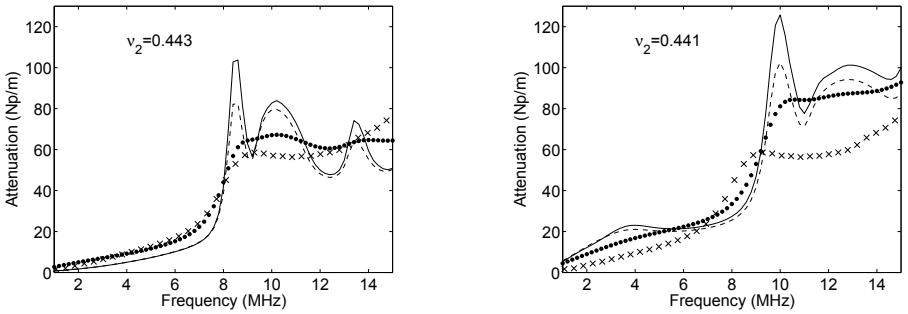

(a) (b)

Figure 2: Predicted and measured attenuation for the 52μm nylon 66 fibres. The experimental attenuation is marked with crosses. The predicted attenuation is modelled in figure (a) with υ =0.443 and in figure (b) with υ = 0.410. The other material property values used in the calculation were $c_2 = 2600$ ms^{-1}, tan $\delta = 0.03$ (solid line)/tan $\delta = 0.2$ (dotted line), $\rho_2 = 1140$ kgm^{-1}. The dashed line includes thermal and viscous terms.

The algorithm used was a constrained non-linear least squares fit [15]. The constraints were limits were set on the material properties (see table 2) so that the minimised cost function would only be a result of realistic values of c_2, ν and $\tan\delta$. The algorithm was set initially to fit the average experimental attenuation curve. It was run a 100 times with randomised initial values for the material properties for each of the three different fibre suspensions. The sensitivity of the algorithm to noise in the data was measured by setting the algorithm to fit the average experimental attenuation curve plus then minus two standard deviations and recording the effect on the material parameter estimations.

4 Results and Discussion

4.1 Parameter Estimation

The predicted attenuation was calculated for two different diameters of fibre suspensions using the values in table 1 over a frequency range matching that of the bandwidth of the transducer. This predicted and the average measured attenuation is plotted for the larger fibre suspension in figures 4.2(a) and 4.2(b) and for the smaller fibre suspension in

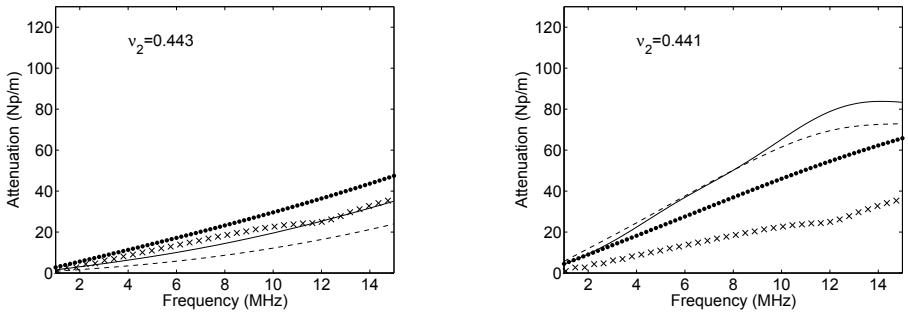

(a) (b)

Figure 3: Predicted and Measured attenuation for the 15 μm nylon 66 fibres. As in figure 4.3(b), the predicted attenuation is modelled in figure (a) with υ =0.443 and in figure (b) with υ = 0.410. The other material property values used in the calculation were as before. Again, the dashed line includes thermal and viscous terms.

figures 4.3(a) and 4.3(b). c_2 and υ in figures 4.2(a) and 4.3(a) are such that the value for G matches the reference values for nylon film. As can be seen for both fibre diameters these values for c_2 and υ_2 give a better fit to the experimental attenuation than the values for c_2 and υ_2 used in figures 4.2(b) and 4.3(b). The latter two figures had values for c_2 and υ_2 that matched the value of E for isotropic nylon 66. This suggests that the model is sensitive to the combined values of c_2 and υ_2 but it also highlights the problem of using isotropic material reference data for fibres that would be better described as transversely isotropic.

Comparing figures 4.2(a) and 4.3(a) we see that the model predicts features in the attenuation in the larger fibre suspension but not in the attenuation in the smaller fibre suspension. The measured attenuation supports this, however the attenuation feature in the larger fibre suspension is not as predominant as that predicted, nor is there more than one feature in the measured attenuation, in the frequency range under consideration. The features are believed to be caused by resonance in the fibres associated with the fibre diameter. Their location in the frequency domain is therefore a function of the diameter of the fibre, as seen in the figures where the material properties are kept constant and the fibre diameters change. Note that the fibre length of the larger fibres and the smaller fibres does in fact differ by 0.2 mm. However it was assumed that the difference in length, which is relatively small in comparison to the difference in diameter, would not cause the difference in the resonance effects seen here for three reasons. Firstly, because the fibres tend to have crushed ends where they have been chopped hence reducing end reflections. Secondly, there is intrinsic attenuation in the fibre material and thirdly, because resonance features in the model are not length dependant due to the fact that the model is based on infinitely long fibres.

The value for B_1 including thermal and viscous effects was solved numerically using the data in table 3, as done by [9]. This was done to examine the effect on the predicted

Table 3: Thermal properties for nylon 66 from [9]

Thermal Material Property	Value
Heat capacity (Jkg°K)	1420
Heat conductivity coefficient ($\mathrm{Wm^{-1}K^{-1}}$)	0.36
Thermal expansivity ($\mu\mathrm{K^{-1}}$)	60

attenuation of neglecting the thermal effects and shear in the fluid. These results are plotted in figures 2 and 3 with dashed lines. They show that including these effects slightly dampens the resonance feature and in general lowers the predicted attenuation but does not affect the location of the resonance feature in the larger fibre. Increasing tan δ also has a dampening effect as illustrated by the dotted lines in figure 2 and 3. Although with the increased tan δ the curves are closer to the shape of the measured attenuation, it too does not affect the location of the resonance feature as illustrated by the plots of the larger fibre.

Noise in the measured attenuation is expressed in terms of the standard deviation as a percentage of the attenuation. The maximum values in the chosen frequency region are 0.2%, 3.4% and 3.9% for the 15 μm, 46 μm and 52 μm fibres, respectively. The maximum standard deviation occurs at the higher frequencies where the signal-to-noise ratio is smaller.

The diameter values used in the predicted attenuation are from table 1. The diameter measurements made of the water saturated fibres compared well to the diameters stated by the manufacturer plus the 8% volumetric swelling that is stated in [16] for water saturated nylon 66.

4.2 Parameter Estimation

Estimates for the material properties were found from the best-fit solution to each of the average measured attenuation curve of the three different fibre suspensions. The 100 random initial values gave rise to a number of clustered values for c_2, υ_2 and tan δ. The c_2 and υ_2 values were used to calculate E and G. Figure 4 is a plot of the resulting estimates for E, G and tan δ for the three different fibre diameter. The size of the marker in figure 4 represents the value of the cost function and the colour, the value of tan δ.

For the 52 μm diameter fibre suspensions, the cluster with the lowest cost function contained 45% of the best-fit solutions to the attenuation. For the 46 μm diameter fibre suspension the cluster contained 30% of the best-fit solutions. These best-fit results are plotted in figure 5. The material property values that gave these best-fit solutions are presented in table 4 and show that the solutions with these low cost functions were much closer to the reference material properties values given in table 5 than the solutions with higher cost functions. This positive results suggests that the model can be used in solving the inverse problem. The solutions that gave higher cost function were presumed to be caused by the optimisation algorithm falsely identifying local minima as the global

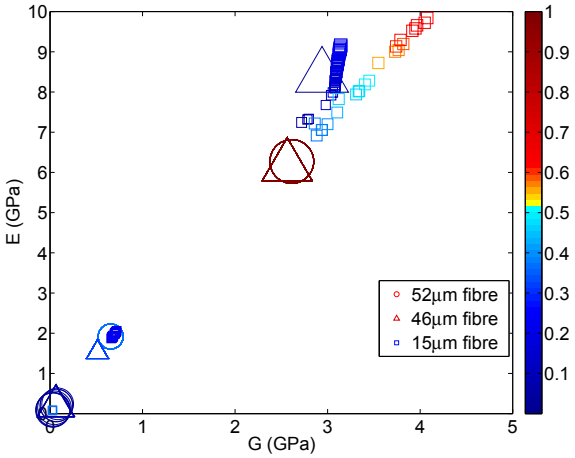

Figure 4: Scatter Plots of the estimated E and G with the value of tan δ represent by colour. The different symbol represent the different fibre suspension. The size of the symbol represents the size of the cost function hence a small symbol represents a better fit.

Table 4: Estimated Values for nylon 66 material properties from the attenuation in the suspensions of the 3 different fibre diameters

Attenuation Value	Measured Diameter 10^{-6} m	c_2 ms^{-1}	ν	tan δ	E GPa	G GPa
Average		2051	0.418	0.222	1.92	0.68
Av. + 2SD	14.8	2072	0.420	0.225	1.94	0.68
Av. - 2SD		2053	0.417	0.217	1.92	0.68
Average		4404	0.488	0.325	1.53	0.51
Av. + 2SD	45.9	6611	0.495	0.334	1.55	0.52
Av. - 2SD		3456	0.480	0.320	1.47	0.49
Average		2897	0.463	0.362	1.92	0.66
Av. + 2SD	51.9	3835	0.481	0.419	1.82	0.68
Av. - 2SD		2460	0.445	0.325	1.98	0.61

Table 5: Table of reference values for nylon 66 material properties. Nylon sheet and block data is obtained from [17] and Goodfellows Cambridge Limited, England respectively, except where marked. Data from [17] shows that the effect of increasing the frequency on the elastic moduli of nylon 66 is offset by the effect of the water saturation, hence elastic data obtained under dry, quasi-static conditions is comparable to that obtained under saturated, high frequency conditions. $E_z, E_{\theta,r}, G_z$ and $G_{\theta,r}$ were derived from compliance data from [17] using a tensor matrix for transversely isotropic materials, such as [18].

Description	ρ_2 kgm^{-1}	c_2 ms^{-1}	ν	$\tan\delta$	E_z GPa	$E_{\theta,r}$ GPa	G_z GPa	$G_{\theta,r}$ GPa
Saturated, transversely isotropic sheets measured at high frequency	1140	-	-	0.10	3.6	2.3	0.74	0.36
Dry, isotropic block measured quasi-statically	1140	2600[1]	0.410	0.03[2]	3.3	3.3	1.17[1]	1.17[1]

[1] calculated from the isotropic values of E and ν
[2] from [17] for dry, isotropic sheet measurements

minimum.

The results of the fitting procedure to the attenuation in the 15 μm fibre suspension are more ambiguous. The size of the marker in figure 4 shows that best fit solutions to the attenuation in this suspension had lower cost function values than the cost function values from the fitting to the attenuation in the other two fibre suspensions. This means that there was a better fit between the model and the measurement data for a suspension with this diameter of fibre than in the suspension of the larger fibres. However, in the case of the small fibre suspension the optimisation procedure converged to a large number of different points. The estimation from the lowest cost function results were $E = 0.08\,\mathrm{GPa}$ and $G = 0.02\,\mathrm{GPa}$, which were over two orders of magnitude less than the reference values. This misidentification of the material parameters is thought to be because there are no resonance features captured with this combination of frequency range and fibre diameter and hence a large number of different values for c_2, υ_2 and $\tan\delta$ provide good fit solutions to the model. In this case, this result indicates the model is not suitable for solving the inverse solution when used with this optimisation procedure.

In the figure we can see a cluster of 26% of the values lying close to the values from the minimum cost function cluster of the other two fibres. These values had the second lowest value of the cost function and were the ones that they lay closest to the reference values of the E and G of all the solutions. Table 4 contains these values since we chose to use them in evaluating the accuracy of the estimates of the material properties. The fibres are more accurately described as transversely isotropic than isotropic hence reference values from drawn nylon film [17] are included in the reference table values. The results

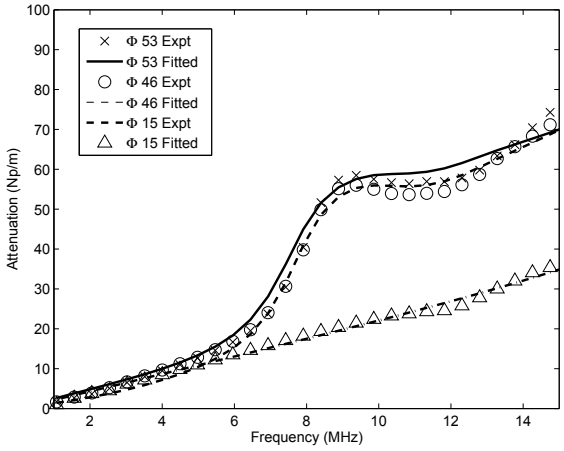

Figure 5: Best fit curves and measurements of the attenuation in the three different fibre suspensions. The values for the material properties from the best fit curves are given in table 4

in table 4 show that estimated values for the shear modulus lie between the value for the G_z and $G_{\theta,r}$. The estimates from the three fibres give values close to each other. However, there are insufficient numbers of different diameters fibres to draw conclusions about the variation between the fibres. We define the sensitivity of the estimation of each parameter to noise in the data as the value estimated from the attenuation plus two standard deviations. Using this definition we can see that the sensitivity of the shear modulus to noise is low.

The estimated value for E is out of the range of values expected for the fibre. It varies between 14% and 36% lower than $E_{\theta,r}$ (54% lower than the isotropic value), however the estimates from the three different fibres are close to each other and have low sensitivity to noise. A probable reason for the low estimation is the assumption in the model of the fibre being isotropic because if $G_{\theta,r}$ is correct, even with a $\upsilon_2 = 0.5$ i.e. incompressible material, the maximum value of E is $3G$ and hence it would only just be in the range given in the table 5. These reference values are possible because of they assume the fibre to be transversely isotropic compared to the model that assumes the material to be isotropic.

The c_2 and υ_2 differ from one fibre to the next and from the reference values in table 5. They also are more sensitive to noise in the attenuation curves than the elastic moduli. This implies that applying the modelling over this range of frequencies there is not sufficient data to specify the individual value of c_2 and υ_2. However, as can be seen from the consistent values obtained for the elastic moduli, their combined values are consistent. It is possible that better estimation of c_2 and υ_2 would be obtained if a greater frequency range was captured.

Comparison between the estimated values of tan δ in table 4 and its reference values in table 5 shows that the estimated values are an order of magnitude larger than expected. Possible reasons for this are that the fibres are in a region of resonance and hence the damping effect is greater. Additionally, the larger estimated value for the loss tangent may be compensating for thermal and fluid shear effects being neglected in the model since neglecting thermal effects and fluid shear effects has a damping effect on the attenuation as previously discussed (see figure 2).

5 Conclusion

The aim of this measurement method was provide ultrasonic based measurements of the material properties of short, uniform fibres in suspension. The measurement method gave reasonable and consistent results for the shear modulus with low sensitivity to noise. The Young's modulus was lower than predicted but consistent and had low sensitivity to noise. The reduced value is thought to be caused by the anisotropic nature of the fibres.

The results suggest that the the frequency range should include at least one resonance feature for the optimisation method used here to unambiguously identify the best-fit to the measured attenuation and give reasonable estimated values of the material parameters. This was despite a better match between the model and the experimental results existing in the region without a resonance feature.

The difference between the predicted and the measured attenuation were not explained by the noise, incorrect tangent delta values or the assumptions of negligible thermal or viscous effects. Given this and the reasonable accuracy of the shear modulus it would seem that the errors come from the assumption of isotropic material. Adding complexity to the model by basing it on transversely isotropic material could improve fit of the model to the experiment data. However, increasing the complexity could introduce problems in solving the inverse problem of estimating the material properties from the measured attenuation. It may slow the estimation procedure and may results in over parameterisation of the model whereby noise would be modelled as well as introducing a larger potential number of solutions that would make identifying the correct solution more difficult.

Further work is needed on the sensitivity of the model to the different parameters also further experiments on isotropic fibres would aid in explaining the reason for the low value of Young's modulus.

6 Acknowledgments

We wish to thank to Swissflock, Emmenbrücke, Switzerland for providing the fibres and Rhodia, France for the nylon fibre properties. Thanks go also to Jan Niemi and Jesper Martinsson for their support and for supplying part of the programming code.

A Appendix

The relationships between the different elastic properties and the compressional wave velocity are the standard relationships and for clarity are give here:

The shear modulus, G, is calculated from

$$G = \frac{(0.5 - \upsilon)}{(1 - \upsilon)} \rho_2 c_2^2. \tag{A.5}$$

Young's modulus, E, is calculated from

$$E = \frac{(1 + \upsilon)(1 - 2\upsilon)}{(1 - \upsilon)} \rho_2 c_2^2. \tag{A.6}$$

References

[1] J. Levlin and L. Söderhjelm, *Pulp and Paper Testing*. Fapet Oy, 1999.

[2] D. Adams, "Ultrasonic transmission through paper fiber suspensions," Ph.D. dissertation, University of London, 1975.

[3] P. Epstein and R. Carhart, "The absorption of sound in suspensions and emulsions. i. water fog in air," *The Journal of the Acoustical Society of America*, vol. 25, no. 3, pp. 553–565, May 1953.

[4] J. Allegra and S. Hawley, "Attenation of sound in suspension and emulsions: Theory and experiments," *The Journal of the Acoustical Society of America*, vol. 51, no. 5, pp. 1545–1564, 2 1972.

[5] A. Harker and J. Temple, "Velocity and attenuation of ultrsound in suspensions of particles in fluids," *Journal of Physics D: Applied Physics*, vol. 21, pp. 1576–1588, 1988.

[6] R. Challis, M. Povey, M. Mather, and A. Holmes, "Ultrasound techniques for characterizing colliodal dispersions," *Reports in Progress in Physics*, vol. 68, pp. 1541–1637, 2005.

[7] L. Flax and W. Neubauer, "Acoustic reflection from layered elastic absorptive cylinders," *Journal of the Acoustical Society of America*, vol. 61, no. 2, pp. 307–312, Feb 1977.

[8] L. Flax, L. Dragonette, and H. Uberall, "Theory of elastic resonance excitation by sound scattering," *Journal of the Acoustical Society of America*, vol. 63, no. 3, pp. 723–730, Mar 1978.

[9] C. Habeger, "The attenuation of ultrsound in dilute polymeric fiber suspensions," *Journal of Acoustical Society of America*, vol. 72, pp. 870–878, sep 1982.

[10] Y. Aitomäki and T. Löfqvist, "Estimating suspended fibre material properties by modelling ultrasound attenuation," in *Mathematical modeling of wave phenomena: 2nd Conference on Mathematical Modeling of Wave Phenomena*, B. Nilsson and L. Fishman, Eds., vol. 834:1. AIP, 2006, pp. 250–259.

[11] A. Bhatia, *Ultrasonic Absorption*. Dover, 1968, ch. 11, p. 272.

[12] L. Kinsler, A. Frey, A. Coppens, and J. Sanders, *Fundamentals of Acoustics*, 4th ed. John Wiley and Sons Inc., 2000.

[13] J. Martinsson, J. Carlson, and J. Niemi, "Model-based phase velocity and attenuation estimation in wideband ultrasonic measurement systems," *IEEE Transactions on Ultrasonics, Ferroelectrics and Frequency Control*, vol. 54, no. 1, pp. 138–146, January 2007.

[14] E. Ehrnrooth, "Softening and mechanical behaviour of single wood pulp fibres - the influence of matrix composition and chemical and physical characteristics," PhD Thesis, Department of Wood and Polymer Chemistry, University of Helsinki, 1982.

[15] T. Coleman and Y. Li, "An interior trust region approach for nonlinear minimization subject to bounds," *SIAM Journal on Optimization*, vol. 6, pp. 418–445, 1996.

[16] A. Anton and B. Baird, *Encyclopedia of polymer science and technology*. Wiley-Interscience, 2003, vol. 3, ch. Polyamides, Fibers, pp. 584–617.

[17] W. Leugh, K. Ho, and C. Choy, "Mechanical relaxations and moduli of oriented nylon 66 and nylon 6," *Journal of Polymer Science*, vol. 22, pp. 1173–1191, 1984.

[18] J. Melo and D. Radford, "Determination of the elastic constants of a transversely isotropic lamina using laminate coefficients of thermal expansion," *Journal of Composite Materials*, vol. 36, pp. 1321–1329, 2002.

Paper E

Damping mechanisms of ultrasound scattering in suspension of cylindrical particles: Numerical analysis

Authors:
Yvonne Aitomäki and Torbjörn Löfqvist

To be submitted
to Journal of the Acoustical Society of America as a letter to the editor

Damping mechanisms of ultrasound scattering in suspension of cylindrical particles: Numerical analysis

Yvonne Aitomäki and Torbjörn Löfqvist

Abstract

The addition of viscosity to the ultrasound scattering models increase complexity. Investigated is the necessity of the addition of viscosity in a suspension of cylindrical scatterers in two different frequency-radius regimes. The modelled attenuation of a scatterer surrounded by a viscous fluid is compared to that where the fluid is non-viscous. The results show that the intrinsic loss in the scatterer and the viscosity both have a damping effect on the attenuation.

The conclusion is that a simpler model where the fluid is assumed to be non-viscous can be used to model attenuation in suspensions of fibres with $\tan\delta \geq 0.1$. This holds if the frequency is not in the region where the viscous skin depth equals the radius.

1 Introduction

Early studies on spherical scatterers have shown the importance of viscosity as a loss mechanism in the attenuation of ultrasound in suspensions [1, 2]. These studies give explicit expressions for the attenuation in suspension of spherical particles showing clearly its dependance on the viscosity. These expressions are valid when the wavelength is much greater than the radius of the particle (long wavelength limit). The importance of viscosity has been shown in a more recent experimental study where suspensions of small solid spheres over a wide range of frequencies were investigated [3]. However, the addition of viscosity adds considerable complexity to the system and in cases where more elaborate geometry is modelled, the viscosity of the fluid is often neglected [4–7].

Ultrasound scattering models based on those discussed above, have been used to solve the inverse problem of obtaining material properties of the scatterers [8, 9]. Solving the inverse problem is optimised if only the parameters influencing the attenuation are included since including redundant parameters has a serious impact on the speed of the optimisation. This is because, in general, the model becomes more complex if it has a greater number of parameters. Also, the addition of any unknown parameter adds another dimension to the search space and hence can have a large impact on the speed of optimisation.

If we are interested in obtaining the material properties of the scatterer, it would be of value to know the loss in accuracy of the attenuation when the fluid is assumed to

be non-viscous. This would provide a basis for appropriate assumptions to be made. It has been shown that when scattering occurs in between two eigenfrequencies of vibration of an elastic body, the scatterer appears as an impenetrable object [10]. Hence, if the interest is in estimating material properties of the scatterer, then the wavelength regime chosen should be where eigenfrequencies of the scatterers exist. The eigenfrequencies are likely to be where the wavelength is of the order of the radius of the scatterers. In this study the influence of viscosity on attenuation where the wavelength is of the same order as the radius is investigated.

One application of this type of model is for estimating the material properties of wood fibres in suspension, such as found in paper pulp. With a view to this application, this paper focuses on cylindrical scatterers with a density close to that of water and with diameters in the order of 10 microns. The aim is to establish if viscosity effects can be neglected when modelling the attenuation of ultrasound in a dilute suspension of such scatterers in water. The model is based on single particle scattering of ultrasound originally derived for spherical particles [1, 2] and adapted for cylindrical scatterers [8]. This is done by comparing the simulated results from the model using the condition that a non-viscous fluid surrounds the scatterers to the results from the model using the condition that a viscous fluid surrounds the scatterers. A numerical comparison is chosen because the number of terms involved in analytical expressions are large, for example, one of the terms is a result of the determinant of a 6 by 6 matrix. Two frequency-scatterer radius regimes are investigated, one where the frequency range is chosen such that the wavelengths are in the order of the radius of the scatterer and the other where the viscous boundary layer is known to effect the attenuation [3]. The model is only valid for low concentrations [11] and hence the comparison are done with a suspension of scatterers of 1% concentration by volume.

2 Theory

In a fluid medium, the total attenuation of an ultrasound plane wave in a known dilute concentration of randomly orientated cylindrical scatterers can be calculated based on the attenuation of a single cylindrical scatterer [8]. This attenuation from a single scatterer can be calculated from the scattering of the wave from an oblique orientated cylinder (see Fig. 1) using the wave equations and associated boundary conditions. The resulting expression by [8] for the attenuation of cylindrical scatterers is

$$\alpha = \frac{-2f_r}{\pi R^2 k_{c_1}} \sum_{n=0}^{\infty} \Re \left(\int_0^{\frac{\pi}{2}} \epsilon_n B_{1n} \cos(\psi) d\psi \right). \tag{1}$$

where f_r is the volume fraction; R is the radius of the scatterer; k_{c_1} is the wave number of the compressional wave in water and is defined as $k_{c1} = \omega/c_1$ where c_1 is the compression wave velocity in the fluid and ω is the angular frequency; $\Re$ denotes the real part of the expression, ψ is the angle of incidence; n is a positive real integer and $\epsilon_n = 1$ if $n = 0$, otherwise $\epsilon_n = 2$ and B_{1n} is the coefficient associated with the reflected compression wave

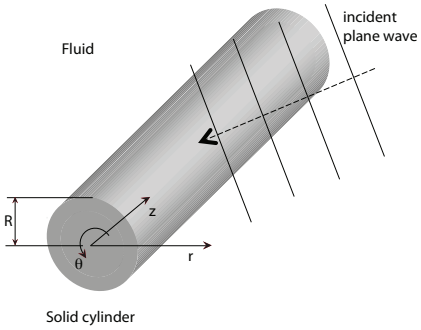

Figure 1: Geometry used for formulating the attenuation from a infinitely long cylinder of radius R.

potential in the fluid. Note that in this paper, the prime superscripts used by [8] have been replaced by a subscript 2 to represent the solid and a subscript 1 to represent the fluid terms.

The B_{1n} coefficients are from the expansion of the of the reflect wave potential, ϕ_{1r}, in Hankel functions (H_n^1) such that

$$\phi_{1r} = \left(B_{0_1} H_0^{(1)}(k_{1cc} r) + 2 \sum_{n=1}^{\infty} i^n \cos(n\theta) B_{n_1} H_n^{(1)}(k_{1cc} r) \right) e^{i(k_{1cs} z - \omega t)}. \quad (2)$$

where k_{cc} is the component of the wave number in the r direction such that $k_{cc} = k_c \cos(\psi)$ where ψ is the angle of incidence. These coefficients and the coefficient associated with other wave potentials (specified later) are calculated from the application of boundary conditions to the expressions for stress and velocity in terms of wave potentials. When these wave potentials are expanded in terms Hankel and Bessel function (Bessel function for the wave potential in the solid since they bounded at $r = 0$) each boundary condition becomes a series in $\cos(n\theta)$. As these are orthogonal, each term in the solved independently of the others (see, for example, [12] for more details).

In the calculation of attenuation, the series in equation 1 was truncated after four terms. This value was chosen as no significant differences in the attenuation are seen when a higher number of terms are included.

To test the effect of viscosity on attenuation, B_{1n} was calculated under two different conditions. Firstly assuming the fluid to be viscous and secondly assuming the fluid to be non-viscous. The thermal effects are not considered.

2.0.1 Viscous fluid condition

With a viscous fluid surrounding the scatterer, for $n > 0$ there are six unknown wave potential coefficients and six boundary conditions. For $n = 0$, this reduces to four unknowns and four boundary conditions. The unknown coefficients are B_{1n} and the coefficient associated with the two orthogonal viscous shear waves (evanescent waves) as well as those associated with the wave potentials in the solid: the compressional wave and the two orthogonal shear waves. In a viscous fluid, the boundary conditions are that the velocities and stresses at the surface of the scatterer in the r, θ and z directions are continuous. B_{1n}, can therefore be expressed as

$$B_{1n} = \frac{Q}{P}, \tag{3}$$

where

$$Q = \begin{vmatrix} b_1 & a_{12} & \dots & a_{16} \\ b_2 & a_{21} & \dots & a_{26} \\ \vdots & \vdots & \ddots & \vdots \\ b_6 & a_{62} & \dots & a_{66} \end{vmatrix} \tag{4}$$

and

$$P = \begin{vmatrix} a_{11} & a_{12} & \dots & a_{16} \\ a_{21} & a_{21} & \dots & a_{26} \\ \vdots & \vdots & \ddots & \vdots \\ a_{61} & a_{62} & \dots & a_{66} \end{vmatrix}. \tag{5}$$

The elements in the matrices are functions of the properties of the fluid and the solid and are given in the appendix.

2.0.2 Inviscid fluid condition

When the surrounding fluid is non-viscous there are no evanescent waves appearing at the surface of the scatterer. Therefore the number of unknown coefficients for $n > 0$, reduces to four as does the number of boundary conditions. For $n = 0$, this reduces further to only three unknowns and three boundary conditions. The remaining coefficients are B_{1n} and the coefficients associated with the wave potentials in the solid. In a non-viscous fluid, the boundary conditions are that the velocities and stresses at the surface of the scatterer in the r are continuous and the stress in the θ and z directions is zero. The solution for B_{1n} is then

$$B_{1n} = \frac{a_{1cc}J_n'(a_{1cc}) - J(a_{1cc})L}{-a_{1cc}H_n^{1\prime}(a_{1cc}) + H_n^{1\prime}(a_{1cc})L} \tag{6}$$

where a_{1cc}, such that $a_{1cc} = k_{1cc}R$ (The prime denotes the first derivative of the Bessel and Hankel functions.) and

$$L = \frac{R}{S}. \tag{7}$$

R and S are a subset of the matrices P and Q, respectively such that

$$R = \begin{vmatrix} a_{44} & a_{45} & a_{46} \\ a_{54} & a_{55} & a_{56} \\ a_{64} & a_{65} & a_{66} \end{vmatrix} \tag{8}$$

and

$$S = \begin{vmatrix} a_{14} & a_{15} & a_{16} \\ a_{54} & a_{55} & a_{56} \\ a_{64} & a_{65} & a_{66} \end{vmatrix}. \tag{9}$$

With the simplification of an non-viscous fluid, B_{1n} is now equivalent to the reflective wave coefficient used in backscattering [10] if the angle of incidence is zero.

In the subsequent calculation of attenuation from B_n as done by [8] which follows the derivation used in spherical particles [1, 2], the subsequent effect of viscosity on the reflected wave at a large distance from the scatterer is considered to be negligible. It is therefore also neglected here and the primary interest is the effect of viscosity on the energy absorbed at the boundary of the scatterer. When the attenuation is calculated from the viscous fluid condition it is termed α_v and when it is calculated from the non-viscous fluid condition it is termed α_{nv}.

3 Method

The attenuation was calculated for the two conditions using equation 1 over the frequency range 1 MHz to 25 MHz for a scatterer with a radius of 20 μm. This radius was used since we chose to test the hypothesis that the viscosity will not affect the attenuation in suspensions of scatterers of this radius or above. For comparison, a suspension of scatterers with a radius approximately equal to the viscosity skin depth, δ, in the frequency range investigated was also tested. This is because it has been shown that viscosity is a primary cause of attenuation when $\delta \approx R$ [3]. δ was calculated as

$$\delta = \sqrt{\eta_1/(\pi\rho_1 f)} \tag{10}$$

Where f is the frequency, η_1 is the viscosity and ρ_1 is the density, of the fluid [13]. When $f = 3.3$ MHz, then $\delta = 0.3\,\mu$m hence the scatterer radius of this second suspension was set to $0.3\,\mu$m.

From the expression for B_{1n}, we can see that the attenuation depends on both the properties of the fluid and of the scatterer. To gain an understanding of the effects of this assumption for different wave velocities the attenuation was calculated for values of the compression wave velocity in the solid, c_2, and Poisson's ratio, v, ranging from $1{\cdot}10^3\,\mathrm{ms}^{-1}$ to $10{\cdot}10^3\,\mathrm{ms}^{-1}$ and 0 to 0.5 respectively. The intrinsic loss in the scatterers also effects B_{1n} and is quantified by the loss tangent, $\tan\delta$ [14]. Note that the term $\tan\delta$ used here is not related to the viscous skin depth δ. Two different values of $\tan\delta$, a high value of 0.1 and a low value of 0.01 and a fixed value for ρ_2 of $1390\,\mathrm{kgm}^{-3}$ were used in the calculations.

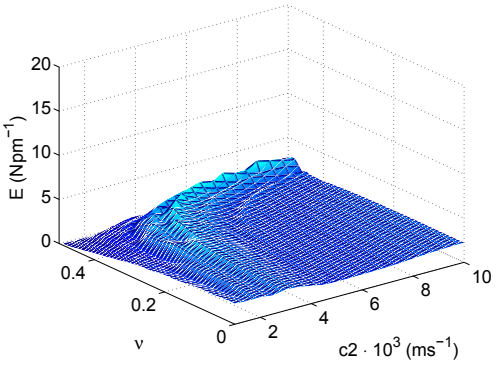

Figure 2: Plot of the error caused by excluding viscous effects for a range of values of c_2 and ν. Here R=20 μm and tan δ =0.1

The difference in the attenuation under the two conditions is expressed in terms of a cost function, V, where

$$V = \frac{1}{N}\sum_{i=1}^{N} |\alpha_{vi} - \alpha_{nvi}|^2 \tag{11}$$

and the ith term is the value at an ith frequency and N is the number of points sampled in the frequency range. The units of V are $\mathrm{Npm^{-1}MHz^{-1}}$.

4 Results and Discussion

Fig. 2 is a plot of V when $R = 20\,\mu$m for a high $\tan\delta$ over a range of values of c_2 and v. As can be seen the difference between the two conditions is negligible. If the $\tan\delta$ is lower, as shown in Fig. 3, the difference increases slightly for certain values of c_2 and v. The maximum difference is 12 $\mathrm{Npm^{-1}MHz^{-1}}$ and occurs at $c_2 = 4 \cdot 10^3\,\mathrm{ms^{-1}}, v = 0.41$. The attenuation curves under the two different conditions at this point are plotted in Fig. 4. It shows that α_v and α_{nv} are aligned except for a resonance feature at 2.5 MHz which does not appear in α_v because the viscosity damps this resonance. When $\tan\delta$ is high, this peak is smaller because high values of $\tan\delta$ also have a damping effect on the resonance.

As discussed in the method, as a comparison α_{nv} and α_v were calculated for $R = 0.3\,\mu$m, which is a condition where one would expect the viscosity to have a significant effect. In this case V was calculated over the same range of c_2 and v for a high and low values of $\tan\delta$ and is shown in Fig. 5 and Fig. 6. As expected α_{nv} and α_v differ significantly over the whole range of c_2 and v values.

In the flatter regions, such as at $c_2 = 6.5 \cdot 10^3\,\mathrm{ms^{-1}}, v = 0.27$, the difference is because $\alpha_v \gg \alpha_{nv}$. This is shown in Fig.7 which is a plot of the attenuation under the two conditions at this point. This figure is with the attenuations calculated using

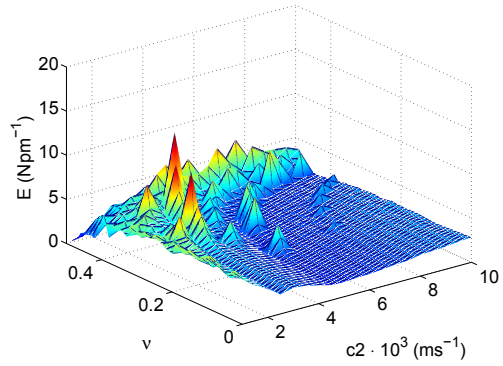

Figure 3: Plot of the error caused by excluding viscous effects for a range of values of c_2 and ν. The values of R and $\tan\delta$ are 20 μm and 0.01, respectively.

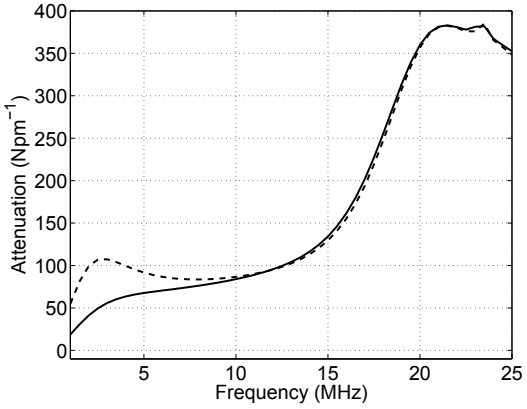

Figure 4: Attenuation calculated using the non-viscous model, α_{nv}, and the viscous model α_v. Here, $R = 20\,\mu m$ and $\tan\delta = 0.01$, $c_2 = 4 \cdot 10^3\ ms^{-1}$ and $v = 0.41$. The solid line is α_v and the dashed line is α_{nv}.

$\tan\delta = 0.01$ but a similar result was obtained when $\tan\delta = 0.1$.

The peaks in plots Fig. 5 and 6 are where $\alpha_{nv} \gg \alpha_v$, as was the case for the scatterer with the large radius. However, when the wavelength of the incident wave is much greater than R, the resonance peak in α_{nv} is at a much higher frequency. In this case the peak is at 185 MHz although its effect is seen at lower frequencies. This is best illustrated by plotting α_{nv} and α_v up to a high frequency as shown in Fig. 8. Note that the higher frequency range used in this plot is simply to illustrate the resonance feature.

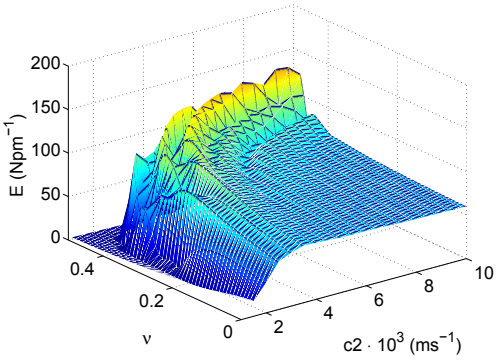

Figure 5: Plot of the error caused by excluding viscous effects for a range of values of c_2 and ν. The values of R and $\tan\delta$ are 0.3μm and 0.1, respectively.

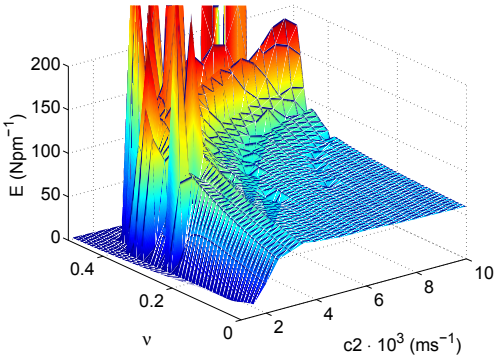

Figure 6: Plot of the error caused by excluding viscous effects for a range of values of c_2 and ν. The values of R and $\tan\delta$ are 0.3μm and 0.01, respectively.

5 Conclusion

If the scatterer has a high intrinsic loss, the non-viscous assumption is valid where the radius of the scatterer is much greater than the viscous skin depth. With low intrinsic loss the two conditions differ slightly even when the scatterer radius is much larger than the viscous skin depth. This is thought to be due to the damping effect the viscosity has on the resonance of the scatterer.

As expected, in the region where the viscous skin depth is approximately that of the radius, the viscosity has a considerable effect. However, this is only due in part to the additional attenuating effect of viscosity in this region. With certain values of compressional wave velocity and Poisson's ratio, the difference in the two conditions is still due to the damping effect the viscosity has on the resonance of the scatterer.

These results suggest that there is a degree of interchangeability between the intrinsic

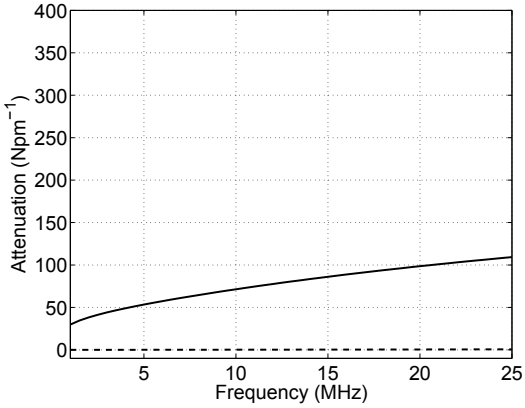

Figure 7: Attenuation calculated using the non-viscous model, α_{nv}, and the viscous model α_v. Here, $R = 20\,\mu m$ and a low $\tan\delta$ with $c2 = 6.5 \cdot 10^3\, ms^{-1}$ and $v = 0.27$. The solid line is α_v and the dashed line is α_{nv}.

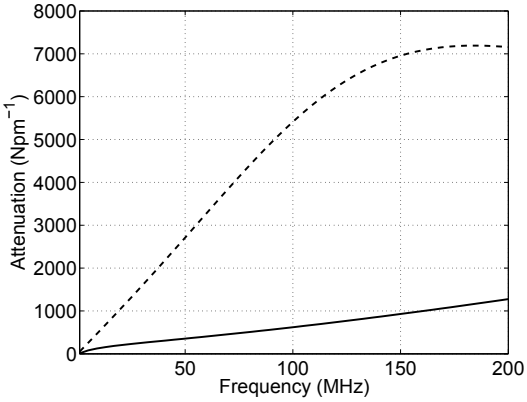

Figure 8: Attenuation calculated using the non-viscous model, α_{nv}, and the viscous model α_v, for $R = 0.3\,\mu m$ and a low $\tan\delta$ where $c2$ and ν are $4{\cdot}10^3\, ms^{-1}$ and 0.41, respectively. The solid line is α_v and the dashed line is α_{nv}.

loss of the scatterer and viscosity since both parameters affect damping, when the radius is not of the order of the viscous skin depth.

This could be used to advantage in solving the inverse problem of estimating the material properties from the attenuation of cylindrical scatters with low density, either by including viscosity and forgoing the estimation of intrinsic loss or excluding viscosity and allowing the estimate of intrinsic loss to be raised. Including viscosity but forgoing the estimation of intrinsic loss could be especially useful if the scatterer is immersed in a well-defined, low viscous fluid like water where the intrinsic loss of the scatterer is

not known and not of interest. In doing so the number of parameters that need to be estimated is reduced. Alternatively, excluding the viscosity and allowing the intrinsic loss to be raised could allow more complex cross sectional geometries to be modelled such as elliptical shapes, layered cylinders or non-isotropic materials without the additional complexity of including viscosity.

A Appendix

The elements of the matrix in equations 4 - 9 are expressed using the following terms and where terms with subscript 1 represent the fluid and terms with subscript 2 represent the solid. $a_c = k_c R$ and k_c is the wave number of the compression wave, $a_{cc} = k_{cc} R$ and k_{cc} is the component of the wave number in the r direction such that $k_{cc} = k_c \cos(\psi)$. $a_{cs} = k_{cs} R$ and k_{cs} is the component of the wave number in the z direction such that $k_c = k_c \sin(\psi)$. Similarly, $a_s = k_s R$ and k_s is the wave number of the shear wave, $a_{sc} = k_{sc} R$ and k_{sc} is the component of the wave number in the r direction such that $k_{sc} = k_s \cos(\psi)$. J_n and H_n^1 are the Bessel functions and Hankel functions of the first order. The prime denotes the first derivative and double prime denotes the second derivative on the Bessel and Hankel functions. ρ_2 is the density, μ_2 is the shear modulus and $\tan\delta$ is loss tangent or intrinsic loss, of the solid. η_1 is the viscosity and ρ_1 is the density of the fluid. The wave numbers are defined as $k_{1c} = \omega/c_1$ where c_1 is the compression wave velocity in the fluid and ω is the angular frequency, $k_{1s} = (i\omega\rho_1/\eta_1)^{\frac{1}{2}}$, $k_{2c} = \omega/c_2(1 + i\tan\delta)$ where c_2 is the compression wave velocity in the solid and $k_{2s} = \omega(\rho_2/\mu_2)^{\frac{1}{2}}$. The elements in the matrix are

$$
\begin{aligned}
a_{11} &= -a_{1cc} H_n^{1\prime}(a_{1cc}) \\
a_{12} &= -i\omega n^2 J_n(a_{2sc}) \\
a_{13} &= -i\omega(-a_{2sc} J_n'(a_{2sc})) \\
a_{14} &= -i\omega a_{2cc} J_n'(a_{2cc}) \\
a_{15} &= -n^2 H_n^1(a_{1sc}) \\
a_{16} &= a_{1sc} H_n^{1\prime}(a_{1sc}) \\
b_1 &= a_{1cc} J_n'(a_{1cc}) \\
a_{21} &= -H_n^1(a_{1cc}) \\
a_{22} &= -i\omega a_{2sc} J_n'(a_{2sc}) \\
a_{23} &= -i\omega(-J_n(a_{2sc})) \\
a_{24} &= -i\omega J_n(a_{2cc}) \\
a_{25} &= -a_{1sc} H_n^{1\prime}(a_{1sc})
\end{aligned}
$$

$$
\begin{aligned}
a_{26} &= H_n^1(a_{1sc}) \\
b_2 &= J_n(a_{1cc}) \\
a_{31} &= -a_{1cs}^2 H_n^1(a_{1cc}) \\
a_{32} &= 0 \\
a_{33} &= -i\omega a_{2sc}^2 J_n(a_{2sc}) \\
a_{34} &= -i\omega a_{1cs}^2 J_n(a_{2cc}) \\
a_{35} &= 0 \\
a_{36} &= -a_{1sc}^2 H_n^1(a_{1sc}) \\
b_3 &= a_{1cs}^2 J_n(a_{1cc}) \\
a_{41} &= -\eta_1((a_{1s}^2 - 2a_{1c}^2)H_n^1(a_{1cc}) - 2a_{1cc}^2 H_n^{1\prime\prime}(a_{1cc})) \\
a_{42} &= 2\mu_2 n^2(J_n(a_{2sc}) - a_{2sc}J_n'(a_{2sc})) \\
a_{43} &= 2\mu_2 a_{2sc}^2 J_n''(a_{2sc}) \\
a_{44} &= (\omega^2\rho_2 R^2 - 2\mu_2 a_{2c}^2)J_n(a_{2cc}) - 2\mu_2 a_{2cc}^2 J_n''(a_{2cc}) \\
a_{45} &= -2\eta_1 n^2(H_n^1(a_{1sc}) - a_{1sc}H_n^{1\prime}(a_{1sc})) \\
a_{46} &= -2\eta_1 a_{1sc}^2 H_n^{1\prime\prime}(a_{1sc}) \\
b_4 &= \eta_1((a_{1s}^2 - 2a_{1c}^2)J_n(a_{1cc}) - 2a_{1cc}^2 J_n''(a_{1cc})) \\
a_{51} &= -\eta_1(a_{1cc}H_n^{1\prime}(a_{1cc}) - H_n^1(a_{1cc})) \\
a_{52} &= (1/2)\mu_2(n^2 J_n(a_{2sc}) - a_{2sc}J_n'(a_{2sc}) + a_{2sc}^2 J_n''(a_{2sc})) \\
a_{53} &= \mu_2(J_n(a_{2sc}) - a_{2sc}J_n'(a_{2sc})) \\
a_{54} &= \mu_2(a_{2cc}J_n'(a_{2cc}) - J_n(a_{2cc})) \\
a_{55} &= -(1/2)\eta_1(n^2 H_n^1(a_{1sc}) - a_{1sc}H_n^{1\prime}(a_{1sc}) + a_{1sc}^2 H_n^{1\prime\prime}(a_{1sc})) \\
a_{56} &= -\eta_1(H_n^1(a_{1sc}) - a_{1sc}H_n^{1\prime}(a_{1sc})) \\
b_5 &= \eta_1(a_{1cc}J_n'(a_{1cc}) - J_n(a_{1cc})) \\
a_{61} &= -2\eta_1 a_{1cs}a_{1cc}H_n^{1\prime}(a_{1cc}) \\
a_{62} &= \mu_2 n^2 a_{1cs}J_n(a_{2sc}) \\
a_{63} &= \mu_2 J_n'(a_{2sc})(a_{2sc}^2 - a_{1cs}^2)a_{2sc}/a_{1cs} \\
a_{64} &= 2\mu_2 a_{2cc}a_{1cs}J_n'(a_{2cc})
\end{aligned}
$$

$$a_{65} = -\eta_1 n^2 a_{1cs} H_n^1(a_{1sc})$$
$$a_{66} = -\eta_1 H_n^{1\prime}(a_{1sc})(a_{1sc}^2 - a_{1cs}^2) a_{1sc}/a_{1cs}$$
$$b_6 = 2\eta_1 a_{1cs} a_{1cc} J_n'(a_{1cc}).$$

Acknowledgment

The authors would like to thank Johan Carlson for this suggestions and comments.

References

[1] P. Epstein and R. Carhart, "The absorption of sound in suspensions and emulsions. i. water fog in air," *The Journal of the Acoustical Society of America*, vol. 25, no. 3, pp. 553–565, May 1953.

[2] J. Allegra and S. Hawley, "Attenation of sound in suspension and emulsions: Theory and experiments," *The Journal of the Acoustical Society of America*, vol. 51, no. 5, pp. 1545–1564, 2 1972.

[3] N. Herrmann and D.J.McClements, "Influence of visco-inertial effect on the ultrasonic properties of mondisperse silican suspensions," *Journal of the Acoustical Society of America*, vol. 106, p. 1178, 1999.

[4] S. M. Hasheminejad and M. Rajabi, "Acoustic scattering characteristics of a thick-walled orthotropic cylindrical shell at oblique incidence," *Ultrasonics*, vol. 47, pp. 32–48, 2007.

[5] D. C. Gazis, "Three-dimensional investigation of the propagation of waves in hollow circular cylinders. i. analytical foundation," *The Journal of the Acoustical Society of America*, vol. 31, no. 5, pp. 568–573, 1959. [Online]. Available: http://link.aip.org/link/?JAS/31/568/1

[6] M. Venkatesan and P. Ponnusamy, "Wave propagation in a solid cylinder of arbitrary cross-section immersed in fluid," *The Journal of the Acoustical Society of America*, vol. 112, no. 3, pp. 936–942, 2002. [Online]. Available: http://link.aip.org/link/?JAS/112/936/1

[7] Y. Angel and C. Artistegui, "Analysis of sound propagation in a fluid through a screen of scatterers," *Journal of the Acoustical Society of America*, vol. 72, p. 118, 2005.

[8] C. Habeger, "The attenuation of ultrsound in dilute polymeric fiber suspensions," *Journal of Acoustical Society of America*, vol. 72, pp. 870–878, sep 1982.

[9] Y. Aitomäki and T. Löfqvist, "Material property estimates from ultrasound attenuation in fibre suspensions," *Ultrasonics*, vol. doi:10.1016/j.ultras.2008.11.005, 2009.

[10] L. Flax, L. Dragonette, and H. Uberall, "Theory of elastic resonance excitation by sound scattering," *Journal of the Acoustical Society of America*, vol. 63, no. 3, pp. 723–730, Mar 1978.

[11] A. K. Hipp, G. Storti, and M. Morbidelli, "Acoustic characterization of concentrated suspensions and emulsions. 1. model analysis," *Langmuir*, vol. 18, no. 2, pp. 391–404, 2002. [Online]. Available: http://pubs.acs.org/doi/abs/10.1021/la015538c

[12] L. Flax and W. Neubauer, "Acoustic reflection from layered elastic absorptive cylinders," *Journal of the Acoustical Society of America*, vol. 61, no. 2, pp. 307–312, Feb 1977.

[13] L. Kinsler, A. Frey, A. Coppens, and J. Sanders, *Fundamentals of Acoustics*, 4th ed. Wiley, 1999, ch. 8.

[14] A. Bhatia, *Ultrasonic Absorption*. Dover, 1968, ch. 11, p. 272.

Paper F

Estimating material properties of solid and hollow fibres in suspension using ultrasonic attenuation

Authors:
Yvonne Aitomäki and Torbjörn Löfqvist

To be submitted
IEEE Transactions on Ultrasonics, Ferroelectrics, and Frequency Control

Estimating material properties of solid and hollow fibres in suspension using ultrasonic attenuation

Yvonne Aitomäki and Torbjörn Löfqvist

Abstract

The aim of this paper is to estimate the material properties of hollow fibres suspended in a fluid using the combination of ultrasound measurements and a simple, computationally efficient analytical model. The industrial application of this method is to evaluate the properties of wood fibres in paper pulp. The necessity of using a layered cylindrical model (LCM) as opposed to a solid cylindrical model (SCM) for modeling ultrasound attenuation in a suspension of hollow fibres is evaluated. The two models are described and used to solve the inverse problem of estimating material properties from attenuation measurements in dilute suspensions of solid and hollow polyester fibres. The results show that the experimental attenuation of hollow fibres differs from that of solid fibres. Results from using a LCM in conjunction with hollow fibre suspension measurements are similar to that of using a SCM used in conjunction with solid fibre suspension measurements. These results compare well to block polyester values for E and G. However, using the SCM with the hollow fibre suspension did not produce realistic estimations for E and G. We conclude that the LCM gives reasonable estimations of hollow fibre properties and the SCM is not sufficiently complex to model hollow fibres in this frequency-diameter region.

1 Introduction

Estimating the material properties of hollow fibres suspended in a fluid using the combination of ultrasound measurements and a simple, computationally efficient analytical model could potentially provide a means of evaluating the properties of wood fibres in paper pulp online. Assuming it were possible, it would provide online feedback on the pulp processing, thereby allowing increased process control and potential efficiency improvements.

An early attempt at interpreting attenuation measurement of wood fibres was done by [1] and has been presented in a report based on his work done on polymer fibers [2]. However attenuation is sensitive to the geometry of the suspended particles (hence its use in particle sizing [3]). Therefore interpreting attenuation measurements without geometric data is unreliable. The onset of optical measurement of pulp which provide geometric information on the wood fibres, opens the possibility of using this data in ultrasound scattering models to estimate their elastic properties.

Estimating the material properties of the fibres from measurement of ultrasound attenuation requires a model, measurement data and an estimation process itself where best fit between the measurement data and the model results is calculated by adjusting the material fibre properties. The method requires a model that gives unambiguous, accurate results. Models such as those derived by [4] could be used to calculate the attenuation in the fibres but the aim is also to use the simplest model possible to provide the necessary material properties. A previous study on solid nylon fibres showed promising results for the estimation of shear and to some extent Young's modulus based on a simple cylindrical scattering model [5,6]. However, since pulp fibres are hollow, the suitability of this model for hollow fibres must be investigated.

A library of information has built up over the years on the acoustic behaviour of cylindrical shells and a comparison of a number of theories was carried out by [7]. The focus of these works, for example [8], is modes of vibration of the cylindrical shell and is summarised by [9]. These modes have an impact on the amplitude of an acoustic waved scattered by a cylindrical shell and hence the attenuation of the acoustic wave. The relationship between modes of vibration and the amplitude of the scattered wave has been studied extensively, for example by [10]. A typical model used as a basis for work done by [11–14], is that of [15], which provides a model for the back-scattering of ultrasound from a layered cylinder. This assumes the fluid medium surrounding the scatters to be non-viscous and since the fluid in pulp is water, which has a low viscosity, this taken as a reasonable assumption.

The following investigation uses a solid model (SCM) [6], attenuation measurements from hollow and solid fibres in suspension and an estimation process to establish the fibre properties that give a best fit between the model and the measurements. The results are then compared to those from using a hollow model (LCM) , the hollow fibre measurement data and the estimation process. The LCM is based on a layered cylinder model [15]. Polyester fibres were chosen since they have a greater uniformity in both geometry and elastic properties than natural fibres. This allows the accuracy of the parameter estimation to be more easily investigated. Conclusions are drawn on the appropriate level of complexity of the model needed to obtain estimates for the elastic properties of the fibres.

2 Theory

In a fluid medium, the total attenuation of an ultrasound plane wave in a suspension of randomly orientated fibres is calculated based on the attenuation of a single fibre [2] and is valid for low concentrations. This single fibre attenuation can be calculated from the scattering of this plane wave from an oblique orientated cylinder using the wave equations and associated boundary conditions. This is done in the two models used here.

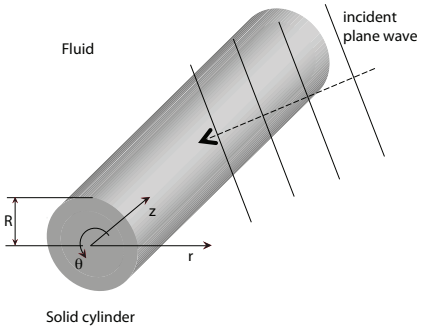

Figure 1: Geometry used for formulating the attenuation from an infinitely long cylinder of radius R.

2.1 Solid fibre model

The solid fibre is modelled using a SCM and is described in detail in [6]. Parameters relating to the fluid surrounding the fibre are given the subscript 1 and those relating to the solid are given the subscript 2. The fibre excitation is illustrated in Fig. 1. The attenuation, α, of the suspension is expressed as

$$\alpha = \frac{-2f_r}{\pi R^2 k_{c_1}} \sum_{n=0}^{\infty} \Re \left(\int_0^{\frac{\pi}{2}} \epsilon_n B_n \cos(\psi) d\psi \right) \tag{1}$$

where f_r is the volume fraction; R is the radius of the fibre; k_{c_1} is the wave number of the compressional wave in water; $\Re$ denotes the real part of the expression, ψ is the angle of incidence; n is a positive real integer; $\epsilon_n = 1$ if $n = 0$, otherwise $\epsilon_n = 2$ and where B_n is the n^{th} expansion coefficient of the wave potential of the reflected wave. The solution for the coefficients B_n, come from using the boundary condition of continuous velocity in the radial direction and continuous stress in radial, tangential and axial directions at the fluid-solid interface. The result is an expression for B_n as a function of the fluid properties: viscosity, η_1, density, ρ_1, and velocity of the compressional wave, c_1, and the fibre properties: radius, R, density, ρ_2, velocity of the compressional wave, c_2, shear wave, c_s and the loss tangent, $\tan \delta$.

In low attenuating suspension, an additional background attenuation, α_{bg}, should be added to the attenuation calculated in equation (1) which is defined as

$$\alpha_{bg} = f_r \alpha' + (1 - f_r)\alpha'', \tag{2}$$

where α' is the intrinsic attenuation of the scatterers and α'' is the intrinsic attenuation of the surrounding fluid [16]. For very dilute suspensions, $f_r \ll 1$ hence $\alpha_{bg} = \alpha''$.

Hence the expression for the attenuation becomes

$$\alpha = \frac{-2f_r}{\pi R^2 k_{c_1}} \sum_{n=0}^{\infty} \Re \left(\int_0^{\frac{\pi}{2}} \epsilon_n B_n \cos(\psi) d\psi \right) + \alpha''. \tag{3}$$

2.2 Hollow fibre model

As above, the parameters relating to the fluid surrounding the fibre are given the subscript 1 and those relating to the solid are given the subscript 2. In addition, parameters relating to the inner fluid are given the subscript 3. In this model we assume that the fluid is non-viscous hence the plane wave can be expressed simply in terms of a scalar potential, ϕ_{c_1}, which is made up of an incident and a reflective part, $\phi_{c_1} = \phi_{o_1} + \phi_{r_1}$. The incident part is then expanded as a series of Bessel functions of the first kind, J_n, and similarly the reflective part is expanded as a series of first order Hankel functions, $H_n^{(1)}$, such that, in cylindrical coordinates,

$$\phi_{o_1} = \left(\sum_{n=1}^{\infty} i^n \epsilon_n \cos(n\theta) J_n(k_{cc_1} r) \right) e^{i(k_{cs_1} z - \omega t)} \tag{4}$$

and

$$\phi_{r_1} = \left(\sum_{n=1}^{\infty} i^n \epsilon_n \cos(n\theta) B_{n_1} H_n^{(1)}(k_{cc_1} r) \right) e^{i(k_{cs_1} z - \omega t)}. \tag{5}$$

where the radial and axial components of the wave number of the compression wave in the fluid are $k_{cc_1} = k_{c_1} \cos(\psi)$ and $k_{cs_1} = k_{c_1} \sin(\psi)$, respectively.

In the solid, the oblique angled plane wave induces both compression and shear waves with wave numbers k_{c_2} and k_{s_2}, respectively. These waves are expressed in terms of scalar and vector potentials and expanded in Bessel function of the first and second kind, Y_n

$$\phi_{c_2} = \left(\sum_{n=1}^{\infty} i^n \epsilon_n \cos(n\theta) \left(B_{n_2} J_n(k_{cc_2} r) + C_{n_2} Y_n(k_{cc_2} r) \right) \right) e^{i(k_{cs_1} z - \omega t)} \tag{6}$$

where, $k_{cc_2} = \sqrt{k_{c_2}^2 - k_{cs_1}^2}$, and

$$k_{s_2}^2 \xi_2 = \left(\sum_{n=1}^{\infty} i^n \epsilon_n \frac{\partial \cos(n\theta)}{\partial \theta} (D_{n_2} J_n(k_{sc_2} r) + F_{n_2} Y_n(k_{sc_2} r)) \right) e^{i(k_{cs_1} z - \omega t)} \tag{7}$$

$$i k_{cs_1} \chi_2 = \left(\sum_{n=1}^{\infty} i^n \epsilon_n \cos(n\theta) (E_{n_2} J_n(k_{sc_2} r) + G_{n_2} Y_n(k_{sc_2} r)) \right) e^{i(k_{cs_1} z - \omega t)} \tag{8}$$

where, $k_{sc_2} = \sqrt{k_{s_2}^2 - k_{cs_2}^2}$, B_{n_2}, C_{n_2}, D_{n_2}, F_{n_2}, E_{n_2} and G_{n_2} is the n^{th} expansion coefficient of the wave potentials.

The inner fluid is assumed to be non-viscous and hence can be expressed in terms of a scalar potential. This is expanded as a series of Bessel functions as it contains the origin, and

$$\phi_{o_3} = \left(\sum_{n=1}^{\infty} i^n \epsilon_n \cos(n\theta) J_n(k_{cc_3} r) \right) e^{i(k_{cs_1} z - \omega t)}. \tag{9}$$

In this case, the inner and outer fluids are the same hence $k_{cc_3} = k_{cc_1}$.

The boundary conditions are that the radial velocity and the stresses are continuous at the surface when $r = R$ and on the inner surface when $r = N$. Since the fluids are assumed to be non-viscous, the tangential and circumferential stresses are zero on these surfaces. Expressing the stresses and velocities in terms of these series expansions of the scalar and vector potentials we obtain the expression for B_{n_1} as

$$B_{n_1} = \frac{a_{cc_1} J_n'(a_{cc_1}) - J(a_{cc_1}) L}{-a_{cc_1} H_n^{1\prime}(a_{cc_1}) + H_n^1(a_{cc_1}) L} \tag{10}$$

where

$$L = \frac{Q}{P} \tag{11}$$

and

$$Q = \begin{vmatrix} a_{21} & a_{22} & a_{23} & a_{24} & a_{25} & a_{26} & 0 \\ a_{31} & a_{32} & a_{33} & a_{34} & a_{35} & a_{36} & 0 \\ a_{41} & a_{42} & a_{43} & a_{44} & a_{45} & a_{46} & 0 \\ a_{51} & a_{52} & a_{53} & a_{54} & a_{55} & a_{56} & a_{57} \\ a_{61} & a_{62} & a_{63} & a_{64} & a_{65} & a_{66} & a_{67} \\ a_{71} & a_{72} & a_{73} & a_{74} & a_{75} & a_{76} & 0 \\ a_{81} & a_{82} & a_{83} & a_{84} & a_{85} & a_{86} & 0 \end{vmatrix},$$

$$P = \begin{vmatrix} a_{11} & a_{12} & a_{13} & a_{14} & a_{15} & a_{16} & 0 \\ a_{31} & a_{32} & a_{33} & a_{34} & a_{35} & a_{36} & 0 \\ a_{41} & a_{42} & a_{43} & a_{44} & a_{45} & a_{46} & 0 \\ a_{51} & a_{52} & a_{53} & a_{54} & a_{55} & a_{56} & a_{57} \\ a_{61} & a_{62} & a_{63} & a_{64} & a_{65} & a_{66} & a_{67} \\ a_{71} & a_{72} & a_{73} & a_{74} & a_{75} & a_{76} & 0 \\ a_{81} & a_{82} & a_{83} & a_{84} & a_{85} & a_{86} & 0 \end{vmatrix}.$$

The matrix elements are functions of the properties of the fluid and the solid and are defined in the appendix.

The attenuation is derived as in the solid model, hence we use equation (1) replacing the expression for B_{1n} with that of equation (10).

Table 1: Table of fibre properties.

Property	Solid Fibre	Hollow Fibre
Outer radius, R (μm)	40 ± 0.19	44 ± 0.18
Inner radius, N (μm)	-	18 ± 0.18
Density (kgm^{-3})	1390	1390
Linear density ($\times 10^6\,\mathrm{kgm}^{-1}$)	17	17
E_z (GPa)	12	7.3

2.3 Suspensions with distributed radii

Since the attenuation is highly dependent on the size of the scatterer, the distribution of the radius is included in the model. Hence equation (12) for the attenuation in a suspension based on scatterers with a single valued radius, has to be modified. A similar approach to that used for polydisperse suspension of spherical particles [17] is applied here to cylindrical particles. The distribution of the radii is described by a histogram of X discrete bin sizes with a volume fraction of scatterers in each bin of f_{rx}. The average radius in each bin, $\bar{R}_x$, is calculated. The attenuation from the SCM (equation (12)) for a suspension of scatterers with distributed radii becomes

$$\alpha_{scm} = \sum_{x=1}^{X} \left(\frac{-2 f_{rx}}{\pi \bar{R}_x{}^2 k_{c_1}} \sum_{n=0}^{\infty} \Re \left(\int_0^{\frac{\pi}{2}} \epsilon_n B_{nx} \cos(\psi) d\psi \right) \right) + \alpha''. \tag{12}$$

The LCM has both an inner radius N and an outer radius, R, that can vary independently hence an additional division is required. The distribution is now described by a two dimensional histogram. The first dimension is a before with X bins and the second dimension is a histogram describing the distribution of the N in Y bins each with a volume fraction in each bin of f_{rxy}. Hence the attenuation from the LCM (equation (13)) with a suspension of scatterers with distributed radii becomes,

$$\alpha_{lcm} = \sum_{y=1}^{Y} \left(\sum_{x=1}^{X} \left(\frac{-2 f_{rxy}}{\pi \bar{R}_{xy}^2 k_{c_1}} \sum_{n=0}^{\infty} \Re \left(\int_0^{\frac{\pi}{2}} \epsilon_n B_{nxy} \cos(\psi) d\psi \right) \right) \right) + \alpha''. \tag{13}$$

3 Experiment

Two samples were prepared, one with solid polyester fibres and the other with hollow polyester fibres. The fibres were supplied by Wellman International Limited, Ireland, and the fibre material in both samples had a density of $1390\,\mathrm{kgm}^{-3}$ and a linear density, ρ_L, of $17{\cdot}10^{-6}\,\mathrm{kgm}^{-1}$. The radius of a sample of 30 fibres was measured using a light microscope. The averages of the measurements are shown in Table 1. The inner diameter of the hollow fibre was calculated from R, ρ_2 and ρ_L and is also given in the table. The radii distribution was calculated from the measurements and is presented in Table 2.

The axial elasticity, E_z, of six hollow and ten solid fibres was measured using an Instron 4411 tensile testing machine. The load was measured by a 5N standard load cell

Table 2: Table of radii distribution

Fibre	Centre of Bin (μm)	Average (μm)	Fraction of total fibres
Solid, R	19	17.9	0.38
	20	20.3	0.36
	22	23.1	0.26
Hollow, R	17.9	18.9	0.21
	22	22.0	0.60
	25	24.0	0.19
Hollow, N	8	8.1	0.39
	9	9.2	0.30
	10	10.3	0.31

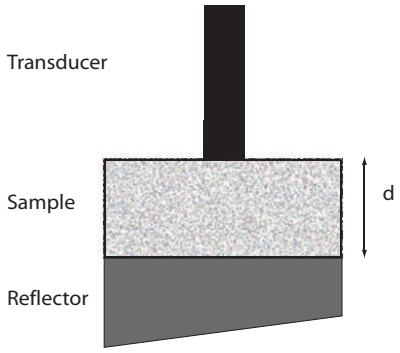

Figure 2: Diagram of the pulse-echo measurement system

and displacement was registered by an electronic unit of the tensile stage. During the measurement, the data were transferred to a PC. The upper grip of the machine was attached through a hinge and thus allowed to self-align. A loading rate of 10% of the fibre length per minute was used. E_z was then calculated from these measurements and the fibre geometry.

A summary of the fibre properties is given in Table 1. The fibres mixed with pure, distilled water to a mass fraction of 0.17± 0.03%. The experiments were carried out using a pulse-echo technique and a diagram of the setup is shown in Fig. 2. A broad-band transducer (V319, Panametrics, Waltham, MA, USA) with a centre frequency of 10 MHz was used. The transducer was excited and the received signal amplified by a pulser/receiver (Model 5073PR, Panametrics). The signal was then digitized using an oscilloscope card (CompuScope 12400, Gage Applied Technologies Inc., Lachine, QC, Canada) with a 12-bit resolution. The sampling rate was set at 200 MHz and all data were stored in a computer for off-line analysis.

The cell was filled with pure, distilled water and a sequence of 300 pulses and echoes

were recorded. The cell was then emptied and filled with a sample of the suspension of solid fibres. A sequence of 500 pulse-echoes were recorded. A sample of the suspension of hollow fibres was then measured in the same way. The temperature of the suspensions and the water varied from a minimum of 20.98±0.2 °C to a maximum of 21.33±0.2 °C during the course of the experiments. The time-of-flight between the pulse and the echo was determined using cross-correlation [18] implemented in Matlab, MathWorks, USA. This time-of-flight and the speed of sound in water, determined from the water temperature, was used to estimate the distance the pulse travelled, i.e. twice the distance labelled d in Fig. 2.

A fast Fourier transform was applied to each echo. Using the average of the water echoes as a reference the attenuation in the sample was calculated for a particular frequency, f, as

$$\alpha_e = \frac{1}{2d} \ln\left(\frac{A_1}{S_1}\right) + \alpha'', \tag{14}$$

where S_1 and A_1 are the frequency dependent amplitudes of the echoes in the sample and water respectively. α'' is the theoretical attenuation of water and assumed to equal $25 \cdot 10^{-15} f^2$ [19].

The standard deviation of the average of the attenuation, σ_α was calculated by an error propagation technique for ultrasound attenuation [20].

4 Estimation Process

Both models were used to solve the inverse problem of estimating the material parameters from α_e over the frequency range 2 MHz - 15 MHz. An iterative search was used to find the values of the material properties, c_2, ν and $\tan\delta$ that minimises the difference between the model attenuation, α_m and the average α_e, over a range of frequencies. This difference is defined as the cost function V and is such that

$$V = \sum_{n=1}^{N} |\alpha_{mn} - \alpha_{en}|^2 \tag{15}$$

where α_m, is the attenuation of the model at the n^{th} frequency interval and α_e is the attenuation calculated from experimental measurements at the n^{th} frequency interval. N is the maximum number of frequency intervals used. The fluid parameters ρ_1 and c_1, were set to 996 kgm^{-1} and 1490 ms^{-1} respectively. The radii used are those in Table 2. ρ_2 was set to 1390 kgm^{-1} since this is the density of the material. However for the calculation of f_r, from the mass fraction, a density of 1115 kgm^{-1} was used which is the density of the hollow fibre structure. The shear wave velocity, c_s, as well as the elastic properties E and G were calculated from the estimated values of c_2, ν and the known ρ_2.

The algorithm used to calculate the cost function, V, was a constrained non-linear least squares fit [21]. The constraints were limits set on the material properties (see Table

Table 3: Limits used in the parameter estimation procedure.

Material Property	Upper Value	Lower Value
c_2	500 ms^{-1}	6000 ms^{-1}
ν	0.2	0.5
$\tan\delta$	0.1	0.5

3) so that the minimised cost function would only be a result of realistic values of c_2, ν and $\tan\delta$. The algorithm was run with 24 different initial values equally spaced over the search space. The estimation of the properties was done on the average of α_e. To assess the effect of noise on the results, the estimation process was also carried out on $\alpha_e \pm \sigma_\alpha$.

The sample rate used in the estimation process, S_p, is a compromise between the accuracy and the speed of optimisation. This was set to use 1 in 4 of the experimental points giving an effective sample rate of 50 MHz since this was sufficient to capture the details of the experimental curves.

5 Results and Discussion

The results of α_e for the solid fibre suspension and the hollow fibre suspension are shown in Fig. 3. A resonance feature in α_e in the solid fibre suspension can be seen clearly at 12 MHz. Such a distinct feature is not seen in α_e in the hollow fibre suspension though the curve between 3-7 MHz is not as flat as that of α_e in the solid fibre suspension. This suggests that there maybe some resonance effects in this frequency range in the hollow fibres. In the solid fibre suspension, σ_α was at a maximum at the two extremes of the frequency range where it was 0.21 Npm^{-1}, though between these extremes, it was 0.01 Npm^{-1}. For the hollow fibres the figures were 0.17 Npm^{-1} at the extremes, otherwise it was a maximum of 0.04 Npm^{-1}.

The results of the parameter estimation from fitting α_{scm} to α_e in the solid fibre suspension are presented in terms of c_2 and c_s in Fig. 4. The figure shows a number of clustered results where the size of the marker indicates the size of V; a small value of V is represented by a small marker. From these marker sizes it can be seen that the cluster at $c_2 = 1720\,\mathrm{ms}^{-1}$, $c_s = 765\,\mathrm{ms}^{-1}$, gives the lowest value of V and hence the best fit to the experimental results. The fact that there are clusters with larger sizes shows that the algorithm is sensitive to the initial values of the optimisation in that it does not successfully converge to the lowest value from all initial values.

The best fit curves associated with the cluster with the lowest V are plotted in Fig. 5. The range of values for elastic moduli E and G from this cluster and from optimisation procedure using $\alpha_e \pm 2\sigma_\alpha$ are given in Table 4. The range of values of the other parameters are also given in Table 4. It can be seen that the results correspond well with block polyester but not with the measured E_z of the fibres of 12 GPa (see Table 1). It is commonly accepted that nylon fibres can more accurately be described as transversely isotropic than isotropic [22]. Also ultrasound frequency measurement of

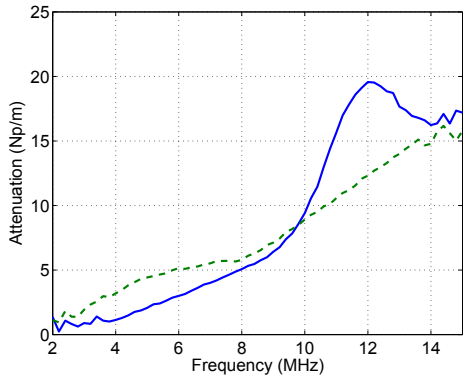

Figure 3: Plot of α_e in hollow fibre (dashed line) and solid fibre (solid line) suspensions (fibre concentration: 0.013% by volume).

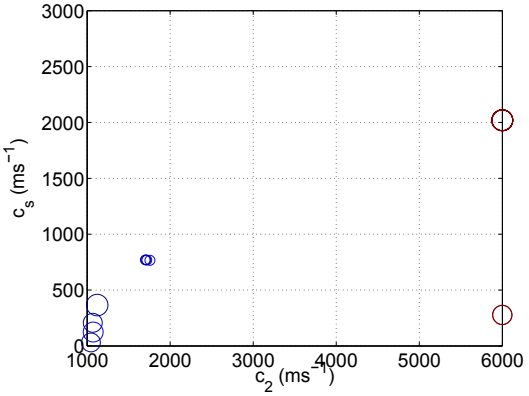

Figure 4: Plot of the estimated compressional wave velocity and shear wave velocity from optimising α_{scm} to α_e in the solid fibre suspension. The shade or colour of the markers represent the value of tan δ and the size of marker, the value of the cost function, V.

the elastic constants studies of drawn nylon film show that the Young's modulus in the drawn direction (corresponding to E_z) is greater than the other directions. Hence the above results suggests that these values are from the cross sectional plane of the fibre (r, θ) rather than the axial direction (z). Support for this can be found from the study of circumferential modes when a cylinder is excited by oblique incidence [23]. However, the differences in material (the latter study used steel and water) makes direct comparison difficult since in the steel case additional approximations can be made.

Fig. 6.6(a) shows the estimated values for c_2 and c_s from optimising the α_{scm} to α_e in the hollow fibre suspension. Fig. 6.6(b) shows the estimated values for E and G. Note

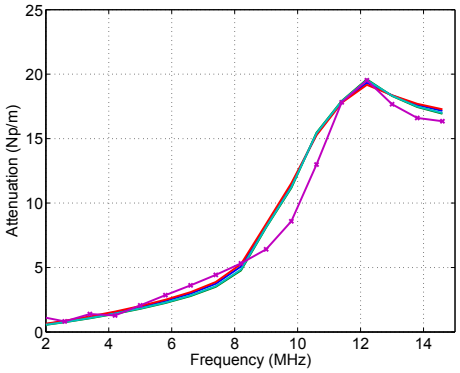

Figure 5: Plot of the best-fit curves of the cluster with the lowest V. Results from optimising α_{scm} to α_e in the solid fibre suspension. Experimental results are marked with crosses.

Table 4: Table of Estimated and Reference values for Polyester Properties

Polyester Sample	Method	E GPa	G GPa	c_2 ms^{-1}	c_s ms^{-1}	ν	tanδ
Solid fibre	U.S+SCM	2.41-2.45	0.83-0.87	1700-1720	760-770	0.372-0.376	0.11-0.12
Hollow fibre	U.S+LCM	1.66-1.69	0.57-0.59	2030-2060	630-620	0.447-0.450	0.10
Hollow fibre	U.S+SCM	0.50-0.51	0.17	1250-1910	340	0.460-0.484	0.13-0.23
Block	Reference[1]	2-4	0.7-1.5	1600-3100	700-1025	0.37-0.44	-

[1] taken from Goodfellow Cambridge Limited, Cambridge, UK.

that the size of the marker is scaled by a factor of ten in comparison with Fig. 4, as the values for V were small. Unlike the solid fibre results there are no values around 2 GPa. There are two clusters with small V but both give very low estimates for E and G as shown in Table 4. The best fit curves from these clusters are shown in Fig. 7. As can be seen, the fit is remarkably good, however the values of the material properties for these best fit curves are 25% of the reference value of E and G and hence are not reasonable.

The results of the optimisation of α_{lcm} to α_e in the hollow fibre suspension are given in Fig. 8. The cluster with the lowest value of V is at $c_2 = 2030\,\mathrm{ms}^{-1}$, $c_s = 620\,\mathrm{ms}^{-1}$. The range of values for elastic moduli E and G from this cluster and from estimating the parameters using $\alpha_e \pm 2\sigma_\alpha$ are given in Table 4. The range of values of the other parameters are also given in Table 4.

The best fit curves associated with this cluster are plotted in Fig. 9. It can be seen that unlike the solid fibre, α_e of the hollow fibre suspension shows no distinct resonance features. There is a slight feature centred around 5 MHz which also exists in the fitted curve. However, the fitted curves also show small resonance features at 7 MHz which does not appear in the experimental values. One possible explanation for this is that

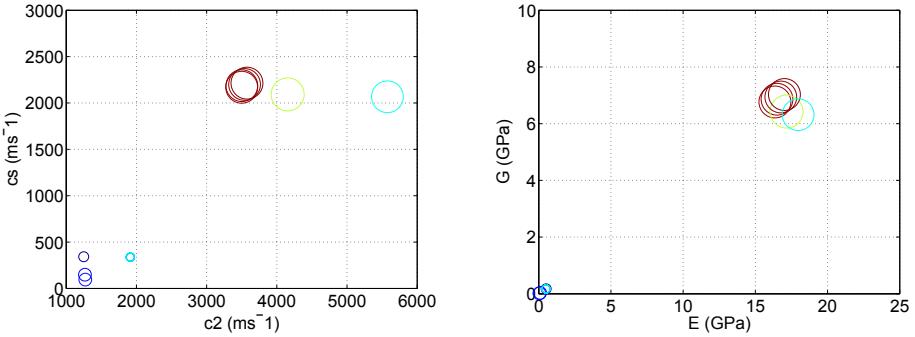

(a) (b)

Figure 6: Fig. 6.6(a) is a plot of the estimated compressional wave velocity and shear wave velocity and Fig. 6.6(b) is a plot of the estimated Young's modulus and shear modulus. Both plots are the results of the parameter estimation procedure when α_{scm} is fitted to α_e in the hollow fibre suspension. The shade or colour of the markers represent the value of tan δ and the size of marker, the value of the cost function, V.

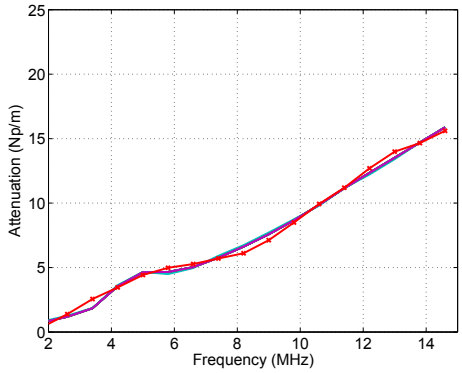

Figure 7: Plot of the best-fit curves of the clusters with two lowest V. The results from the parameter estimation procedure when α_{scm} is fitted to α_e in the hollow fibre suspension. Experimental results are marked with crosses.

the fibres are not isotropic, hence the material properties are dependent on the angle of incidence in a way that is not captured by the model since the model assumes the fibres to be isotropic. These anisotropy in the material properties could cause resonance across a broader range of frequencies.

Since the results of the estimation depend on S_p and to some extent on the choice of limits chosen on the optimisation, some additional clarification of these subjects is given here.

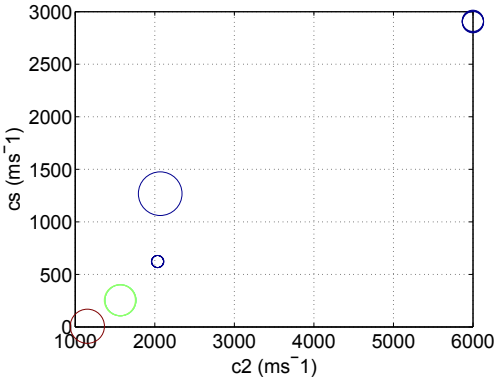

Figure 8: Plot of the compressional wave velocity, c_2 and shear wave velocity, c_s from results of the parameter estimation procedure when α_{lcm} is fitted to α_e in the hollow fibre suspension. The shade or colour of the markers represent the value of tan δ and the size of marker, the value of the cost function, V.

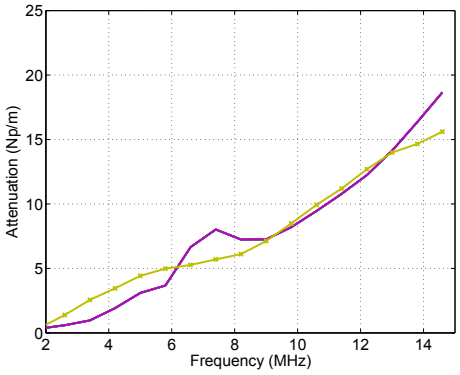

Figure 9: Plot of the best-fit curves of the remaining cluster of results from the parameter estimation procedure when the hollow model is used to model α_e in the hollow fibre suspension. Experimental results are marked with crosses.

The boundary on the volume fraction was set as $\pm 20\%$. This was to take into account the accuracy of the scales used for weighing the fibres which gives an error of $\pm 17\%$. An additional few percent was added to allow for other losses in fibres such as fibres floating on the surface. The lower boundary of the loss tangent was set at a fairly high value of 0.1. The reason this was chosen is that the layered model used has no damping mechanisms if the loss tangent is not set since the viscosity is not taken into account. This means that any resonance peaks tend to be very large. It is also possible, with the low S_p,

that these peaks lie between two sample points and hence are not correctly rejected as a poor fit. Using a higher loss tangent removes these problems and gives more consistent optimisation results. Values for the loss tangent at ultrasonic frequencies for polyester are difficult to obtain, though other polymers such as nylon have values of 0.1 [24].

6 Conclusion

The hollow model when used in conjunction with the hollow fibre suspension measurements gave similar estimation of E and G to those from the solid model used in conjunction with the solid fibre suspension measurements. These compare well to values of E and G for block polyester. However the estimated value for E from this method does not reflect the measured axial value of E.

The solid model when used in conjunction with a hollow fibre suspension does not give reasonable estimates of the material properties of fibres, at least in this frequency-diameter region. Hence, despite giving a good fit to the experimental results the model is not capturing the behaviour of the hollow fibres. We conclude, therefore, that in this frequency-diameter region, it is necessary to use the more complex hollow model when estimating material properties such as the elastic modulii from suspensions of hollow fibres.

$$a_{11} = -i\omega a_{2cc} J_n'(a_{2cc})$$

$$a_{12} = -i\omega a_{2cc} Y_n'(a_{2cc})$$

$$a_{13} = -i\omega n^2 J_n(a_{2sc})$$

$$a_{14} = -i\omega n^2 Y_n(a_{2sc})$$

$$a_{15} = i\omega a_{2sc} J_n'(a_{2sc})$$

$$a_{16} = i\omega a_{2sc} Y_n'(a_{2sc})$$

$$a_{21} = \frac{(\omega^2\rho_2 R^2 - 2Ga_{2c}^2) J_n(a_{2cc}) - 2Ga_{2cc}^2 J_n''(a_{2cc})}{i\omega\rho_1 R^2}$$

$$a_{22} = \frac{(\omega^2\rho_2 R^2 - 2Ga_{2c}^2) Y_n(a_{2cc}) - 2Ga_{2cc}^2 Y_n''(a_{2cc})}{i\omega\rho_1 R^2}$$

$$a_{23} = 2Gn^2 (J_n(a_{2sc}) - a_{2sc} J_n'(a_{2sc}))/(i\omega\rho_1 R^2)$$

$$a_{24} = 2Gn^2 (Y_n(a_{2sc}) - a_{2sc} Y_n'(a_{2sc}))/(i\omega\rho_1 R^2)$$

$$a_{25} = 2Ga_{2sc}^2 J_n''(a_{2sc})/(i\omega\rho_1 R^2)$$

$$a_{26} = 2Ga_{2sc}^2 Y_n''(a_{2sc})/(i\omega\rho_1 R^2)$$

$$a_{31} = 2(a_{2cc} J_n'(a_{2cc}) - J_n(a_{2cc}))$$

$$a_{32} = 2(a_{2cc} Y_n'(a_{2cc}) - Y_n(a_{2cc}))$$

$$a_{33} = n^2 J_n(a_{2sc}) - a_{2sc} J_n'(a_{2sc}) + a_{2sc}^2 J_n''(a_{2sc})$$

$$a_{34} = n^2 Y_n(a_{2sc}) - a_{2sc} Y_n'(a_{2sc}) + a_{2sc}^2 Y_n''(a_{2sc})$$

$$a_{35} = 2(J_n(a_{2sc}) - a_{2sc} J_n'(a_{2sc}))$$

$$a_{36} = 2(Y_n(a_{2sc}) - a_{2sc} Y_n'(a_{2sc}))$$

$$a_{41} = 2a_{2cc} a_{1cs}^2 J_n'(a_{2cc})$$

$$a_{42} = 2a_{2cc} a_{1cs}^2 Y_n'(a_{2cc})$$

$$a_{43} = n^2 a_{1cs}^2 J_n(a_{2sc})$$

$$a_{44} = n^2 a_{1cs}^2 Y_n(a_{2sc})$$

$$a_{45} = a_{2sc}^3 J_n'(a_{2sc}) - a_{2sc} J_n'(a_{2sc}) a_{1cs}^2$$

$$a_{46} = a_{2sc}^3 Y_n'(a_{2sc}) - a_{2sc} Y_n'(a_{2sc}) a_{1cs}^2$$

$$a_{51} = -i\omega a_{3cc} J_n'(a_{3cc})$$

$$a_{52} = -i\omega a_{3cc} Y_n'(a_{3cc})$$

$$a_{53} = -i\omega n^2 J_n(a_{3sc})$$

$$a_{54} = -i\omega n^2 Y_n(a_{3sc})$$

$$a_{55} = i\omega a_{3sc} J_n'(a_{3sc})$$

$$a_{56} = i\omega a_{3sc} Y_n'(a_{3sc})$$

$$a_{57} = -a_{4cc} J_n'(a_{4cc})$$

$$a_{61} = \frac{(\omega^2\rho_2 N^2 - 2Ga3c^2) J_n(a_{3cc}) - 2Ga_{3cc}^2 J_n''(a_{3cc})}{i\omega\rho_1 N^2}$$

$$a_{62} = \frac{(\omega^2\rho_2 N^2 - 2Ga3c^2) Y_n(a_{3cc}) - 2Ga_{3cc}^2 Y_n''(a_{3cc})}{i\omega\rho_1 N^2}$$

$$a_{63} = 2Gn^2 (J_n(a_{3sc}) - a_{3sc} J_n'(a_{3sc}))/(i\omega\rho_1 N^2)$$

$$a_{64} = 2Gn^2 (Y_n(a_{3sc}) - a_{3sc} Y_n'(a_{3sc}))/(i\omega\rho_1 N^2)$$

$$a_{65} = 2Ga_{3sc}^2 J_n''(a_{3sc})/(i\omega\rho_1 N^2)$$

$$a_{66} = 2Ga_{3sc}^2 Y_n''(a_{3sc})/(i\omega\rho_1 N^2)$$

$$a_{67} = J_n(a_{4cc})$$

$$a_{71} = 2(a_{3cc} J_n'(a_{3cc}) - J_n(a_{3cc}))$$

$$a_{72} = 2(a_{3cc} Y_n'(a_{3cc}) - Y_n(a_{3cc}))$$

$$a_{73} = n^2 J_n(a_{3sc}) - a_{3sc} J_n'(a_{3sc}) + a_{3sc}^2 J_n''(a_{3sc})$$

$$a_{74} = n^2 Y_n(a_{3sc}) - a_{3sc} Y_n'(a_{3sc}) + a_{3sc}^2 Y_n''(a_{3sc})$$

$$a_{75} = 2(-a_{3sc} J_n'(a_{3sc}) + J_n(a_{3sc}))$$

$$a_{76} = 2(-a_{3sc} Y_n'(a_{3sc}) + Y_n(a_{3sc}))$$

$$a_{81} = 2a_{3cc} a_{4cs}^2 J_n'(a_{3cc})$$

$$a_{82} = 2a_{3cc} a_{4cs}^2 Y_n'(a_{3cc})$$

$$a_{83} = n^2 a_{4cs}^2 J_n(a_{3sc})$$

$$a_{84} = n^2 a_{4cs}^2 Y_n(a_{3sc})$$

$$a_{85} = a_{3sc}^3 J_n'(a_{3sc}) - a_{3sc} J_n'(a_{3sc}) a_{4cs}^2$$

$$a_{86} = a_{3sc}^3 Y_n'(a_{3sc}) - a_{3sc} Y_n'(a_{3sc}) a_{4cs}^2$$

References

[1] C. Habeger and G. Baum, "Ultrasonic characterizations of fibre suspension," The Institue of Paper Chemistry, Appleton, Wisconsin, IPC Technical Paper series 118, Nov 1981.

[2] C. Habeger, "The attenuation of ultrsound in dilute polymeric fiber suspensions," *Journal of Acoustical Society of America*, vol. 72, pp. 870–878, sep 1982.

[3] R. Challis, M. Povey, M. Mather, and A. Holmes, "Ultrasound techniques for characterizing colliodal dispersions," *Reports in Progress in Physics*, vol. 68, pp. 1541–1637, 2005.

[4] S. M. Hasheminejad and M. Rajabi, "Acoustic scattering characteristics of a thick-walled orthotropic cylindrical shell at oblique incidence," *Ultrasonics*, vol. 47, pp. 32–48, 2007.

[5] Y. Aitomäki and T. Löfqvist, "Material property estimates from ultrasound attenuation in fibre suspensions," *Ultrasonics*, vol. doi:10.1016/j.ultras.2008.11.005, 2009.

[6] ——, "Estimating suspended fibre material properties by modelling ultrasound attenuation," in *Mathematical modeling of wave phenomena: 2nd Conference on Mathematical Modeling of Wave Phenomena*, B. Nilsson and L. Fishman, Eds., vol. 834:1. AIP, 2006, pp. 250–259.

[7] A. Leissa, *Vibrations of Shells*. NASA, Washington, DC. Tech. Rep. NASA SP-288, 1973.

[8] W. Flugge, *Stresses in shells*. Springer, 1973.

[9] R. Blevins, *Formulas for natural frequency and mode shapes*, 2nd ed. Van Nostrand Reinhold Company, 1979.

[10] S. K. Numrich and H. Uberall, *Physical Acoustics Vol. XXI*. Academic Press, 1992, ch. Scattering of sound pulses and the ringing of target resonances, p. 235.

[11] J. Dickey, G. Frisk, and H. Uberall, "Whispering gallery wave modes on elastic cylinders," *Journal of the Acoustical Society of America*, vol. 59, no. 6, pp. 1339–1346, June 1976.

[12] H. Uberall, L. Dragonette, and L. Flax, "Relation between the creeping waves and the normal modes of vibration of a curved body," *Journal of the Acoustical Society of America*, vol. 61, no. 3, pp. 711–715, Mar 1977.

[13] J. Diarmuid-Murphy, J. George, A. Nagl, and H. Uberall, "Isolation of the resonant component in acoustic scattering from fluid-loaded elastic spherical shells," *Journal of the Acoustical Society of America*, vol. 65, no. 2, pp. 368–373, Feb 1979.

[14] H. Uberall, G. Gaunaurd, and J. Diarmuid Murphy, "Acoustic surface wave pulses and the ringing of resonances," *Journal of the Acoustical Society of America*, vol. 72, no. 3, pp. 1014–1017, Sept 1982.

[15] L. Flax and W. Neubauer, "Acoustic reflection from layered elastic absorptive cylinders," *Journal of the Acoustical Society of America*, vol. 61, no. 2, pp. 307–312, Feb 1977.

[16] A. K. Hipp, G. Storti, and M. Morbidelli, "Acoustic characterization of concentrated suspensions and emulsions. 1. model analysis," *Langmuir*, vol. 18, no. 2, pp. 391–404, 2002. [Online]. Available: http://pubs.acs.org/doi/abs/10.1021/la015538c

[17] R. E. Challis, J. S. Tebbutt, and A. K. Holmes, "Equivalence between three scattering formulations for ultrasonic wave propagation in particulate mixtures," *J. Phys. D: Appl. Phys.*, vol. 31, pp. 3481–3497, 1998.

[18] S. Orfanidis, *Optimum Signal Processing. An Introduction*, 2nd ed. Prentice-Hall, Englewood Cliffs, NJ,, 1996.

[19] L. Kinsler, A. Frey, A. Coppens, and J. Sanders, *Fundamentals of Acoustics*, 4th ed. John Wiley and Sons Inc., 2000.

[20] J. Martinsson, J. Carlson, and J. Niemi, "Model-based phase velocity and attenuation estimation in wideband ultrasonic measurement systems," *IEEE Transactions on Ultrasonics, Ferroelectrics and Frequency Control*, vol. 54, no. 1, pp. 138–146, January 2007.

[21] T. Coleman and Y. Li, "An interior trust region approach for nonlinear minimization subject to bounds," *SIAM Journal on Optimization*, vol. 6, pp. 418–445, 1996.

[22] D. Hadley, P. R. Pinnock, and I. M. Ward, "Anisotropy in oriented fibres from synthetic polymers," *Journal of Materials Science*, vol. 4, no. 2, pp. 152–165, 1969.

[23] Y. Fan, F. Honarvar, A. N. Sinclair, and M. R. Jafari, "Circumferential resonance modes of solid elastic cylinders excited by obliquely incident acoustic waves," *The Journal of the Acoustical Society of America*, vol. 113, no. 1, pp. 102–113, 2003. [Online]. Available: http://dx.doi.org/10.1121/1.1525289

[24] J. Ferry, *Viscoelastic Properties of Polymers*, 3rd ed. John Wiley & Sons Inc, 1980, ch. 2, pp. 46–47.

Paper G

Comparison of softwood and hardwood pulp fibre elasticity using ultrasound

Authors:
Yvonne Aitomäki, Jan Niemi and Torbjörn Löfqvist

To be submitted

Comparison of softwood and hardwood pulp fibre elasticity using ultrasound

Yvonne Aitomäki, Jan Niemi and Torbjörn Löfqvist

Abstract

A method based on ultrasound scattering for estimating the elastic properties of fibres in suspension is tested on pulp. Estimates of the elastic moduli are found by measuring and modelling the attenuation of ultrasound in hardwood and softwood pulps. The method gives an single unambiguous value for moduli of each fibre type. The results show that the refined hardwood and softwood fibres have the equal elastic properties after chemical treatment and refining. Further work on the method is required to validate these results.

1 Introduction

Fibre properties in pulp contribute significantly to the characteristics of the finish paper product. One of these properties is the flexibility of fibres which affects the strength of the paper since greater flexibility improves bonding between the fibre [1]. It would therefore be advantageous to measure the flexibility of fibres during the production. The flexibility of a fibre is defined as function of both the elastic modulus of the structure and its cross sectional geometry, more specifically, its second moment of area [2]. Individual fibre tests [3] showed that the flexibility of fibres can be altered by the refining energy in that it increases the second moment of area. Their results also showed a large difference between the elasticity of fibres at two different fraction levels. Fractioning fibres separates fibres according to a combination of length and flexibility whereby short or flexible long fibre pass through a mesh [1]. In these individual fibre test, measurement of the two different fractions showed that the flexibility of fibres is not only due to differences in the second moment of area but to their elasticity.

Some of the current methods of measuring fibre flexibility are from single fibres measurement in the laboratory [3, 4]. Measurements of the fibres flexibility can also be obtained from devices such as the SFTI Fibermaster (Lorentzen-Wettre, Sweden), by measuring the way a fibre is deformed by different rates of flow through the instrument. This is however, a relative measure of flexibility and it is difficult to separate the contribution of the geometry from the elastic properties of the fibres [5].

A potential method of measuring the elastic properties of fibre and hence their flexibility is to measure the elastic modulus by ultrasound. However, ultrasound scattering has a large dependence on the size of the scatterer which is why it has be used for particle sizing in opaque mixtures [6]. Therefore an integral part of this method is its use in conjunction with optical measurement devices such as a PulpEye (Eurocon Analyzer AB,

Sweden) or the STFI Fibermaster. The ultrasound method has been tested on hollow polymer fibres and shows some promising results [7]. Since ultrasound is non-destructive, non-contact quick and inexpensive it lends itself to online material characterisation.

Although this model shows promising results for synthetic fibres it is less certain whether it is suitable for testing wood fibres which are considerably less cylindrical in form than synthetic fibres. Wood fibre also have a more complex fibre wall structure than synthetic fibres. This added complexity may cause additional anisotropic behaviour that is not included in the model.

This study is therefore a preliminary investigation on whether ultrasound can be used to measure the elastic properties of fibres in pulp. A comparison is done between softwood pulp and hardwood pulp. The method is based on solving the inverse problem. This is where measurements are taken and the problem is to establish the parameter values that would produce such measurements. The method therefore has three parts: measuring ultrasound attenuation from fibres in suspension, modelling the attenuation and optimising the fit between the model and the measurements. The optimisation gives an estimate of the material properties that give the best fit to the measurements. The method requires knowledge of the geometric properties of the fibres.

2 Method

2.1 Experimental setup

The ultrasound was measured using a pulse-echo technique in the measurement cell illustrated in Fig. 1. The cell was inserted in as a module in PulpEye (Eurocon Analyzer AB, Sweden) optical based pulp analyzer. The propagating ultrasonic signal travels through the suspension, reflects back at a polished steel reflector and is then received by the transducer. The distance between the transducer and the reflector was 19.2 mm. The ultrasound was generated by a PVDF transducer from GE Sensing & Inspection Technologies, PA, USA, with a center frequency of 25 MHz. The transducer was excited and amplified by a dual pulser/receiver model DPR500 from JSR ultrasonics, NY, USA. The captured ultrasonic signal from the pulser/receiver was digitized by an oscilloscope card (CompuScope 12400, from Gage Applied Technologies Inc., Canada), sampling at 100 MHz with a 12-bit resolution. The data was store on a PC for later analysis.

Note that the measurement cell is a combined optical and ultrasonic measurement device but, for clarity, the optical section has not been shown since this was not used in this study.

The softwood pulp was that used for kraftliner Brown and the hardwood pulp was that used for kraftliner white. Both of are were chemical pulps after the refining stage and were delivered from SCA Munksund, Sweden. The pulp was first fractioned using a Britt Jar, with a mesh 50, to remove the fines contents in the pulp sample. After the measurements a smaller sample of each pulp was used to determine the total mass consistency (method standard ISO 4119:1995 [8]). The fibre geometry was analyzed by PulpEye using a camera based method.

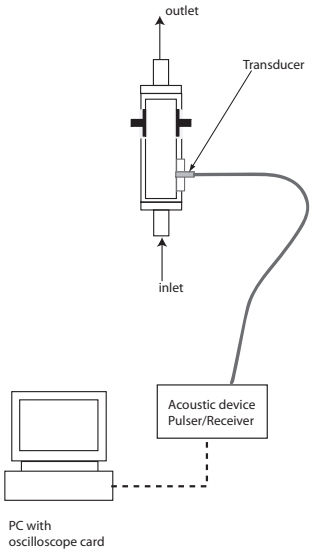

Figure 1: Diagram of the experimental setup

The samples were poured into the PulpEye and cycled in a closed loop. During the each experiment the system was pressurized. This means that size of air bubbles in the samples are reduced. After a initial pumping sequence to make the samples more homogeneous, the measurement started. The measurement procedure was repeated twice in order to reduce variation in the measurements average.

For each pulp sample, 300 ultrasonic pulses was recorded. The temperature in the suspension was monitored during the whole experiment and ranged from 10.0-10.7℃. After thoroughly rinsing the system, the PulpEye was filled with water and three reference signals were measured and the temperature was recorded as 10.1℃.

A discrete Fourier transform was performed on the stored signals, which were then averaged. The attenuation was then calculated as

$$\alpha_e = \frac{1}{2d} \ln\left(\frac{P_s}{P_w}\right) + \alpha'', \tag{1}$$

where P_s and P_w are the amplitudes of the echoes in the sample and water respectively. α'' is the theoretical attenuation of water and assumed to equal $36.1{\cdot}10^{-15} f^2$ [9].

The standard deviation of the mean was calculated by propagating errors through the above equation. The frequency range is set by the spectral content of the received pulse echo. In this study, the frequency range is found to be 4-29 MHz.

2.2 Model and Optimisation

The second part of the method requires a model of the attenuation of ultrasound in a suspension of fibres. It is based on the attenuation, α_m, of an ultrasound wave scattered by a layered cylinder. The expression for α_m is derived elsewhere [7] and is

$$\alpha_m = \sum_{y=1}^{Y}\left(\sum_{x=1}^{X}\left(\frac{-2f_{rxy}}{\pi \bar{R_{xy}}^2 k_{c_1}}\sum_{n=0}^{\infty}\Re\left(\int_0^{\frac{\pi}{2}}\epsilon_n B_{nxy}\cos(\psi)d\psi\right)\right)\right) + \alpha''. \qquad (2)$$

In this expression the distribution of the cross sectional geometry is described by a two dimensional histogram where the first dimension is of x intervals of the radial sizes X and the second dimension is y intervals of the lumen sizes Y. The volume fraction in each interval is given by f_{rxy}. R_x is the average radius of the fibres within the interval X. k_{c1} is the wave number of the compression wave in the fluid. $\Re$ denotes the real part of the expression, ψ is the angle of incidence; n is a positive real integer; $\epsilon_n = 1$ if $n = 0$, otherwise $\epsilon_n = 2$ and where B_{nxy} is the n^{th} expansion coefficient of the wave potential of the reflected wave for X, Y fibre size interval. The expression for B_{nxy} is a function of the fibre properties and the properties of the water and is given in a previous publication [7]. α'' is the intrinsic attenuation of water. A layered cylinder is used since, as the afore mentioned study shows, a solid fibre model is not sufficiently complex to capture the behaviour of the ultrasound.

The elastic moduli, Young's modulus, E, and the shear modulus, G, are estimated by the method. These are calculated from the properties estimated from the model which are the compression wave velocity, c_2, the shear wave velocity, c_s, and the intrinsic loss, $\tan\delta$. The properties of water are assumed to be known and the values used in the model are the compression wave velocity, $c_1 = 1496\,\text{ms}^1$ and the density, $\rho_1 = 996\,\text{kgm}^{-3}$. The water is assumed to be non-viscous which has be found to be a reasonable assumption if the solid is viscoelastic [7]. Studies have shown the fibre material to be viscoelastic [10].

The fibre diameters, ϕ were sorted into size grouping and the percentage in each group was calculated. The average diameter of each group was also calculated. These numbers are presented in Table 1 and were used in equation 2.

The average diameter of the softwood fibre was 29.8± 2.2 μm and the average wall thickness was 2.42 μm. This gives an average lumen size of 24.9 μm and makes up for 84% of the fibre. In the calculation we assume that the lumen is this percentage in all the fibres. For hardwood fibres, the assumption is that the lumen makes up 81% of the fibre. This is based on an average wall thickness of 1.80 μm and an average diameter of 18.55± 0.92 μm.

The dry mass fraction of the pulps were measured as 0.206% and 0.232% for the hardwood and the softwood samples, respectively. From the geometry of the fibres and taking the density of the wood fibre material as $1500\,\text{kgm}^{-3}$ [4], this gives a density for the hardwood fibre structure as $491\,\text{kgm}^{-3}$ and for the softwood fibre structure as $442\,\text{kgm}^{-3}$. These are typical values for pine. The volume fraction is therefore 0.34% and 0.41% for the hardwood and the softwood pulps, respectively.

The algorithm used in the optimisation is a non-linear least square fit with boundaries on the parameters [11]. These boundaries used are given in Table 2. In addition the

Table 1: Table of radii distribution

Fibre	Upper limit of Bin (μm)	Average (μm)	Percentage of fibres %
Softwood, ϕ	≤ 16	14.8	5.6
	22	20	19.4
	28	26.2	30.4
	34	31.9	22.8
	$\leq$35	45.1	21.8
Hardwood, ϕ	10	9.5	2.2
	16	14.9	37.9
	18	19.4	45.6
	22	25.4	11.6
	25	33.7	2.7

Table 2: Limits used in the parameter estimation procedure.

Material Property	Lower Value	Upper Value
c_2	500 ms^{-1}	6000 ms^{-1}
ν	0.2	0.5
$\tan\,\delta$	0.1	0.5

volume fraction was allowed to vary down to 0.15% to allow for the fact that a proportion of the fibres are collapsed and therefore the number of fibres per unit volume is less. The results of the optimisation algorithm can depend on the initial values. This is because the algorithm is not always able to locate the best-fit between the measured attenuation and the modelled attenuation. To improve the chances of the best fit being located, 16 different initial values for the parameters being estimated, were used. These were spaced evenly across the allowed search space.

3 Results

Figure 2 is a plot of the experimental measurements of the attenuation in the softwood and the hardwood pulp. The standard deviation of the mean, σ_m, of the measurements was a maximum of $1.2\,\mathrm{Npm}^{-1}$ for the softwood and the hardwood pulps. However, these maximum in σ_m were only at the highest frequencies, otherwise σ_m was less than $0.3\,\mathrm{Npm}^{-1}$. The gradients for both pulps appear constant and do not appear to show any of the resonance peaks that have been observed in experimental attenuation in synthetic fibre suspension [12,13]. However, if the attenuation was due solely to the wave travelling through the fibre material, without scattering or resonance, it would be proportional to the quantity of the material and its intrinsic attenuation. Therefore it would be expected that the pulp with the higher volume fraction would have a large attenuation unless the intrinsic loss was significantly higher. The results show however that larger attenuation

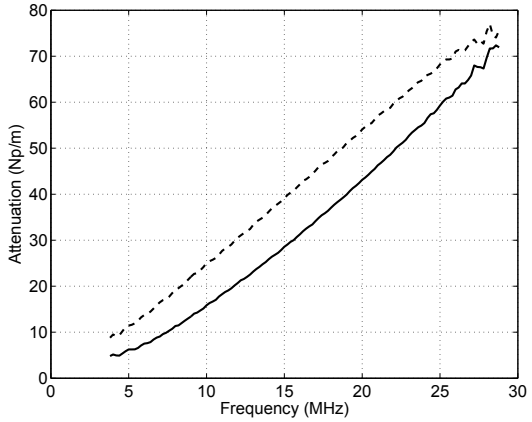

Figure 2: Plot of α_e in softwood fibre (solid line) and hardwood fibre (dashed line) pulps.

Table 3: Table of Estimated Values for Hardwood and Softwood Properties

Fibre Type	E GPa	G GPa	c_2 ms^{-1}	c_s ms^{-1}	ν	$\tan\delta$
Softwood fibres	1.56-1.60	0.52-0.53	6000	590-604	0.495	0.1-0.08
Hardwood fibre	1.56-1.57	0.52-0.53	6000	590-592	0.495	0.05

is in the suspension with the slightly lower volume fraction. This indicates that either there are significant differences in intrinsic attenuation properties of the material or that the attenuation is a result of a more complex interaction between the fibres and the ultrasound. In the model, the attenuation is based on the latter.

In solving inverse problems, it is common to obtain ambiguous results. In our case, the fitting procedure did successfully identify one result that had a lower error difference between the measured and modelled attenuation. The solution with the lowest error for the softwood and the hardwood pulps are plotted in figures 7.3(a) and 7.3(b). The estimates of the material properties of these best-fits are given in table 3 for both types of pulp. As can be seen from 7.3(a), the fit to the attenuation in the softwood pulp is good and the estimate values of the Young's modulus match the values from a study on individual fibre measurements [3]. The hardwood fibre estimates of all the properties are very close to that of the softwood fibres. The best fit curve captures the overall trend of the measurement curve but there exists two resonance features in the modelled attenuation that are not seen in the experimental results.

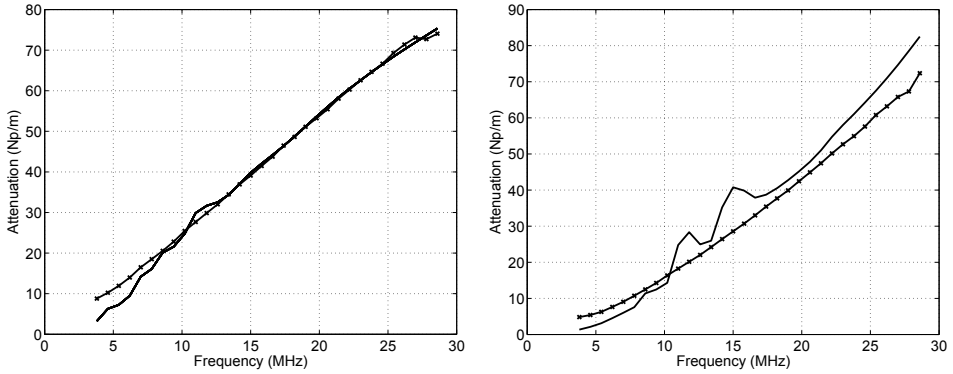

(a) (b)

Figure 3: Results from optimising α_m to α_e in the pulp. Experimental results are marked with crosses. Fig. 7.3(a) is the best-fit for the softwood pulp and Fig. 7.3(b) is the best-fit to the hardwood pulp.

4 Discussion

As discussed in the introduction, the emphasis of this study is on evaluating the method and to a less extent interpreting the results of the comparison between the two pulp. This method has previously been tested on synthetic fibres which although were hollow and varied in diameter, were cylindrical. Wood fibre cross section would be more accurately described by an ellipse than circular, however the mathematical solutions to the scattering problem with this geometry are considerable more complex.

Therefore the assumption this method relies on is that the elliptical shape of a layered scatterer will only affect the attenuation to a certain degree. This is thought to be a reasonable assumption because the attenuation is an average over all angles of incidence and is based on the calculation of the energy over the surface of the scatterer at a large distance away from it. However variations in the shape would cause the resonance from different fibres to be at slightly different frequencies hence clear peaks will not be seen and there will be some discrepancies between the model and the measured attenuation.

Inherent in this is that differences in the elastic properties of the material have a larger impact on the attenuation than the differences in shape. Given this is true, it should therefore be possible to establish the elastic properties without modelling the exact shape of the layered scatterer which in this case is the fibre.

The absence of the peaks in measured attenuation of the hardwood pulp can therefore be explained by the fact that the fibres are not perfect cylinders and vary in shape. The reason for the fact that no resonance peaks are found in the softwood despite the value of the material properties being almost identical is that the diameter distribution of the softwood fibres is greater than the hardwood fibres (see Table 1). A greater distribution in diameter means that the resonance peaks occur across a broader range of frequencies

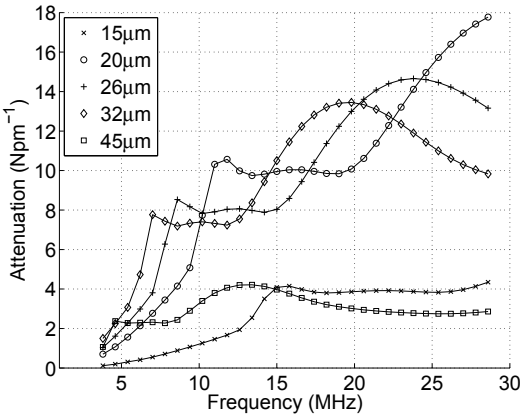

Figure 4: Plot of the attenuation due to the different diameter (given in table 1) that summed, give the best fit to the measured attenuation in the softwood fibre pulp (shown in Fig. 7.3(a))

and when these are summed together the result is that there is virtually no evidence of the resonance peaks are seen in the final curve. To illustrate this point Fig. 4 shows a plot of the attenuation from the different diameters that make up the total modelled attenuation in Fig. 7.3(a).

Examining the results it is seen that the estimated values for c_2 for both the softwood and the hardwood pulp were equal to the boundary value set for the optimisation process. Since this velocity is that of steel it is highly unlikely to be the true value of the c_2. However, the estimated value for Young's modulus is a typical value. The most likely source of this error is due to the assumption in the model that the material is isotropic as opposed to transversely isotropic. It maybe possible to use a transversely isotropic material but this introduces five independent elastic constants instead of two and hence could introduce further ambiguities into the results of the optimisation. Hence, an alternative option is to not limit the value of c_2, allow it to be adjusted to compensate for the error in assuming the material to be isotropic and only use the value of the Young's modulus that is calculated from it.

The $\tan\delta$ for the hardwood fibres was equal to the boundary value set for the optimisation process. This was also true of the volume fraction for hardwood fibres. So, with the volume fraction at its minimum value and knowing that a low tangent delta value lowers the attenuation at all points except for the resonance peaks, it would appear that the model is predicting the attenuation to be higher than the measurement value. This could be an effect of a large number of collapsed fibres.

The estimated value for E of 1.6 GPa compares well with the upper range of individual fibre measurements [3], this, however, is unexpected. This is because others studies on polymer fibres have previously shown that the estimated value is close to that of the transverse Young's modulus, $E_{\theta r}$ and not the longitudinal direction, E_z. This supported to some extent by studies on the modes of vibration in nylon cylinder in water [7] but

the relationship of the modes of vibration to a specific modulus was not done. It could be that the wood material is now isotropic possibly due to the action of the refining process. However, this is unlikely and if the material was isotropic then the reason for the model giving very high values for c_2 could not be true. We would suggest therefore that the value estimated is $E_{\theta r}$ and that E_z is typically much higher than this. The pulp used in the individual study was refined thermomechanical pulp of black spruce whereas the pulps used here was refined kraft pulp. It is therefore expected that there would be considerable differences in the elastic properties. This supports the suggestion that the value estimated using the ultrasound method is that of $E_{\theta r}$. The individual fibres testing was also done at much lower frequencies which could also be a cause of difference in the measurements .

Not all the initial values converged on the lowest difference between the measured attenuation and the modelled attenuation. Modification to the error difference calculation could improve the number of values that converged to the best fit value so that the optimisation would be less sensitive to the initial values. This would make it unnecessary to have several initial values and hence the optimisation process would be more efficient.

A considerably improvement would be to included the measurement the wall thickness with respect to the fibre diameter for each fibre. This would allow account to be taken of the fact that the wall thickness can vary in proportion to the size of the fibre.

5 Conclusion

The method successfully identifies a single value for the shear modulus and the Young's modulus. The results show that the hardwood fibres and softwood fibres which are processed for the use in Kraftliner have almost identical elastic properties. However, some further work is needed to establish the accuracy of the estimation.

Most importantly, it needs to be established if the elastic properties of the fibres are more important to the attenuation that the exact geometry of the fibre. This can be done by investigating the effect of the ellipsoidal rather than cylindrical form of the fibres. This could be tested experimentally by scaling the system such that the dimension of the scatterer is increased, and the frequency range decreased, to such a degree that the scatterer shape could be more easily controlled. If it is found that variation in the the scattering geometry has a large impact on the attenuation then the model would have to be replaced with a model that has the more complex ellipsoidal geometry.

The effect of collapsed fibres on the attenuation should also be further investigated as well as the possibilities of identifying mixtures of fibres with different elastic properties.

An improved test of this model would be to compare pulp before and after refining or comparing sample from different pulp treatments.

References

[1] H. Karlsson, *Fibre Guide*. Lorentzen & Wettre, Kista, Sweden, 2006.

[2] A. Kaw, *Mechanics of composite materials*. Taylor & Francis, 2006.

[3] J. Tchepel, J. Provan, A. Nishida, and C. Biggs, "A procedure for measuring the flexilibity of single wood-pulp fibres," *Mechanics of Composite Materials*, vol. 42, no. 1, pp. 83–92, 2006.

[4] E. Ehrnrooth, "Softening and mechanical behaviour of single wood pulp fibres - the influence of matrix composition and chemical and physical characteristics," PhD Thesis, Department of Wood and Polymer Chemistry, University of Helsinki, 1982.

[5] A. Hagedorn, J. Orccotoma, P. Schueler, B. Snow, and J. Jarvinen, "Optimizing machine efficiency through fibre quality management," in *2006 TAPPI Papermaker's Conference*. Technical Association of the Pulp and Paper Industry, 2006.

[6] A. Dukhin and P. Goetz, *Ultrasound for Characterizing Colloids: Particle Sizing, Zeta Potential, Rheology*. Elsevier Science, 2002.

[7] Y. Aitomäki, "Online fibre property measurements: Foundations for a method based on attenuaion," Ph.D. dissertation, Luleå University of Technology, 2009.

[8] *Pulps - Determination of stock concentration*, International Organization for Standards, 1995.

[9] F. Fisher and V. Simmons, "Sound absorption in sea water," *Journal of the Acoustical Society of America*, vol. 62, no. 3, pp. 558–564, Sept 77.

[10] L. Salmen, "Viscoelastic properties of in situ lignin under water-saturated conditions," *Journal of material science*, vol. 19, no. 9, pp. 3090–3096, Sept. 1984.

[11] T. Coleman and Y. Li, "An interior trust region approach for nonlinear minimization subject to bounds," *SIAM Journal on Optimization*, vol. 6, pp. 418–445, 1996.

[12] Y. Aitomäki and T. Löfqvist, "Material property estimates from ultrasound attenuation in fibre suspensions," *Ultrasonics*, vol. doi:10.1016/j.ultras.2008.11.005, 2009.

[13] C. Habeger, "The attenuation of ultrsound in dilute polymeric fiber suspensions," *Journal of Acoustical Society of America*, vol. 72, pp. 870–878, sep 1982.